Measurement and interpretation of the bunched beam transfer function in SIS-18 with space charge

Vom Fachbereich Elektrotechnik und Informationstechnik
der Technischen Universität Darmstadt

zur Erlangung
der Würde eines Doktor-Ingenieurs (Dr.-Ing.)
genehmigte

Dissertation

von
Dipl.-Phys. Oleksandr Chorniy
geboren am 26. Oktober 1980 in Smolino, Ukraine

Referent: Prof. Dr.-Ing. Thomas Weiland
Korreferent: Prof. Dr. Oliver Boine-Frankenheim

Tag der Einreichung: 15. April 2008
Tag der mündlichen Prüfung: 27. Mai 2008

D 17
Darmstadt 2008

Abstract

Longitudinal Beam Transfer Function (BTF) measurements are employed as a diagnostic tool to determine synchrotron frequencies and damping rates in a synchrotron. The BTF method is employed to measure an effective impedance.

The aim of our theoretical study was to understand the influence of space charge effects and longitudinal impedances on the BTF. The BTF models developed in this work are based on the linearized Vlasov equation and on the equation of motion for a driven oscillator with damping factor. To verify the theoretical models numerical simulations studies have been performed. For these studies a PIC (particles-in-cell) code has been developed.

As part of this work longitudinal BTF measurements using bunched beams were performed in the SIS. In the experiment we excited the bunches using rf phase modulation. The longitudinal bunch oscillations were detected as a function of the rf phase modulation frequency. The measurements were done at different beam intensities. For the interpretation of experimental results the theoretical framework developed in this work was used.

Contents

Chapter 1

Introduction

The synchrotron SIS at "Gesellschaft fuer Schwerionenforschung" (GSI) is used for acceleration of intense heavy ion beams up to medium energies [1]. High intensity beams are required for nuclear physics experiments. The number of the successful events is proportional to the beam intensity on the target. Plasma physics experiments require high beam intensities to create high density matter.

During synchrotron cycle ions are grouped together in longitudinal direction forming the bunches. One of the effects observed during the synchrotron cycle in SIS are longitudinal persistent dipole oscillations of bunches [2, 3]. These are oscillations of the bunch center-of-mass with respect to the synchronous particle. In the Experimental Storage Ring (ESR) unstable dipole oscillations accompanied by fast particle losses were observed [4]. Bunch instability in the SIS is expected after the upgrade where it is planned to increase the beam intensity. Dipole oscillations are driven by longitudinal impedances. The mechanism which damps the dipole oscillations is Landau damping due to the nonlinearity of the Radio Frequency (rf) fields [5]. At high beam intensities Landau damping is lost due to space charge effects, as it will be shown later.

The impedances that potentially drive the dipole oscillations can be written in the form of an effective dipole impedance. As long as the dipole oscillations are damped by Landau damping or by electron cooling, no information about the impedances can be extracted. Dipole oscillations can be artificially excited by phase modulation of the rf signal. The amplitude and the phase of the induced dipole oscillations can be measured with respect to the phase modulation signal. These measurements are called longitudinal bunched Beam Transfer Functions Measurements (BTFM). To determine the effective dipole impedance in a real machine the BTFM can be used.

One of the first BTFM in a hadron synchrotron was performed in 1977 by F. Pederson and F. Sacherer in CERN [6]. The theoretical Beam Transfer Function (BTF) model for these measurements was represented by a simple oscillator model with damping factor. The space charge impedance and the effective dipole impedance were not included in the model. The particle distribution was not included as well. The BTFM deviated from the theoretical BTF model. This gave rise for further studies of Landau damping in bunched beams. Later, the particle distribution and the synchrotron frequency were taken into

account in the BTF model [7].

One of the most detailed theoretical studies related to the bunched beam BTF was performed by E. Shaposhnikova [8]. The theoretical results were used for the analysis of Landau damping in a single and double rf system [9]. In [8] a general approach is presented which contains not only rf phase modulation but rf amplitude modulation as well.

Since the 90s the BTFM has become a very important tool. They have been used to determine the synchrotron frequency, damping rates and bunches length [10, 11, 12]. The theoretical and experimental studies of the longitudinal motion under rf phase modulation with high modulation amplitudes have been performed in many laboratories [13, 14, 15, 16, 17, 18]. The main topics in these studies were beam splitting, resonance islands and bifurcations. Recently, it was shown that the effect of beam splitting in electron beams increases the stability properties with respect to the coupled bunch instabilities [19]. These effects are not considered in this thesis. Here only the case of rf phase modulation with low modulation amplitude is considered.

In general, the rf phase modulation can be provided either by the addition of a phase error in the rf control system [10] or by rf cavity de-tuning. To detect the dipole oscillations Digital Signal Processors (DSP) based phase detectors are usually used. The BTF is obtained by means of a comparison of the DSP signal with the rf phase modulation signal. In most of mentioned experiments low frequency network analyzers are used for the rf phase modulation and as a comparator.

At GSI the BTF method as a diagnostics tool for the coasting beams is well established. In 1990 longitudinal coasting BTFM were done in the Experimental Storage Ring (ESR) [20]. The measurement results were compared with data from Schottky diagnostics[21]. The longitudinal impedance of the rf cavity was obtained from the longitudinal coasting BTFM[22, 23, 24].

For the longitudinal coasting BTFM a network analyzer was used. The modulation frequency in the case of coasting BTFM lies in the MHz range. The modulation frequency in the longitudinal bunched BTFM lies in the kHz range which cannot be achieved by the network analyzers presently available at GSI. Additionally, there was no clear measuring technique for longitudinal dipole oscillations. Thus the longitudinal bunched BTFM have received no attention at GSI so far. In this thesis the results from the longitudinal bunched BTFM, or further BTFM, without involving network analyzer are presented. The measurement technique was developed during this work.

This thesis is organized as follows:

A theoretical treatment and numerical simulations are presented in the first part of this thesis. In the theoretical part the space charge and the effective dipole impedances are included in the BTF models. In the simulation part the BTFM were performed to check the BTF models from the theoretical part. In the second part of this thesis the results of BTFM in the SIS are presented.

In Chapter 2 an overview of the GSI facility is presented. A special attention is given to the description of the SIS. A role of the SIS in the FAIR(Facility for Antiproton and Ion Research) project is discussed. The rf system which operates the rf cavity in the SIS is described.

Chapter 3 introduces the particle motion in the rf fields. This Chapter includes a basic theory of synchrotron motion. A storage operation mode is considered.

In Chapter 4 the collective effects and the impedances are introduced. The connection between the real impedances and the effective dipole impedance is shown. The effective dipole impedance and space charge impedance are added to the synchrotron equation of motion. Dispersion relation as a basic theoretical tool for the investigation of beam stability is presented.

In Chapter 5 the BTF models for low and high beam intensity are introduced. The space charge and the effective dipole impedances are included in the BTF models.

Chapter 6 shows a numerical simulation scheme for the BTF simulation studies. The BTFM is performed numerically in order to check the BTF models.

In Chapter 7 the BTFM performed in the SIS are discussed. The rf phase modulation via the rf cavity de-tuning is described as well as the BTF measuring technique. The BTFM are compared with the BTF models.

Conclusion summaries the main results achieved during this work.

Chapter 2

GSI and the SIS (SchwerIonen Synchrotron)

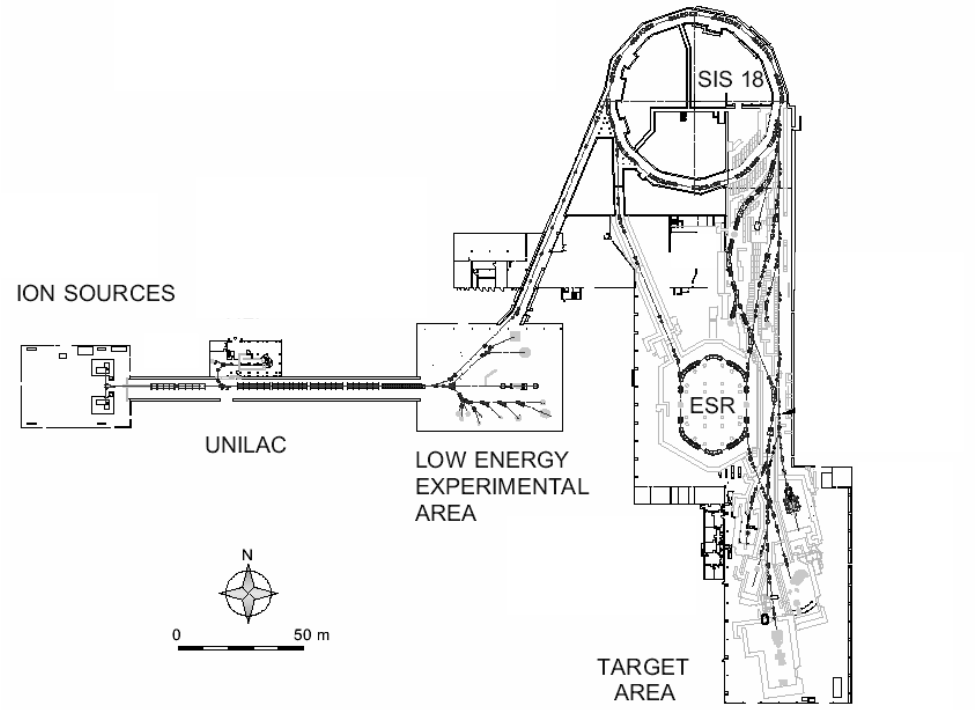

Figure 2.1: Accelerator facilities and experimental areas at GSI.

GSI was founded in 1969 and is a member of the Helmholtz association of National

Research Centers. GSI's facility performs the acceleration of protons and heavy ions. The research programm at GSI covers a broad range of activities: atomic physics, nuclear and hadron physics, plasma physics, materials research, biophysics and cancer therapy [25]. The research program includes also the development and upgrade of the existing accelerator facility. The main priority is the operation with highest beam intensities. A schematic view of the GSI is shown in Fig. 2.1. The heavy ion accelerator facility at GSI consists of three main parts:

- Universal linear accelerator (Unilac).
- SchwerIonenSynchrotron (SIS).
- ExperimentierSpeicherRing (ESR).

Accelerator	Particle energy	Number of ions per cycle
Unilac	11.4 MeV/U	U: $2 \cdot 10^{10}$ Ne: $1 \cdot 10^{11}$
SIS (presently)	U: 50-1400 MeV Ne: 50-2000 MeV p: 4.5 GeV	$< 7 \cdot 10^9$ $5 \cdot 10^{10}$ $2 \cdot 10^{10}$
ESR	U: 3-560 MeV Ne: 3-830 MeV	typically $< 10^9$

Table 2.1: Heavy ion energies achieved in the GSI's accelerators.

Starting from different ion sources the ions go to the SIS through the Unilac. The Unilac is used for pre-acceleration of ions and serves as the injector machine. The Unilac accelerates the ions up to the energy of 11.4 MeV/u. The energy of accelerated ions in the SIS at magnetic rigidity 18 Tm lies in the range from 1 GeV for U^{+73} to 4.5 GeV for protons. The accelerated ions are delivered either by fast extraction to the storage ring ESR or by slow extraction to the experimental hall. In the ESR the ions are accumulated. Using electron cooling the beam lifetime is increased significantly and the ions can be stored in the ESR during a long time. The particles energies and particle intensities presently achieved at GSI are presented in the Table 2.1.

2.1 Present status of the SIS

The scheme of the SIS is presented in Fig. 2.2. At the moment SIS serves as injector machine for the ESR. The main parameters of the SIS are shown in Table 2.2. The

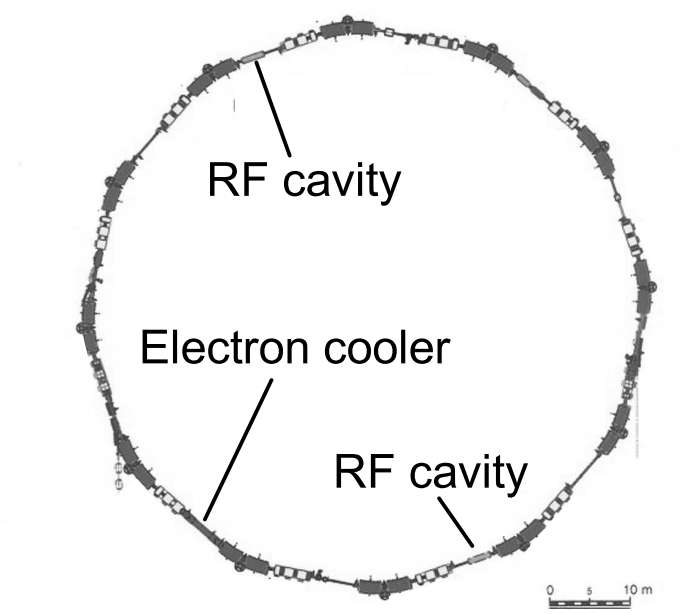

Figure 2.2: Overview of the heavy ion synchrotron SIS.

whole SIS acceleration cycle can be divided into the steps: injection, capture, acceleration, de-bunching, extraction. During multi-turn injection an ion pulse with energy of 11.4 MeV/u is injected in the SIS from the Unilac. The pulse duration varies from 1 to 400 μs. To increase the beam intensity during one SIS cycle the multi-multi-turn injection is performed. During multi-multi-turn injection several pulses are injected in the SIS. To decrease the longitudinal and transverse beam emittances electron cooling is used. After injection, the rf cavity voltage amplitude is increased and the particles are captured in a rf bucket. The design capture times lies in the range of 15 ms. When the capture is finished acceleration starts. The frequency of the rf voltage is increased during acceleration while the rf voltage amplitude is decreased in order to keep the rf bucket size constant. After acceleration the beam can be extracted by fast extraction. Another possibility is to de-bunch the beam by slow decrease of the rf voltage amplitude and then perform slow extraction.

The time between the injection start and the acceleration start is called the injection

Circumference	216 m
Maximum bending power	18 T·m
Magnets	24 Dipoles, 1.8 T 12 Triplettlenses 12 Sextupolelenses
Magnet Power	Dipoles 3.6 kA at 12 kV Field Ramp 10 T/s
rf Acceleration	2 Cavities at 16 kV Frequency Span 0.8-5.6 MHz
Vacuum	operational 10^{-10} Torr bakable to 300^0C
Beam Diagnosis	12 Position Monitors 2 Phase Probes 1 DC Transformers 1 fast, 1 slow Pulse Transformer 1 Faraday Cup 1 Beam Scraper

Table 2.2: The main parameters of the SIS facility.

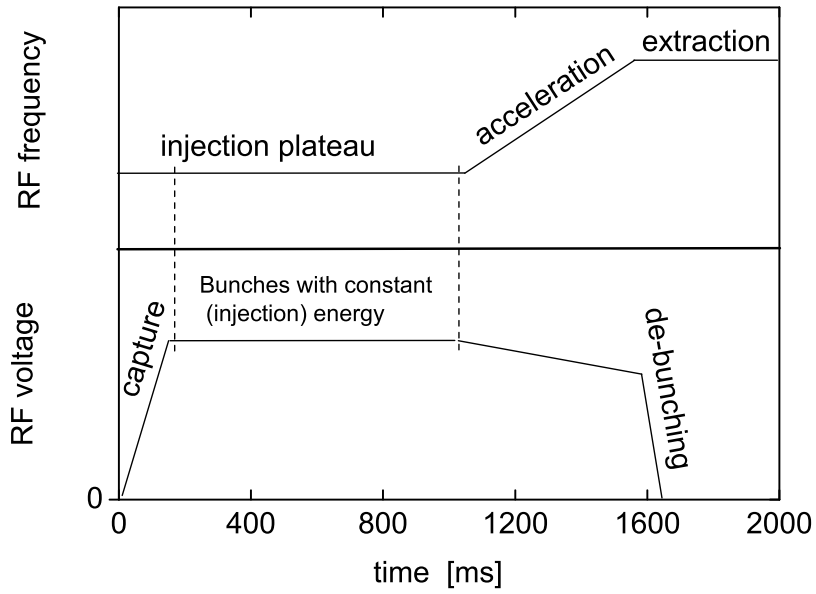

Figure 2.3: Scheme of the typical SIS cycle with injection plateau of 1 s.

plateau. The schematic picture of typical SIS cycle with the injection plateau of about 1 s is shown in Fig. 2.3. For machine experiments with bunched beam at injection energy the injection plateau can be increased up to seconds. During the injection plateau the synchrotron is operated in the so-called storage mode.

2.2 Role of the SIS in the FAIR project

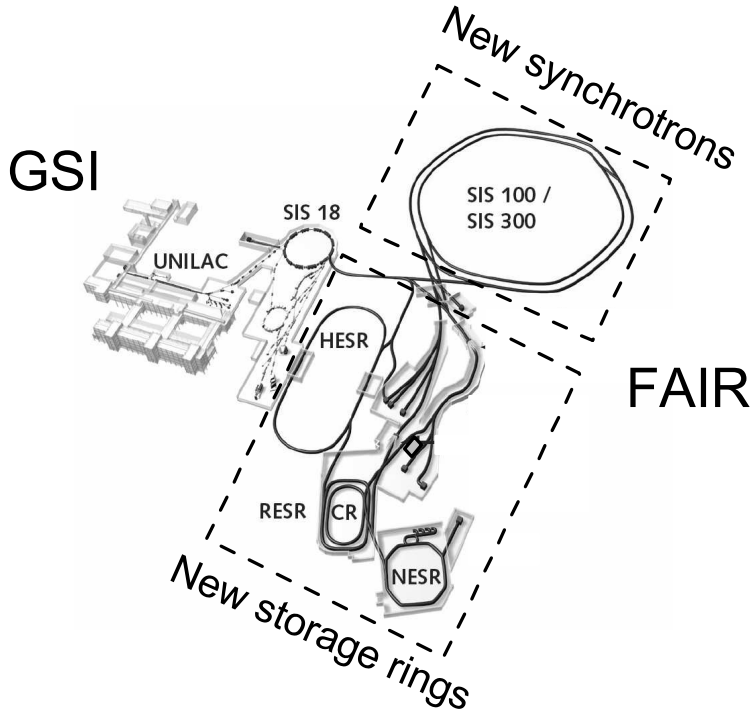

Figure 2.4: Overview of the FAIR project

The SIS will play an important role in the FAIR(Facility for Antiproton and Ion Research)project [26]. The future FAIR accelerators together with the present GSI facility are presented in Fig. 2.4. The maximum energy of the beam in the SIS100 lies in the range from 2.7 GeV/u for U^{+28} to 29 GeV for protons. The maximum intensity is $5 \cdot 10^{11}$ for U^{+28}.

	SIS presently	SIS after upgrade	SIS after upgrade (to SIS100)
Reference ion	U^{+73}	U^{+73}	U^{+28}
Repetition rate	0.3 Hz	1 Hz	2.7 Hz
Maximum intensity	$< 7 \cdot 10^9$	$2 \cdot 10^{10}$	$1.5 \cdot 10^{11}$
Maximum energy	1GeV/u	1GeV/u	0.2 GeV/u

Table 2.3: SIS parameters for the FAIR project

The SIS will serve as an injector for the SIS100. The present status of SIS does not allow to achieve the required beam intensity in the SIS100. To prepare the booster operation the SIS will be upgraded. The main aim of SIS upgrade is to increase the beam intensity by an order of magnitude compared to the present status. In Table 2.3 the beam parameters in the SIS which are required for the FAIR project are given. To achieve higher intensities many improvements will be done including the upgrade of the rf system. The upgrade of the rf system consists in the installation of a new rf cavity working at harmonic two. The new rf cavity will be operated together with one of the existing SIS rf cavities, working at harmonic four [27]. The new rf cavity will provide a larger rf bucket area that allows to increase the number of captured ions. The combination of the new cavity with the existing one will create a double harmonic rf bucket. Flattening of a bunch profile in a double rf bucket decreases the peak current in a bunch. On the other hand, at high beam intensities bunch instabilities in the SIS are expected. The instability growth rates for the SIS with the existing rf cavities are analyzed in this work.

2.3 General principles of acceleration

Synchronization and phase focusing is required during acceleration of a bunch. Synchronization is fulfilled if the rf voltage frequency is chosen as an integer multiple of the revolution frequencies. This number is called the harmonic number. The longitudinal focusing of the particles inside rf bucket is defined as phase focusing. It can be achieved by a proper phase between the rf voltage and the synchronous particle.

The rf cavity provides an electric field which is parallel to the longitudinal particle direction. The longitudinal direction is the direction along a ring. Particles experience the effect of rf fields when they cross a cavity gap. This is the gap between the electrodes of rf cavity. The electric field provided by the rf cavity is time dependent and its direction may be towards or opposite to the particles direction. Thus going through rf cavity the particles may gain or loose energy due to interaction with the electric field. In the simplest

case, the electric fields, provided by the rf cavity, depend on time as a single harmonic function [28], p.110

$$E_z(t) = E_{z0} \cdot \sin(\omega_{rf} t + \phi),$$

where $\omega_{rf} = h\omega_0$ is the rf frequency and ϕ is the phase between the electric field and the particle at the times when particle arrive into the cavity. It is assumed that electric field is homogenous in the radial and in the longitudinal direction. The energy gain $\triangle E$ of a particle traveling the cavity gap is written as [29], p.233

$$\triangle E = q \int E_z(t) dt,$$

where q is the particle charge. It can be obtained as [30]

$$\triangle E = q E_{z0} L_g T_{tr} \sin(\phi),$$

where L_g is the gap width, $T_{tr} = \sin(hL_g/2R)/(hL_g/2R)$ is the so called transit time factor. The particle needs a finite time to pass the cavity while the longitudinal field in the cavity varies with time. Thus the energy gain is electric field in the gap averaged over the transit time. This fact is reflected by the transit time factor. In the SIS cavities the gap is very small and $T_{tr} \approx 1$. The rf voltage seen by the particle is defined as

$$V_{rf} = E_{z0} L_g \sin\phi = V_0 \sin\phi$$

with rf voltage amplitude V_0.

2.4 Radio Frequency (rf) system in the SIS

Presently, two identical rf cavities are operated in the SIS. Their positions are shown in Fig. 2.2. The rf cavity in the SIS consists of two groups of ferrite rings with gap in between. The working range of a single cavity lies in the frequency range from 0.8 to 5.6 MHz. The maximum rf voltage amplitude of one cavity is 16 kV. The rf cavities are operated with harmonic number four. Thus the rf system is able to accelerate four bunches simultaneously.

It is important to know the impedance of rf cavity. The equivalent electric circuit of rf system can be represented as a RLC circuit as it is shown in Fig. 2.5. The impedance of the rf cavity is determined by the shunt impedance and the quality factor. The shunt impedance of the cavity is defined as the ratio of the square voltage seen by the beam to the dissipated power[30]. The quality factor depends on the rf cavity wall resistance and rf cavity characteristic impedance. A ferrite cavity has a resonant frequency, i.e. the frequency at which the rf voltage amplitude is maximum for a fixed generator current amplitude. The impedance of the RLC circuit that is equivalent to the impedance of rf cavity is calculated as

$$Z_{cav} = \frac{R_{sh}}{1 + iQ(\frac{\omega_r}{\omega} - \frac{\omega}{\omega_r})}, \tag{2.1}$$

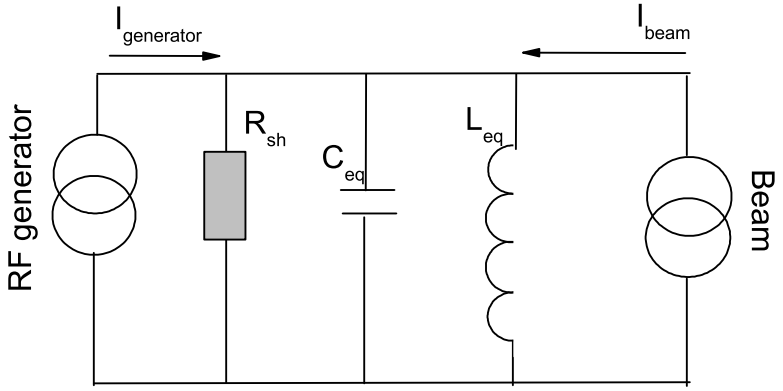

Figure 2.5: Parallel equivalent circuit of the rf system with cavity.

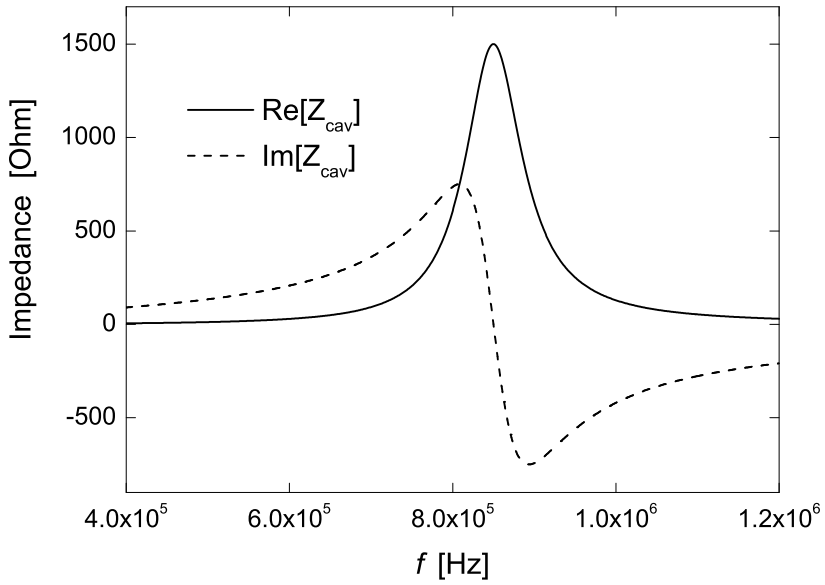

Figure 2.6: Impedance of the SIS cavity with quality factor $Q = 10$, shunt impedance $R_{sh} = 1500$ Ohm and resonant frequency $f_r = \frac{\omega_r}{2\pi} = 849$ kHz . The values were obtained by rf group at GSI [31].

where the quality factor Q and the cavity resonant frequency are determined as

$$Q = R_{sh}\sqrt{\frac{C_{eq}}{L_{eq}}} \qquad \omega_r = \frac{1}{\sqrt{L_{eq}C_{eq}}} \tag{2.2}$$

with L_{eq} and C_{eq} as the equivalent inductance and capacitance. The measured impedance of the SIS cavities is shown in Fig. 2.6.

To match the rf frequency in the cavity the rf system uses a bias current. The rf system also adjusts the phase between the bunch and the electric field inside the gap. This ability of rf system to change the relative phase is used for the rf phase modulation. The principle of the phase adjustment between the particle and rf voltage can be demonstrated in a simple way. The rf voltage acting on the particle is determined by the generator current multiplied by the cavity impedance:

$$V_{rf} \approx I_g e^{i\omega_{rf}t} Abs(Z_{cav}) e^{i\theta} \qquad \theta = Arg(Z_{cav}), \tag{2.3}$$

where $I_g e^{i\omega_{rf}t}$ is the generator current loaded to the cavity, Z_{cav} is the cavity impedance value at the frequency ω_{rf}. By changing the bias current the resonant frequency is changed. Thus the cavity impedance is shifted and the phase θ is changed. In Chapter 7 it will be shown how the dynamical change of cavity resonant frequency is used for the longitudinal bunched BTFM.

Chapter 3

Particle dynamics in rf fields

In this Chapter the particle dynamics in the presence of rf fields is introduced. Synchrotron motion is the motion of a particle with respect to the synchronous one. In this thesis the synchrotron equation of motion is restricted to the case of storage mode operation, e.g. without acceleration. Hamiltonian formalism is involved to derive the stationary longitudinal particle distribution and line density. Due to the rf field nonlinearity the synchrotron frequency is a function of the particle oscillation amplitude.

3.1 Single particle equation of motion in rf buckets

For stored beams the synchronous particle is defined as the particle that moves with fixed energy around the synchrotron. In the case of heavy ion beams the radiation losses is negligibly small and it is assumed that the synchronous particle receives no energy from an rf cavity. A non-synchronous particle is defined as a particle with an energy that is different from the energy of the synchronous particle.

There is a range of possibilities for the selection of variables that is used to describe the motion of the non-synchronous particle [29], p.237, [28], p.113, [32], p.300. In this thesis we will use the phase variable ϕ which describes position deviation and the phase velocity $\dot{\phi}$ which describes energy deviation. The relative phase is defined as

$$\phi = \frac{2\pi h}{T_0}(\tau - T_0), \tag{3.1}$$

where $\tau - T_0$ is the difference in revolution period of the synchronous and the non-synchronous particles. It is assumed that the relative phase changes smoothly with time

$$\frac{d\phi}{dt} = \frac{\triangle\phi}{T_0}, \tag{3.2}$$

where $\triangle\phi$ is the particle phase change during one turn in a synchrotron and T_0 is the revolution period. In one turn the particle phase changes as (from Eq. (3.1))

$$\triangle\phi = 2\pi h\frac{\triangle\tau}{T_0}. \tag{3.3}$$

In the following we will derive $\triangle\tau$.

The orbit length C depends on the particle momentum p. A relationship between these two parameters is defined through the so-called "momentum compaction factor" [32], p.296. The relationship is calculated as

$$\frac{dC}{C} = \alpha_p \frac{dp}{p},$$

where dC is the difference in the orbit length for the synchronous and for the non-synchronous particles and dp is the difference in particles momentum of synchronous and non-synchronous particles. From the particle travel time $\tau = \frac{C}{v}$ and particle velocity v we obtain [28]:

$$\frac{d\tau}{\tau} = \frac{dC}{C} - \frac{dv}{v}. \tag{3.4}$$

Using the relativistic relation $dv/v = 1/\gamma^2 \cdot dp/p$ with Eq. (3.4) we obtain:

$$\frac{d\tau}{\tau} = \eta \frac{dp}{p}, \tag{3.5}$$

where $\eta = \alpha_p - 1/\gamma^2$ is the so-called "phase slip factor" [30]. Here we are interested in low γ-value. For low particle energies η is negative. Combining Eqs. (3.2), (3.3), (3.5) we obtain

$$\frac{d\phi}{dt} = \frac{2\pi h}{T_0}\eta\delta, \tag{3.6}$$

where $\delta = \frac{p - p_0}{p_0}$ is the relative particle momentum change in one turn, p_0 is the momentum of the synchronous particle and p is the momentum of non-synchronous particle. Eq. (3.6) is the first equation of longitudinal motion.

The second longitudinal equation of motion is derived by taking into account the influence of rf voltage. Assuming that particle momentum changes smoothly with time, we obtain

$$\frac{dp}{dt} = \frac{\triangle p}{T_0}. \tag{3.7}$$

The change in momentum due to the rf field will be derived using

$$\triangle E = qV_{rf}. \tag{3.8}$$

The change in particle energy $\triangle E$ due to rf voltage is described by Eq. (3.8). Energy of the particle is connected with the particle momentum via

$$E^2 = m^2c^4 + p^2c^2.$$

After simplifications the next relation is obtained [32], p.300:

$$\triangle E = \beta c \triangle p.$$

Using this equation with Eqs. (3.7), (3.8) one obtains

$$\frac{dp}{dt} = \frac{qV_0}{L}\sin\phi.$$

The second longitudinal equation of motion is written as

$$\frac{d}{dt}(\frac{p-p_0}{p_0}) = \dot{\delta} = \frac{qV_0}{L\gamma m\beta c}\sin\phi. \tag{3.9}$$

Combining Eqs. (3.6), (3.9) the second order differential equation can be obtained:

$$\ddot{\phi} + \omega_{s0}^2 \sin\phi = 0, \tag{3.10}$$

where ω_{s0} is the parameter which is called the synchrotron frequency:

$$\omega_{s0} = \frac{hqV_0}{LRm^*}, \tag{3.11}$$

with the effective mass $m^* = -\gamma m/eta$. Synchrotron equation of motion (3.10) describes the oscillations of non-synchronous particle around the synchronous particle. These oscillations are called synchrotron oscillations. Comparing Eq. (3.10) with Eq. (3.9) the particle phase velocity in the frame co-moving with the synchronous particle can be derived:

$$\dot{\phi} = -\frac{h}{R}\eta\beta c\delta. \tag{3.12}$$

The longitudinal equations of motions (3.6), (3.9) can be re-written using Eq. (3.12) as

$$\begin{cases} \dfrac{d\phi}{dt} = \dot{\phi} \\ \\ \dfrac{d\dot{\phi}}{dt} = -\omega_{s0}^2 \sin\phi \end{cases}. \tag{3.13}$$

Both Eqs. 3.13 together have the structure of Hamiltonian equations

$$\frac{dq}{dt} = \frac{\partial H}{\partial p} \quad \frac{dp}{dt} = -\frac{\partial H}{\partial q}, \tag{3.14}$$

where the canonical conjugated variables corresponds to the physical variables ϕ and $\dot{\phi}$. From the equations of motion a single particle Hamiltonian can be extracted as

$$H = \frac{\dot{\phi}^2}{2} + \omega_{s0}^2 Y_{rf}(\phi), \tag{3.15}$$

where

$$Y_{rf}(\phi) = \frac{1}{V_0}\int_0^{\phi} V_{rf}(\phi')d\phi' \tag{3.16}$$

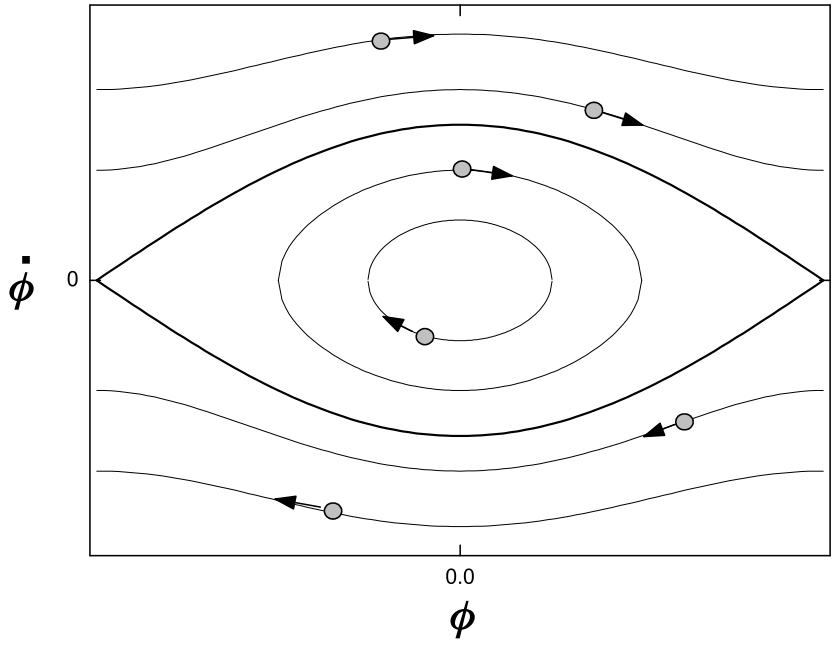

Figure 3.1: Particles trajectories in phase space inside and outside the rf bucket.

is the rf potential function. By using the Hamiltonian the particle trajectories in the longitudinal phase space [29] presented by ϕ , $\dot{\phi}$ coordinates can be calculated. The equation of the trajectory can be written as

$$\dot{\phi}(\phi) = \pm\sqrt{2[H_0 - \omega_{s0}^2 Y_{rf}(\phi)]}, \tag{3.17}$$

where the Hamiltonian value H_0 is calculated using initial values of ϕ and $\dot{\phi}$. In Fig. 3.1 the trajectories for particles with different H_0 are shown. The region of closed trajectories around the synchrotron particle is called the rf bucket.

3.2 Bunch distributions

Inside the rf bucket the particles are grouped together forming a bunch. The line density is defined as

$$\lambda(\phi) = \frac{1}{N}\frac{dN}{d\phi},$$

where N is the number of particles. On the other hand the line density can be obtained as the projection of distribution function $\psi(\phi, \dot{\phi})$ in phase space on the longitudinal direction:

$$\lambda(\phi) = \int_{-\infty}^{+\infty} \psi(\phi, \dot{\phi}) d\dot{\phi}.$$

The two dimensional phase space is represented by the two variables ϕ and $\dot{\phi}$. The phase space distribution and the line density are shown in Fig. 3.2.

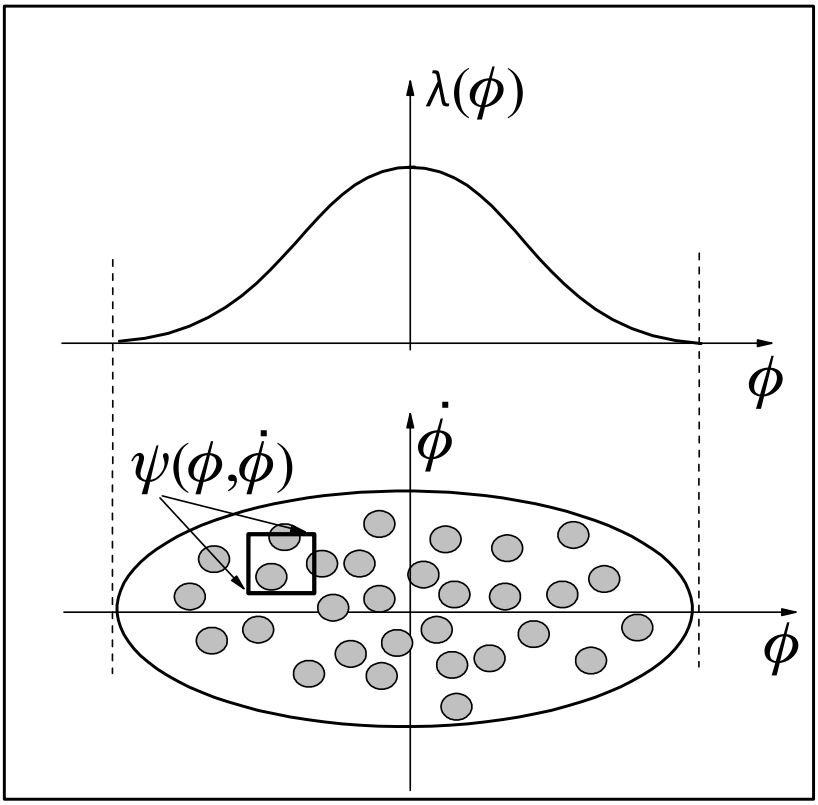

Figure 3.2: The line density as the projection of distribution $\psi(\phi, \dot{\phi})$ on longitudinal axis ϕ.

It is important to note that the distributions functions are normalized to one:

$$\int_{-\infty}^{+\infty} \lambda d\phi = 1$$

$$\int_{-\infty}^{+\infty} \int_{-\infty}^{+\infty} \psi(\phi, \dot{\phi}) d\phi d\dot{\phi} = 1.$$

A stationary, or matched, distribution is defined as a time independent distribution. According to a statement from theoretical mechanics [33] the poisson brackets of a such a distribution with a Hamiltonian must be equal to zero

$$[\psi, H] = \frac{\partial \psi}{\partial \phi}\frac{\partial H}{\partial \dot{\phi}} - \frac{\partial \psi}{\partial \dot{\phi}}\frac{\partial H}{\partial \phi} = 0.$$

Thus a stationary distribution is an arbitrary function of the Hamiltonian, i.e. $\psi = \psi(H)$.

There are two widely used distributions. The first one is a Gaussian distribution. Due to intra-beam scattering the natural particle distribution is a Gaussian distribution in particle energy. Intra-beam scattering is Coulomb scattering of a charged particle in a beam [34]. This scattering is a random process. Thus, according to the central limit theorem of statistical mechanics, any processes of a random, statistically independent nature acting on a particle distribution in a harmonic oscillator potential will lead to displacements in the particles positions that obey a Gaussian distribution [35]. Since the particle distribution of a beam is confined by a focusing force and the individual particles are performing oscillations, there is a continuous exchange between position (potential energy) and velocity (kinetic energy) so that energy distribution is also a Gaussian distribution. Since the Hamiltonian is directly proportional to the full particle energy, it can be written

$$\psi(H) = \psi_0 e^{-\frac{H}{2H_{rms}}},$$

where ψ_0 is a normalized constant and $H_{rms} = v_{rms}^2/2$ is the Hamiltonian which is proportional to the root mean square value of the particles energies in a bunch. The line density $\lambda(\phi)$ is the projection of phase space distribution $\psi(\phi, \dot{\phi})$ onto ϕ axis. Using the expression for the Hamiltonian (3.15) we can write the expression for the line density in terms of the rf potential:

$$\lambda(\phi) = \lambda_0 e^{-\frac{Y_{rf}(\phi)}{\sigma^2}},$$

where $\sigma = \dfrac{\dot{\phi}_{rms}}{\omega_{s0}}$ is proportional to the rms value of the particles phase velocities, $Y(\phi)$ is the total potential and λ_0 is a normalized constant. The line density solution can be written as

$$\lambda(\phi) = \lambda_0 e^{-\frac{1-\cos\phi}{\sigma}}. \tag{3.18}$$

For short bunches the line density can be approximately written as a a Gaussian function

$$\lambda(\phi) \approx \frac{1}{\sqrt{2\pi}\sigma_{rms}} e^{-\frac{\phi^2}{2\sigma}}, \tag{3.19}$$

with σ as the longitudinal rms size of the bunch. In Fig. 3.3 the comparison between exact and approximate solution is shown. Since the discrepancy is small the approximate solution can be used even for relatively large bunch lengths.

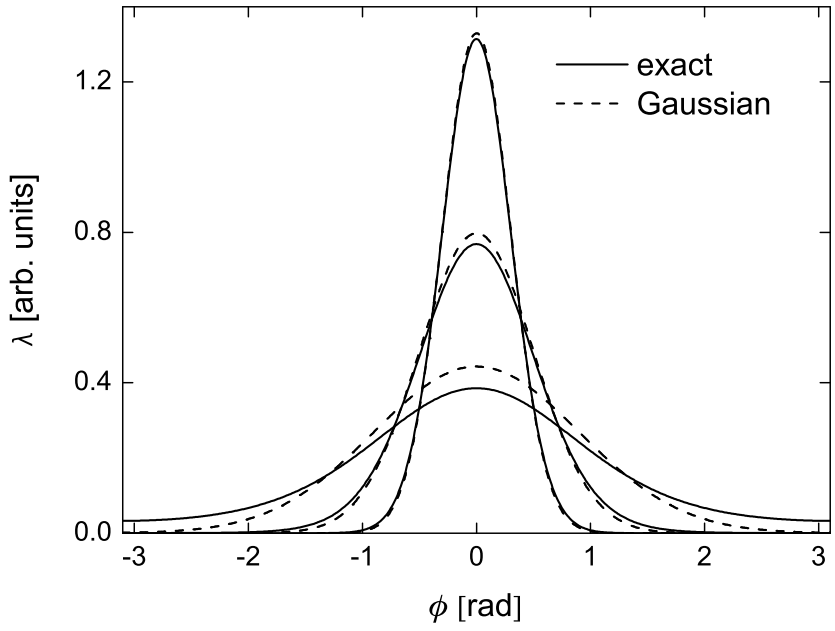

Figure 3.3: Comparison of the line densities obtained with exact(Eq. (3.18)) and approximate (Eq. (3.19)) equations for different parameters σ: 0.3, 0.5, 0.9.

Another distribution used in beam physics calculations is the elliptic distribution. It was implemented firstly in the middle of 80s. The line density obtained from the elliptic distribution was used as a best fit for the measured line density of the proton bunches in CERN [36]. If the elliptic distribution is used in the form

$$g(H) = c\sqrt{H_m - H}, \tag{3.20}$$

then the line density is obtained as

$$\lambda(\phi) = \frac{1}{u_m}(Y_{rf}(\phi_m) - Y_{rf}(\phi)), \tag{3.21}$$

where H_m is the value of the Hamiltonian for the bunch boundary particle, ϕ_m is the half-bunch length, and u_m obtained from the normalizing condition:

$$u_m = 2\int_0^{\phi_m} (Y_{rf}(\phi_m) - Y_{rf}(\phi))d\phi.$$

The line densities obtained from a Gaussian and elliptic distributions are called rms equivalent for short bunches if $\phi_m \approx \sqrt{5}\sigma_{rms}$ [35]. The example of the rms-equivalent bunches is shown in Fig. 3.4.

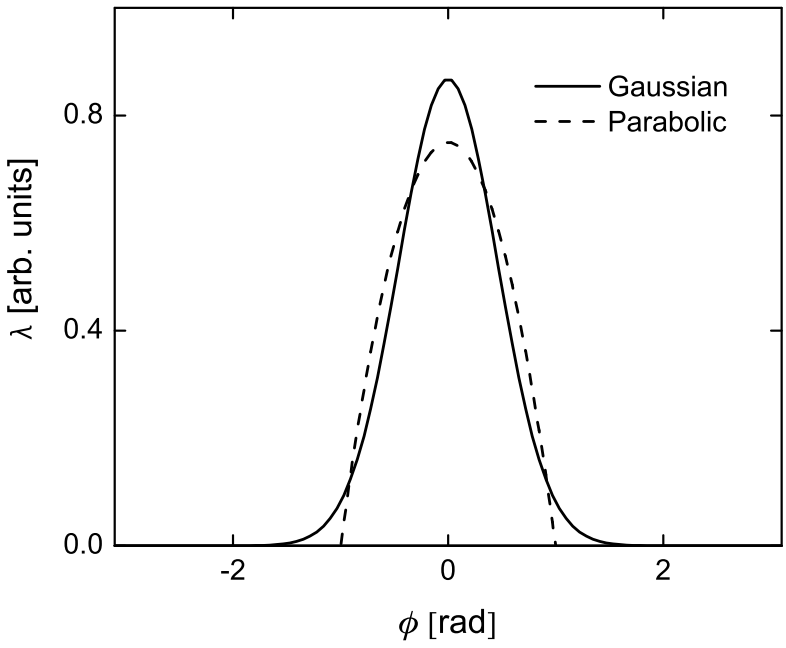

Figure 3.4: rms equivalent Gaussian and parabolic line densities with bunch length $\phi_m = 60^0$.

The particle distribution is important to know in the case of collective effects. In this case a synchrotron frequency is different for different distributions. If the collective effects are not included than the synchrotron frequency is the same for both Gaussian and elliptic distributions.

3.3 Synchrotron frequency

As described in the previous section, the non-synchronous particle performs oscillations termed synchrotron oscillations, here we will obtain the period of these oscillations. Using the Hamiltonian [3.15] we write:

$$\omega_{s0}^2 Y_{rf}(\hat{\phi}) = \frac{\dot{\phi}^2}{2} + \omega_{s0}^2 Y_{rf}(\phi),$$

where $\hat{\phi}$ is the particle oscillating amplitude (Fig. 3.5). Extracting $\dot{\phi}$ and using

$$dt = \frac{d\phi}{\dot{\phi}} \qquad T_s(\hat{\phi}) = 2\int_0^{\hat{\phi}} \frac{d\phi}{\dot{\phi}} \tag{3.22}$$

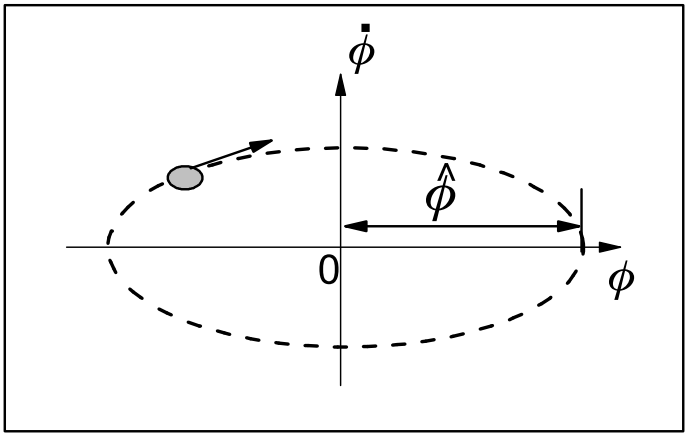

Figure 3.5: Particle oscillation in phase space. $\hat{\phi}$ is the particle oscillating amplitude.

the synchrotron period $T_s(\hat{\phi})$ as a function of $\hat{\phi}$ can be obtained from

$$T_s(\hat{\phi}) = \frac{2\sqrt{2}}{\omega_{s0}} \int_0^{\hat{\phi}} \frac{d\phi}{\sqrt{Y_{rf}(\hat{\phi}) - Y_{rf}(\phi)}}. \tag{3.23}$$

According to Eq. (3.23),the synchrotron frequency defined as $\omega_s(\hat{\phi}) = 2\pi/T_s(\hat{\phi})$ reads

$$\frac{\omega_s(\hat{\phi})}{\omega_{s0}} = \frac{\pi}{\sqrt{2}} \left(\int_0^{\hat{\phi}} \frac{d\phi}{\sqrt{\cos\phi - \cos\hat{\phi}}} \right)^{-1}, \tag{3.24}$$

with $Y_{rf}(\phi) = 1 - \cos\phi$. The integral (3.24) can be written in the form of the complete elliptic integral of the first kind $K(x)$ [37] :

$$\frac{\omega_s(\hat{\phi})}{\omega_{s0}} = \frac{\pi}{2} \frac{1}{K(\sin\frac{\phi}{2})}.$$

An approximate solution for the synchrotron frequency can be obtained for small $\hat{\phi}$ [30]:

$$\frac{\omega_s}{\omega_{s0}} = 1 - \frac{\hat{\phi}^2}{16}. \tag{3.25}$$

In Fig. 3.6 the exact (3.24) and the approximate (3.25) solutions are compared.

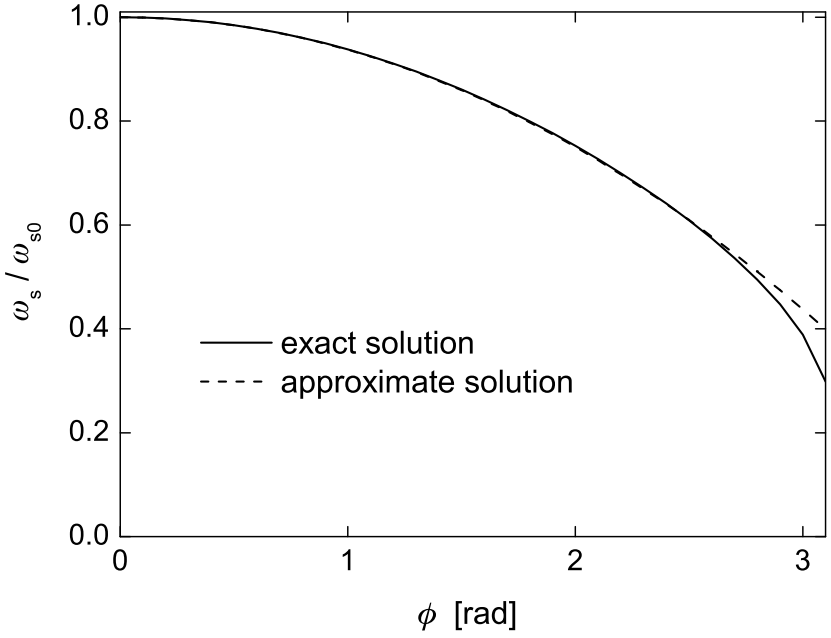

Figure 3.6: Dependence of the relative synchrotron frequency on the particle oscillating amplitude. Exact (3.24) and approximate (3.25) curves is plotted.

The particles in the bunch oscillate with $\omega_s(\hat{\phi})$. The bunch itself can perform dipole oscillations. The frequency of these dipole oscillations is called as coherent. The coherent frequency Ω_c obtained in [38] is

$$\Omega_c^2 = \omega_{s0}^2 \int_{-\phi_m}^{+\phi_m} \lambda'(\phi) \frac{V_{rf}}{V_0}(\phi) d\phi.$$

So far particle dynamics without collective effects has been described. The coherent frequency in this case is a real number, an imaginary part is absent. Later it will be shown that in the presence of collective effects the imaginary part can have non-zero value. Depending on the sign of the imaginary part the dipole oscillations can grow or be damped.

Chapter 4

Longitudinal collective effects

In addition to the interaction of the beam with the rf cavities, the beam interaction with the self-produced fields is described. This interaction is called the collective effects. To describe the collective effects the concept of longitudinal ring impedance is introduced. The

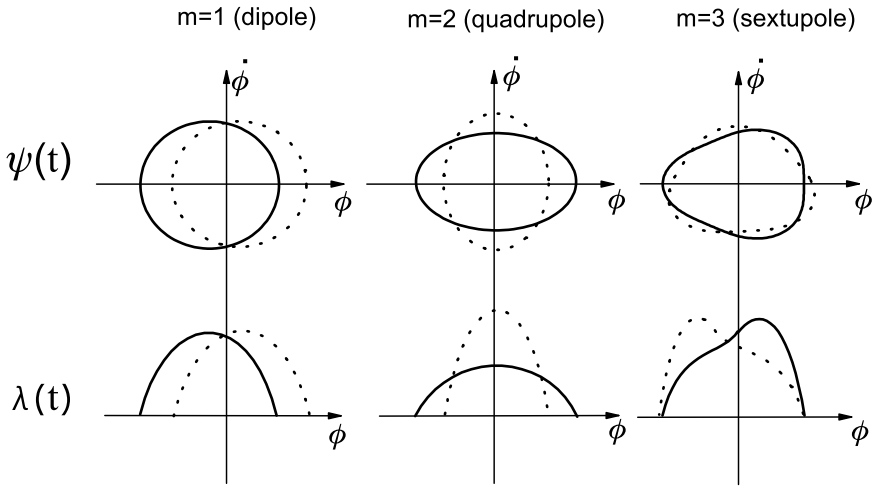

Figure 4.1: Different modes of bunch oscillation.

influence of the the space charge impedance on the stationary bunch consists in reduction of the focusing rf force, if η is negative [38]. The stationary, or matched, line density of the bunch affected by space charge impedance is presented.

The stable bunch has been discussed so far. Despite of the particles in the stable

bunch perform oscillations the bunch itself does not perform any motion. In reality a bunch can oscillate in dipole, quadruple and higher order modes (Fig. 4.1). This motion is called coherent modes and these modes can be amplified by the impedance [39]. Thus an amplitude of oscillations may grow that is called instability.

At low beam intensities the collective effects are negligible. When the beam intensity is increased the collective effects plays an important role. Instabilities caused by these effects can limit the maximum beam intensity in a synchrotron.

4.1 Longitudinal impedances

Consider a bunched beam with average current I circulating in a ring. The beam induces electromagnetic fields. Since the beam pipe is a good conductor the currents will be created on the surface of the beam pipe. In turn these currents generate an electromagnetic field that act back on the beam. The connection between induced field and beam current is described by the longitudinal impedance. The longitudinal impedance is defined as

$$Z_{||}(\omega) = -\frac{\oint E_{||}(\omega, s)ds}{I(\omega)},$$

where $E_{||}$ is the longitudinal electric field seen by the particle and $I(\omega)$ is the frequency component of the beam current. The integration is done over the path that beam goes in synchrotron. The impedance gathers all the details of the electromagnetic interaction between the beam and its surroundings. The concept of impedance in accelerators was introduced in 1967 by. A. Sessler and V. Vaccaro [40]. The impedance of a synchrotron consists of a sum of impedances coming from different synchrotron components. The impedance sources can have narrow band or broad band character in its spectra (Fig. 4.2). In the SIS we consider four main impedance sources:

- Space charge impedance (electromagnetic interaction between the beam particles).
- rf cavity impedance (impedance of the rf cavity itself).
- "Cavity-like structure" impedance (e.g. due to the variations in the beam pipe cross-section) plus high order rf cavity impedance.
- "Resistive wall" impedance (due to finite conductivity of the beam pipe).

The rf cavity impedance and "cavity-like structure" impedance can be described by the RLC circuit impedance that is written as

$$Z_{||} = \frac{R}{1 + iQ(\frac{\omega_r}{\omega} - \frac{\omega}{\omega_r})}, \tag{4.1}$$

where R is impedance value at resonance, ω_r is the resonance frequency, Q is the quality factor. In Fig. 4.2 the absolute values of resonant impedances with different Q are presented. The x-axis in Fig. 4.2 represents the harmonics of revolution frequency ω_0. The

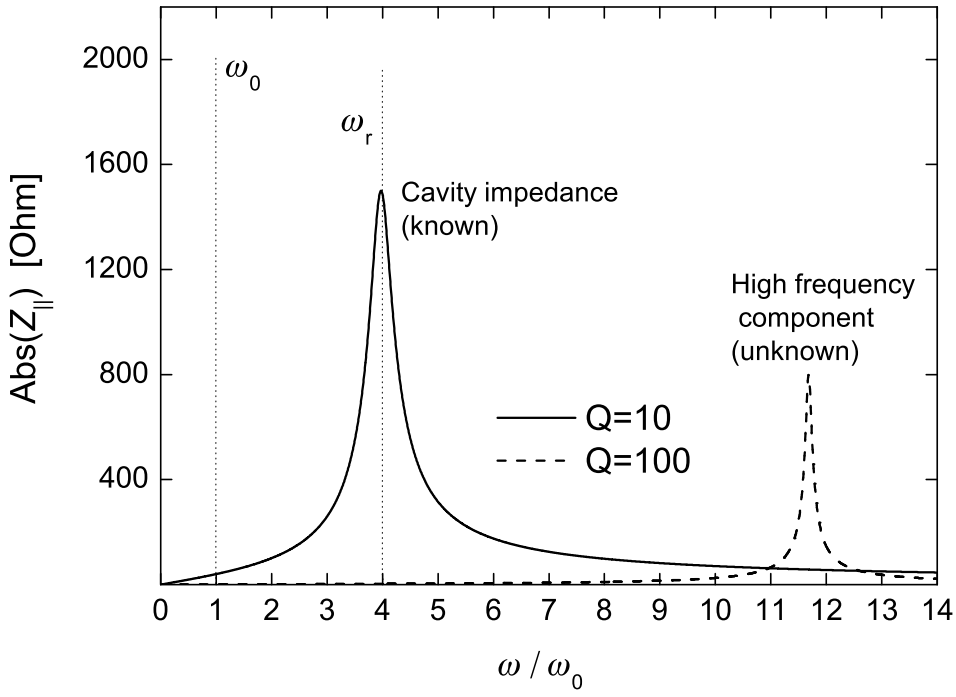

Figure 4.2: "Cavity-like structure" impedances with different Q-values.

revolution frequency $f_0 = \omega_0/2\pi$ at injection energy in the SIS is equal to 214 kHz. The resonant frequency of rf cavity impedance is equal to $4 \cdot \omega_0$. The higher harmonic components are unknown. The space charge and resistive wall impedances have no resonance and thus it is always broad-band.

The interaction of beam with impedances produce a voltage defined in frequency domain as the product of impedance and beam current:

$$V(\omega) = -I(\omega)Z_{||}(\omega).$$

4.2 Space charge field

One of the important contributions to the total longitudinal impedance in the SIS is the space charge impedance. The charged particles in a bunch interact with each other and with the pipe wall. The resulting electric space charge field induces a voltage that counteracts the rf voltage.

Single particle motion is governed by the external focusing force and the additional force

generated by the beams. The line density is determined by the motion of each particle. A self consistent distribution function can be obtained.

4.2.1 Voltage induced by a stationary bunch

In order to obtain the induced voltage the beam current in frequency domain has to be known. Fourier analysis is used to obtain the frequency spectrum. The line density and the rf voltage have been defined as a function of ϕ. In frequency domain we will use p-variable which represents the frequency ω in units of revolution frequency ω_0:

$$p = \frac{\omega}{\omega_0}.$$

For periodic line density

$$\lambda(\phi + L) = \lambda(\phi), \tag{4.2}$$

the spectrum in the frequency domain has a discrete frequencies $\omega = \omega_0 p$ and p is an integer. The beam current depends on the line density as

$$I(\phi) = Nq\beta c\frac{h}{R}\lambda(\phi).$$

This current can be expanded in Fourier series:

$$I(\phi) = \sum_{p=-\infty}^{+\infty} I_p e^{ip\phi}. \tag{4.3}$$

Current spectrum I_p can be calculated as

$$I_p = \frac{1}{2\pi}\int_{-\pi}^{\pi} I(\phi)e^{-ip\phi}d\phi.$$

Consider a bunch with a Gaussian line density (Eq. 3.19) the current spectrum is obtained as

$$I_p = \frac{qN}{T_0}e^{-\frac{p^2\sigma_{rms}^2}{2}}.$$

In Fig. 4.3 the current spectrum for bunch with $\phi_m = 60^0$ is shown. The current components I_p multiplied by the impedance $Z_p^{||} = Z_{||}(p\omega_0)$ create an additional voltage calculated as

$$V_{add}(\phi) = -\sum_{p=-\infty}^{+\infty} I_p Z_p^{||} e^{ip\phi}. \tag{4.4}$$

The additional voltage $V_{add}(\phi)$ depends on the coordinate ϕ and does not include the time variable. The time dependence appears if the dipole oscillations is included in the

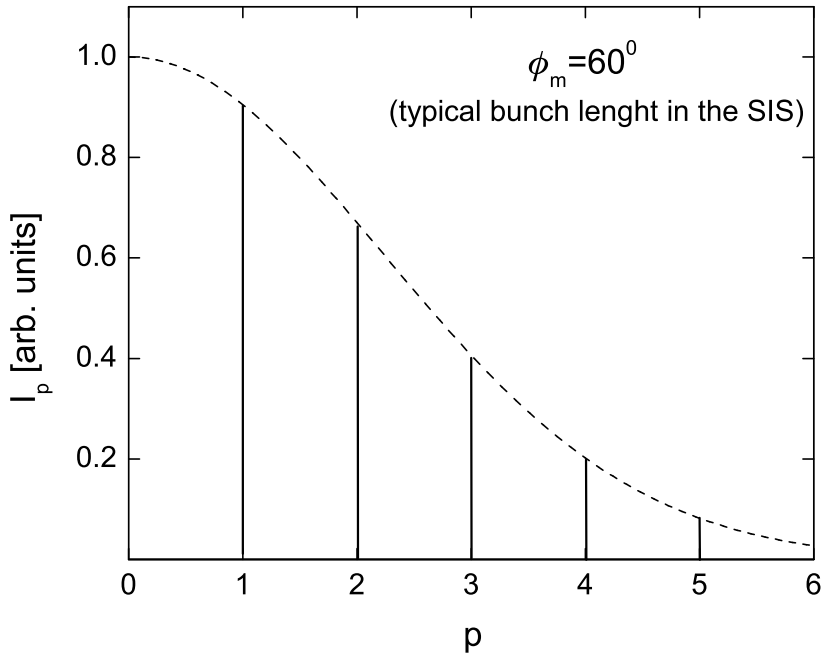

Figure 4.3: Spectrum of the current components for a Gaussian bunch with bunch length $\phi_m = 60^0$.

procedure above. Without dipole oscillations the effective voltage seen by the bunch is time independent and is written as

$$V_{tot} = V_{rf}(\phi) + V_{add}(\phi).$$

It is important to note that the value $V_{add}(\phi)$ depends on the type of impedance. The broader the impedance the more current harmonics will contribute to $V_{add}(\phi)$.

4.2.2 Space charge impedance

To compute the space charge field the following assumptions must be valid:

- The beam is uniformly distributed transversely.
- A beam pipe with infinitely conducting walls.

These assumptions allow to consider the space charge field variation only on ϕ-axis and to remove other fields that arises due to reflection from the pipe walls. A beam with radius a and beam pipe with radius b is assumed. A schematic picture is shown in Fig. 4.4. To

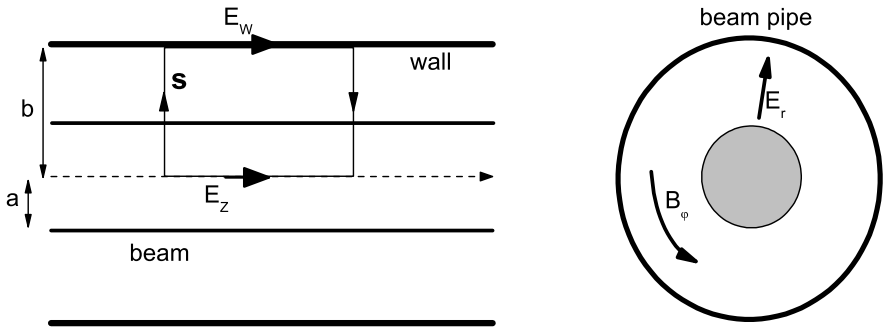

Figure 4.4: Beam inside beam pipe and induced fields.

calculate the electric field Faraday's law in integral form is used:

$$\oint \overrightarrow{E}\, d\overrightarrow{l} = \frac{\partial}{\partial t} \oint \overrightarrow{B}\, d\overrightarrow{A}. \tag{4.5}$$

The radial electric field of the beam and the azimuthal magnetic field is written as

$$E_r = \begin{cases} \dfrac{q\lambda(z)}{2\pi\epsilon_0}\dfrac{r}{a^2} \\ \\ \dfrac{q\lambda(z)}{2\pi\epsilon_0}\dfrac{1}{r} \end{cases} \qquad B_\varphi = \begin{cases} \dfrac{\mu_0 q\lambda(z)\beta c}{2\pi}\dfrac{r}{a^2} & r \le a \\ \\ \dfrac{\mu_0 q\lambda(z)\beta c}{2\pi}\dfrac{1}{r} & r > a \end{cases},$$

with $\lambda(z) = h/R \cdot \lambda(\phi)$. If the bunch length ϕ_m much more larger than beam radius a then other field components can be neglected. Taking the integral (4.5) over the contour s (Fig.4.4) we obtain:

$$E_z dz + \frac{Nq}{2\pi\epsilon_0} g_0(\lambda(z+dz) - \lambda(z)) = -\frac{\mu_0 q\beta c}{2\pi}\frac{\partial\lambda(z)}{\partial t}dz,$$

where $g_0 = 0.5 + ln(a/b)$ is the geometrical factor. The time derivative of line density $\lambda(z)$ can be written as the derivative of the current $I(\phi)$ over ϕ as $\partial\lambda(z)/\partial t = -h/R \cdot \partial I(\phi)/\partial\phi$. The expression for the longitudinal electric field is:

$$E_z = -\frac{qg_0}{2\pi\epsilon_0\gamma^2}\frac{h}{\beta cR}\frac{\partial I(\phi)}{\partial\phi}. \tag{4.6}$$

On the other hand E_z can be defined as $E_z = -V_{sc}(\phi)/L$. Fourier series for the current $I(\phi)$ (Eq. 4.3) and for the voltage $V(\phi)$ (Eq. 4.4) can be used for the calculation of the space charge impedance. The obtained expression is written as [41]

$$Z_p^{sc} = p\frac{iZ_0 g_0}{2\gamma^2\beta},$$

where $Z_0 = 377$ Ohm is the impedance in the vacuum. The space charge impedance per harmonic is found as

$$\frac{Z_{sc}}{p} = \frac{iZ_0 g_0}{2\gamma^2\beta} = iX_s$$

with the space charge reactance X_s. The space charge voltage can be written as

$$V_{sc}(\phi) = -qh^2\beta c X_s \frac{N}{R}\frac{\partial\lambda(\phi)}{\partial\phi}. \tag{4.7}$$

The space charge voltage affects the stationary line density, as it will be shown in the following section.

4.2.3 Self-consistent line density with space charge

The space charge potential can be found by integrating Eq. (4.7) in the same way as for rf potential Eq. (3.16):

$$Y_{sc}(\phi) = qh^2\beta c X_s \frac{N}{RV_0}(\lambda_0 - \lambda(\phi)), \tag{4.8}$$

where $\lambda_0 = \lambda(\phi = 0)$ is the line density at the location of the synchronous particle. The single particle Hamiltonian is

$$H = \frac{\dot{\phi}^2}{2} + \omega_{s0}^2(Y_{rf}(\phi) + Y_{sc}(\phi)) \tag{4.9}$$

where $Y_{rf} + Y_{sc}$ is the total potential.

For a Gaussian distribution the matched line density is defined as

$$\lambda(\phi) = \lambda_0 e^{-\frac{Y_{rf}(\phi) + Y_{sc}(\lambda(\phi))}{\sigma^2}}.$$

This equation can be solved through a numerical iteration scheme.

For the elliptic distribution the line density with space charge is obtained as

$$\lambda(\phi) = \frac{1}{u_m}(Y_{rf}(\phi) - Y_{rf}(\phi_m)) \qquad u_m = 2\int_0^{\phi_m}(Y_{rf}(\phi_m) - Y_{rf}(\phi))d\phi$$

where the bunch half-length ϕ_m can be obtained from Eq. (4.9). For the elliptic distribution the space charge potential (4.8) is directly proportional to the rf potential. The total potential then can be written in the form

$$Y(\phi) = Y_{rf}(\phi)(1 - \frac{V_{s0}}{V_0}),$$

where V_{s0} is the amplitude of the space charge voltage obtained as

$$V_{s0} = sgn(m^*)q\beta_0 cRX_s\frac{N}{u_m}.$$

At the limiting intensity when $V_{s0} = V_0$ the space charge field cancels the external rf field. Below this intensity the matched voltage amplitude for the bunch with half-length ϕ_m and with maximum momentum spread $\delta_m = \dot{\phi}_m R/(h\eta\beta)$, can be obtained as [38]

$$\omega_{s0}^2 = -(1+\Sigma)\frac{\dot{\phi}_m^2 R^2}{2h^2 Y_{rf}(\phi_m)},$$

where Σ is the so-called space charge parameter:

$$\Sigma = -\frac{q^2 h X_s \lambda_0}{\pi R m \beta c \eta \delta_m} \tag{4.10}$$

with the maximum value of line density λ_0

The increase of the space charge parameter has no influence on the line density obtained from the elliptic distribution but it has an influence on the synchrotron frequency in the bunch.

For a given space parameter the rms equivalent Gaussian distribution can be obtained. In Fig. 4.5 it can be seen that for large space charge parameters the line density obtained from a Gaussian distribution converges with the line density obtained from the elliptic distribution (Fig. 3.4). This is one of the reasons why parabolic bunch forms are used for space charge dominated beams [35, 42]. For the Gaussian distribution and for the elliptic distribution the space charge impedance affects the synchrotron frequency. This is described in detail in the next section.

4.2.4 Synchrotron frequency and Landau damping

After the calculation of the self-consistent line density for a given space charge parameter Σ the form of the space charge potential is known. The synchrotron frequency as a function of the particle oscillation amplitude can be calculated using a total potential. The obtained synchrotron frequency will be different from the synchrotron frequency in the absence of space charge Eq. (3.25).

For the elliptic bunch distribution with space charge the total potential can be written as

$$Y = \frac{Y_{rf}}{(1+\Sigma)}.$$

Taking Eq. (3.22) and using the total potential instead of the rf potential the synchrotron frequency is obtained as

$$\frac{\omega_s(\hat{\phi})}{\omega_{s0}} = \frac{1}{\sqrt{1+\Sigma}}(1-\frac{\hat{\phi}^2}{16}),$$

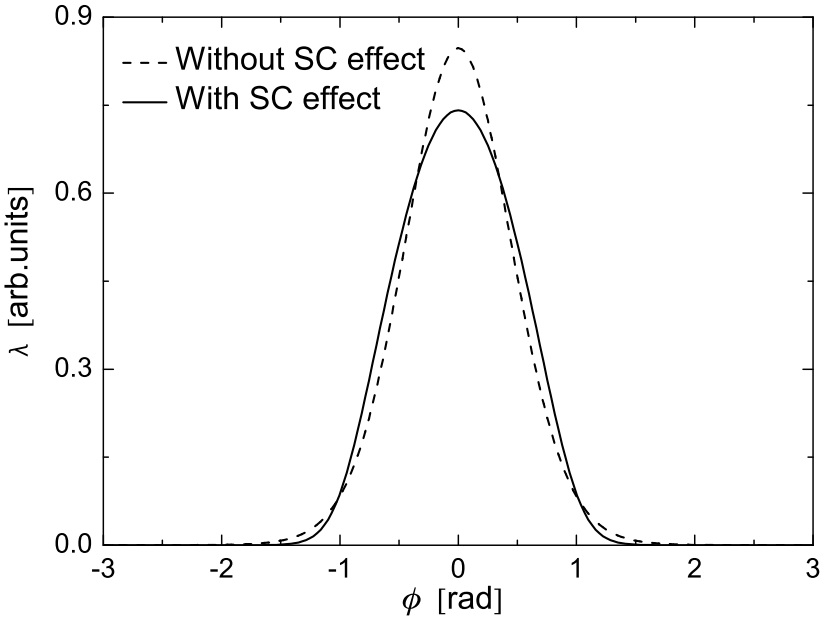

Figure 4.5: Gaussian self-consistent line density distribution with space charge obtained for $\phi_m = 60^0$ and $\Sigma = 1$.

or, in the case of low intensity when $\Sigma << 1$,

$$\frac{\omega_s(\hat{\phi})}{\omega_{s0}} \approx 1 - \frac{\hat{\phi}^2}{16} - \frac{\Sigma}{2}. \tag{4.11}$$

The frequency shift due to space charge is

$$\frac{\triangle\omega}{\omega_{s0}} = -\Sigma/2 \tag{4.12}$$

is called linear synchrotron frequency shift. This shift does not depend on the amplitude ϕ.

For a Gaussian distribution with space charge the exact synchrotron frequency can be calculated only numerically. An approximate analytical solution can be found for short bunches and low intensity ($\Sigma << 1$) as in [43]. The solution can be written as

$$\frac{\omega_s(\hat{\phi})}{\omega_{s0}} = 1 - \frac{3}{2}\Sigma\left(1 - \frac{3\hat{\phi}^2}{8\sigma^2}\right) - \frac{\hat{\phi}^2}{16}, \tag{4.13}$$

where it can be seen that the frequency shift due to space charge depends on the oscillation amplitude and is called non-linear synchrotron frequency shift.

In Fig.4.6 the exact synchrotron frequencies with linear and non-linear shifts are presented. The coherent frequency Ω_c is plotted as well. Without space charge the coherent frequency lies inside the synchrotron frequency band:

$$\omega_s(0) < \Omega_c < \omega_s(\phi_m).$$

This provides the Landau damping for bunches [44]. Landau damping suppresses the bunch oscillations and can be defined as inability of an harmonic force to excite an ensemble of oscillators because of the spread in frequencies among the oscillators [45].

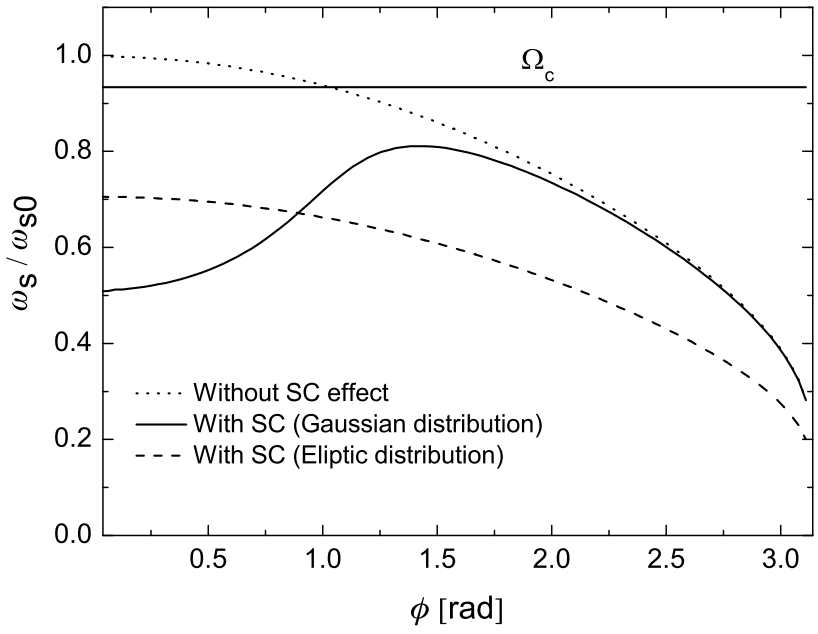

Figure 4.6: Synchrotron frequency as a function of the particle amplitude $\hat{\phi}$ for the cases without ($\Sigma = 0$) and with ($\Sigma = 1$) space charge effect. The results are obtained for the bunch half-length length $\phi_m = 60^0$.

Space charge shifts the synchrotron frequency downwards and with space charge parameter $\Sigma = 1$ the coherent frequency Ω_c is above the synchrotron frequency band. If the coherent frequency Ω_c is outside the range of synchrotron frequencies then Landau damping is lost [38, 36]. The condition for loss of Landau damping can be easily defined for elliptic distribution as

$$\Omega_c > \omega_s(0).$$

For short bunches the coherent frequency simplifies to

$$\frac{\Omega_c}{\omega_{s0}} = \sqrt{1 - \frac{\phi_m^2}{10}}. \tag{4.14}$$

Using Eq. (4.11) the threshold space charge parameter is obtained as

$$\Sigma_{th} \approx \frac{\phi_m^2}{10}. \tag{4.15}$$

Thus for a bunch with half-bunch length of 60^0 the threshold parameter is calculated as $\Sigma_{th} = 0.1$.

For a Gaussian distribution the threshold parameter is obtained numerically. For an rms equivalent bunch with half-bunch length of 60^0 the threshold parameter is obtained as $\Sigma_{th} \approx 0.04$ that is less than in the case of the elliptic distribution. Thus for loss of Landau damping it is enough that the condition (4.15) is fulfilled.

When Landau damping is lost undamped longitudinal dipole oscillations occur. These oscillations are driven by an effective dipole impedance which will be described in the next section. An effective impedance produces a non-zero imaginary part of the coherent frequency which leads to an exponential grow of coherent oscillations.

4.3 Effective dipole impedance

When the bunch performs dipole oscillations the current spectrum will be modified. In this case in addition to the main harmonics sidebands induced by the dipole motion appear. The impedances that has an effect on the dipole motion can be written in a form of the so-called effective dipole impedance. This impedance induces a coherent frequency shift and may lead to unstable dipole oscillations.

4.3.1 Spectrum of an oscillating bunch

Consider a bunch that executes dipole oscillations with frequency Ω_c. Since the bunch oscillates rigidly the current $I(\phi)$ is transformed to $I(\phi - \bar{\phi})$, where $\bar{\phi}$ is the coordinate of the bunch center. For small $\bar{\phi}$ the Taylor expansion can be used:

$$I(\phi - \bar{\phi}) = I(\phi) - I'(\phi)\bar{\phi}$$

with $\bar{\phi}$ being described with harmonic law $\bar{\phi} = \hat{\bar{\phi}}\cos(\nu\phi)$, where $\nu = \Omega_c/\omega_0$ is the coherent frequency tune. The current can be represented again in Fourier series as

$$I(\phi - \bar{\phi}) = \sum_{p=-\infty}^{\infty} I_p e^{ip\phi} + \frac{\bar{\phi}}{2}\Big(\sum_{p=-\infty}^{\infty} ipI_p(e^{i(p-\nu)\phi} + e^{i(p+\nu)\phi})\Big).$$

In comparison with the current $I(\phi)$ for a stationary bunch Eq. (4.3) the second term is added. The second term appears due to dipole oscillations. Thus, the total current spectrum consists of the spectrum of the main harmonics I_p plus the satellites $I'_p = pI_p$. The total spectrum is shown in Fig. 4.7.

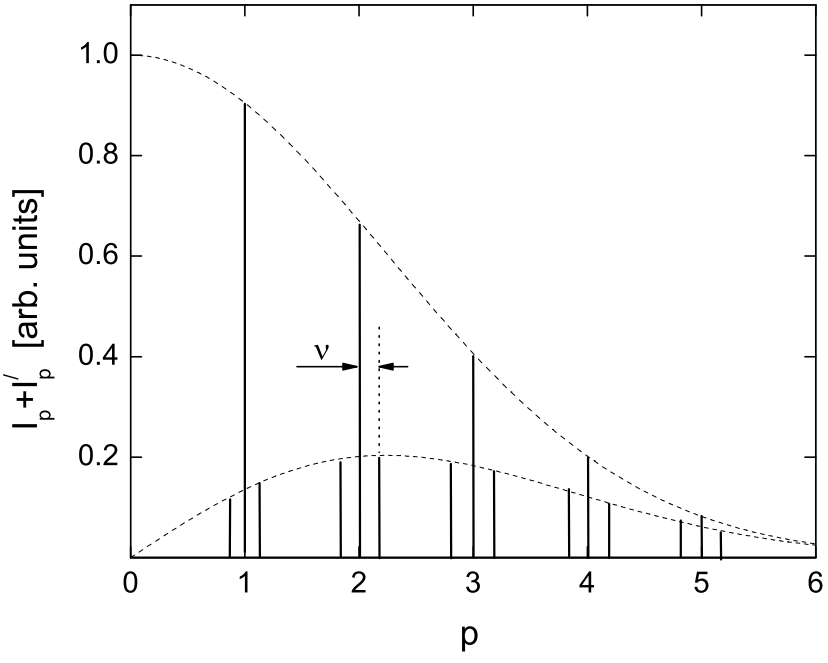

Figure 4.7: Spectrum of an oscillating bunch as the spectrum of a stationary bunch plus the spectrum of dipole oscillations.

4.3.2 Coherent frequency shift

The average voltage seen by the particles in the bunch is determined as electric energy averaged over one turn in a synchrotron divided by the average charge:

$$<V>= \frac{1}{2\pi I_0}\int_{-\pi}^{\pi} I(\phi)V(\phi)d\phi.$$

After rather lengthly calculations (see Appendix A) the average voltage is obtained as

$$<V>= \frac{V_0}{\omega_{s0}}(\Omega_c Z_I \cdot \bar{\phi} + Z_R \cdot \dot{\bar{\phi}}), \tag{4.16}$$

where $Z_r + iZ_i = Z$ are the real ind imaginary parts of the effective dipole impedance. The variables $\bar{\phi}$ and $\dot{\bar{\phi}}$ represent the phase and the phase velocity of the bunch in the frame connected with the synchronous particle.

The synchrotron equation of motion including the effective dipole impedance is written as

$$\ddot{\bar{\phi}} + \omega_{s0}^2 \sin\phi = -\omega_{s0}\Omega_c Z_I \cdot \bar{\phi} + \omega_{s0} Z_R \cdot \dot{\bar{\phi}}.$$

In the case of the linear approximation $\sin\phi \approx \phi$ the equation simplifies to

$$\ddot{\bar{\phi}} + \omega_{s0}^2\phi = -\omega_{s0}\Omega_c Z_I \cdot \bar{\phi} + \omega_{s0} Z_R \cdot \dot{\bar{\phi}}.$$

Looking for solutions $\bar{\phi} = \hat{\bar{\phi}} e^{i\Omega t}$ we obtain the next expressions:

$$\Omega - \omega_{s0} = \triangle\Omega \qquad \triangle\Omega = \frac{i\omega_{s0}}{2} Z, \tag{4.17}$$

where $\triangle\Omega$ is the coherent frequency shift. Thus in the linear approximation the coherent frequency Ω depends linearly on the coherent frequency shift:

$$\Omega = \Omega_R + i\Omega_I = (\omega_{s0} - \triangle\Omega_R) - i\triangle\Omega_I. \tag{4.18}$$

When nonlinear terms in the sinus expansion are taken into account $\sin\phi = \phi - \phi^3/3$, the connection of the coherent frequency with the coherent frequency shift is provided by the dispersion relation [46]:

$$1 = -\pi\triangle\Omega \int_{-\infty}^{\infty} \frac{f'(\hat{\phi})\hat{\phi}^2 d\hat{\phi}}{\Omega - \omega_s(\hat{\phi})}, \tag{4.19}$$

where the bunch distribution function $f(\hat{\phi})$ is written in dependence on the particle amplitude $\hat{\phi}$. For a given coherent frequency shift $\triangle\Omega$ the value of Ω can be obtained. The imaginary part of the coherent frequency Ω_I determines the exponential growth or damping rate depending on the sign of the Ω_I. The dependence of Ω_I on $\triangle\Omega$ can be plotted with the help of the stability diagram (Fig. 4.8). To plot the stability diagram the real and imaginary parts of $\triangle\Omega$ divided by the frequency spread S are used as axes and the obtained curves for constant Ω_I are plotted. The rms synchrotron frequency spread is determined as $S = \omega_{s0}\sigma^2/16$. The stability boundary is the border between the stable area ($\Omega_I \leq 0$) and the unstable area ($\Omega_I > 0$). Value of $\triangle\Omega$ allows us to find in which region the "working point" lies. This value is provided by the effective dipole impedance according to Eq. (4.17). The effective dipole impedance can be measured in an experiment. In Chapter 7 the value of the effective dipole impedance will be obtained from BTFM in the SIS.

The next question is related to the space charge influence on the stability boundary. Taking the coherent frequency shift $\triangle\Omega$ due to the effective dipole impedance as coherent force and the incoherent frequency shift $\triangle\omega$ due to space charge as incoherent force the synchrotron equation of motion can be written as [47]

$$\ddot{\bar{\phi}} + (\omega_{s0}^2 - 2\omega_{s0}\triangle\omega)\phi = 2\omega_{s0}(\triangle\Omega - \triangle\omega)\bar{\phi}. \tag{4.20}$$

The resulting dispersion relation is obtained as

$$1 = -\pi \int_{-\infty}^{\infty} (\triangle\Omega - \triangle\omega) \frac{f'(\hat{\phi})\hat{\phi}^2 d\hat{\phi}}{\Omega - \omega_s(\hat{\phi})}. \tag{4.21}$$

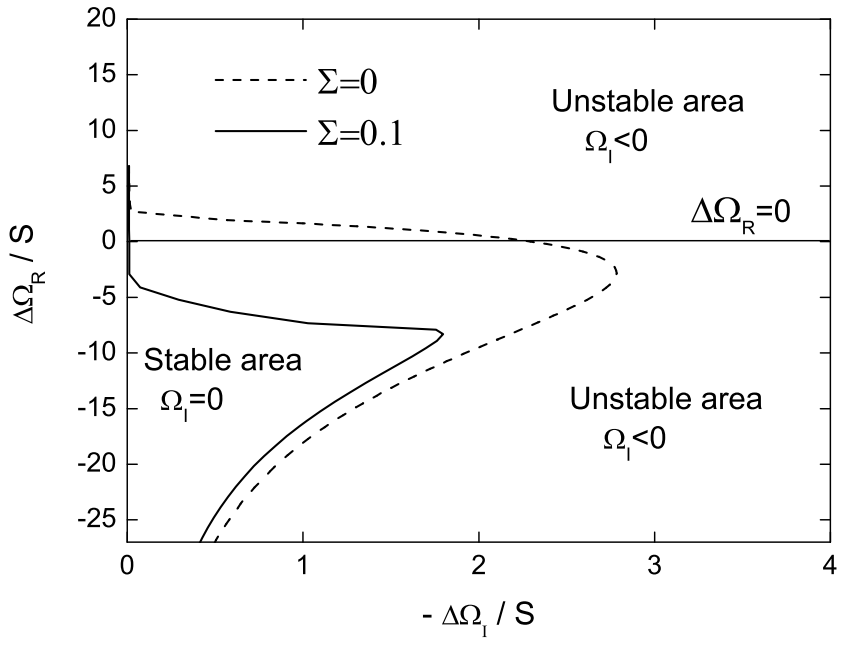

Figure 4.8: Stability boundary for a Gaussian distribution as a function of the normalized coherent frequency shift for different space charge parameters. The rms equivalent bunch half-length is 60^0.

In Fig. 4.8 the resulting stability boundaries are plotted for different space charge parameters. The stability boundary is shifted by space charge below the $\triangle\Omega_R = 0$ line. In this case, for any $\triangle\Omega_I > 0$ the unstable dipole oscillations occurs. If $\triangle\Omega$ is obtained from the measured effective impedance the instability growth rate Ω_I can be calculated from dispersion relation (4.21). In Chapter 7 the threshold intensity of unstable dipole oscillations in the SIS will be obtained.

Chapter 5

Longitudinal Beam Transfer Function (BTF)

In the presence of the permanent rf phase modulation the bunch oscillates. If the modulation frequency is close to the bunch coherent frequency than the amplitude of dipole oscillations will be much higher then the modulation amplitude. The longitudinal bunched BTF is defined as the amplitude and the phase of dipole oscillations related to the rf phase modulation amplitude and phase.

If space charge parameter equals zero Landau damping is present. The BTF in this case is well-known and was approved in experiments [11]. The BTF will be calculated for non-zero space charge parameters.

At high space charge parameters Landau damping is lost. A damping can be provided by the electron cooling. The BTF for this case will be derived from a driven cold oscillator model. The effective dipole impedance will be added in the BTF.

5.1 rf phase modulation

The equation of motion in a rf bucket with rf phase modulation is obtained in the following. The rf voltage with phase modulation is written as

$$V_{rf}(\phi, t) = V_0 \sin(\phi + \triangle\phi(t)),$$

where $\triangle\phi(t)$ is the rf phase modulation. We are interested in a harmonic modulation that can be represented as $\triangle\phi(t) = \hat{\phi}_m \sin(\omega_m t)$ with $\hat{\phi}_m$ and ω_m as amplitude and frequency of phase modulation.

The equation of motion with rf phase modulation is written as

$$\ddot{\phi} + \omega_{s0}^2 \sin(\phi - \hat{\phi}_m \sin(\omega_m t)) = 0.$$

Assuming a short bunch, after linearization of the second term the equation of motion can be written as

$$\ddot{\phi} + \omega_{s0}^2 \phi = \omega_{s0}^2 \hat{\phi}_m \sin(\omega_m t),$$

where the term on right-hand side is the same for all particles. Thus the rf phase modulation acts coherently on all particles and it induces only dipole oscillation of a bunch. A picture of the bunch oscillations induced by the rf phase modulation is shown in Fig. 5.1.

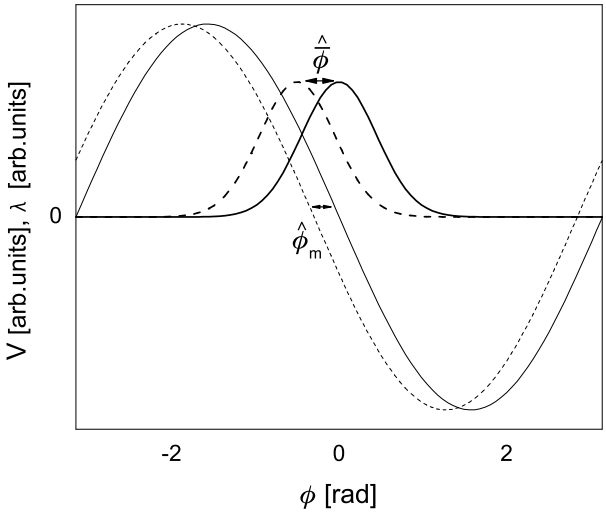

Figure 5.1: Mechanism of rf phase modulation. In the reference frame of the synchronous particle dipole oscillations of the rf wave form are observed. The amplitude of the rf phase oscillations is $\hat{\phi}_m$. As a result, a bunch oscillates with the amplitude $\hat{\hat{\phi}}$.

In measurements or in simulations three different types of rf phase modulation can be used to evaluate BTF: fixed frequency, frequency sweep, white noise. The simplest method is to excite the beam with a fixed frequency ω_m^i according to the formula

$$\phi_{mod} = \hat{\phi} \sin \omega_m^i t. \tag{5.1}$$

In this case only one value BTF^i can be measured in one measurement:

$$BTF^i = \frac{\hat{\hat{\phi}}}{\hat{\phi}}.$$

By changing the frequency from measurement to measurement by the value of $\triangle\omega_m$ a discrete BTF values is measured that can be compared with theory. In this case the resolution of BTFM is determined by the number of measurements.

The measurement time can be decreased if a frequency sweep is used. The form of the excitation is the same as in the first method, but the modulation frequency ω_m is linearly ramped with time t:

$$\omega_m(t) = \omega_m^{st} + \frac{\omega_m^{fin} - \omega_m^{st}}{t_{sw}} t,$$

where ω_m^{st} and ω_m^{fin} are the initial and the final values of the modulation frequency that determine the bandwidth of the measurements. t_{sw} is the sweep time during which the frequency change occurs. Thus the BTF is measured during one cycle.

Another method to measure the BTF is via white noise rf phase modulation. The phase modulation signal in this case is

$$\phi_{mod} = \hat{\phi}_m \sum_{k=1}^{n} \sin(\omega_m^k t + \phi_k). \tag{5.2}$$

The frequencies ω_k^m are uniformly distributed around the synchrotron frequency. The phases ϕ_k are uniformly distributed. The number of frequencies and phases are given by n. The BTF with white noise rf phase modulation is determined as:

$$BTF = \frac{FFT[\bar{\phi}]}{FFT[\phi_{mod}]}, \tag{5.3}$$

where FFT is the fast Fourier transform of the signal. The resolution in this case is determined by the modulation time.

In the next Chapters the application of these methods to BTF simulations and experiments is shown.

5.2 BTF of a bunch with electron cooling

If the space charge parameter exceeds a threshold value Landau damping is lost and the only damping mechanism is provided by electron cooling. In this case the bunch can be treated like a single particle and the BTF is described by a simple oscillator with damping factor. The effective impedance can be easily calculated using BTFM.

5.2.1 Physics of electron cooling

The concept of electron cooling was developed by Budker in 1967 [48] in Institute for Nuclear Physics in Novosibirsk and proved experimentally [49]. Electron cooling is used for the reduction of the area in phase space occupied by the ions. The co-moving electrons reduce the ion momentum spread. The effect of electron cooling in the longitudinal direction can be explained as follows. In the cooler section the ion beam is overlapped with a co-moving electron beam. The electron beam flows in the same direction as ion beam with the energy matched to the synchronous one. If the ion has an energy which deviates from the synchronous then this ion will counteracts with the electrons. If the ion energy less or larger than synchronous then this ion will gain or lose energy due to interaction with electrons until the ion energy will be equal to the synchronous one. Thus during synchrotron oscillation the ion experiences many collisions with electrons and the kinetic energy of synchrotron oscillation is decreased. The electrons act as a friction force for the ions. This force is linear with respect to the ion phase velocity at low values of this phase

velocity. Thus the cooling force on an individual ion can be represented by a damping factor or cooling rate [50]:

$$\frac{F_{cool}}{m}\frac{h}{R} = -\gamma_c \dot{\phi},$$

with the damping factor γ_c and the particle phase velocity$\dot{\phi}$. The effective cooling force on a bunch is written as

$$\frac{F_{cool}}{m}\frac{h}{R} = -\gamma_c \dot{\bar{\phi}},$$

where $\dot{\bar{\phi}}$ is the bunch phase velocity.

5.2.2 Model of a simple oscillator with damping factor

Here we assume, that electron cooling is the only damping mechanism. The bunch can be treated as a simple oscillator with a resonance frequency equal to Ω_c. The equation of a simple oscillator including a damping term and an external force is written as

$$\ddot{\bar{\phi}} + 2\gamma_c \dot{\bar{\phi}} + \Omega_c^2 \bar{\phi} = \omega_{s0}^2 \hat{\phi}_m e^{i\omega_m t}, \tag{5.4}$$

where $\hat{\phi}_m$ is the amplitude of the periodic force, ω_m is the modulation frequency of the force, $\bar{\phi}$ is the longitudinal coordinate of the bunch center with respect to the bucket center, Ω_c is the coherent frequency and γ_c is the damping decrement that characterizes the effect of electron cooling. After comparably long time $t >> 1/\gamma_c$ the solution for $\bar{\phi}$ is obtained as [33]

$$\bar{\phi} = \frac{\omega_{s0}^2 \hat{\phi}_m}{\Omega_c^2 - \omega_m^2 + i2\gamma_c\omega_m} e^{i\omega_m t} = \hat{\bar{\phi}} e^{i\omega_m t}.$$

The BTF in this case is equal to the relation of the response $\hat{\bar{\phi}}$ to the amplitude of the modulation force $\hat{\phi}_m$. Assuming $\Omega_c = \omega_{s0}$ for short bunches the expression for the BTF is written as

$$BTF = \frac{\Omega_c^2}{\Omega_c^2 - \omega_m^2 + i2\gamma_c\omega_m}. \tag{5.5}$$

Usually BTFM are performed with a modulation frequency being close to the coherent frequency and the BTF expression simplifies to

$$BTF = \frac{1}{2}\frac{\Omega_c}{\Omega_c - \omega_m + i\gamma_c}. \tag{5.6}$$

Thus the BTF is a complex number. The quantities that can be measured during an experiment are the BTF amplitude A_{BTF} and phase θ_{BTF}. The BTF amplitude corresponds to absolute value and BTF phase corresponds to the argument of the complex BTF. The BTF amplitude and phase obtained from Eq. (5.6) are shown in Fig. 5.2.

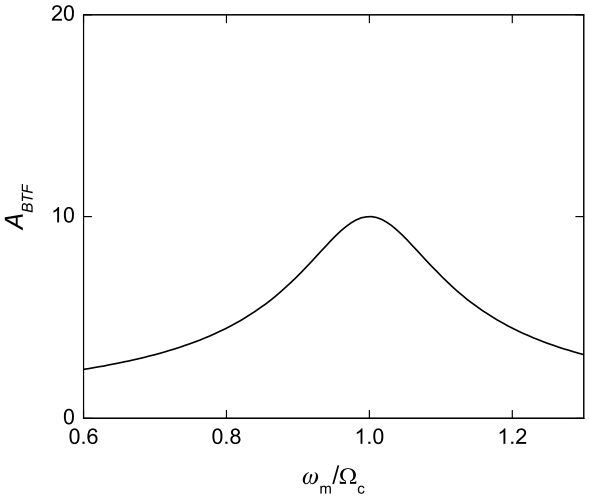

a)

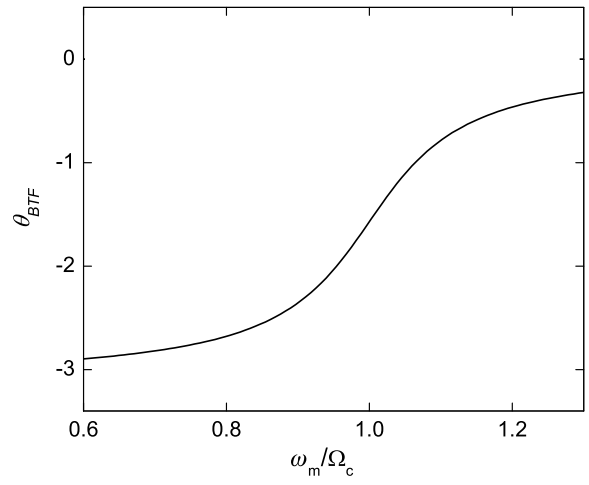

b)

Figure 5.2: BTF amplitude and BTF phase as function of modulation frequency ω_m. Calculated from Eq. (5.6).

5.2.3 Influence of the effective dipole impedance on the BTF

The equation of bunch center motion in the presence of electron cooling and the effective dipole impedance is written as

$$\ddot{\bar{\phi}} + \Omega_c^2 \bar{\phi} + 2\gamma_c \dot{\bar{\phi}} = -\omega_{s0}\Omega_c Z_I \bar{\phi} + \omega_{s0} Z_R \dot{\bar{\phi}} + \omega_{s0}^2 \hat{\phi}_m e^{i\omega_m t}. \tag{5.7}$$

Under assumption $\omega_{s0} = \Omega_c$, Eq. (5.7) can be re-written as

$$\ddot{\bar{\phi}} + 2(\gamma_c - \frac{\Omega_c Z_R}{2})\dot{\bar{\phi}} + \Omega_c^2(1 + \frac{Z_I}{2})^2\bar{\phi} = \omega_{s0}^2\hat{\phi}_m e^{i\omega_m t} \tag{5.8}$$

that is similar to Eq. (5.4). Thus the BTF_Z with the effective dipole impedance is similar to the BTF without effective dipole impedance in Eq. (5.6):

$$BTF_Z = \frac{1}{2}\frac{\Omega_c}{\Omega_c^Z - \omega_m + i\gamma_c^Z}, \tag{5.9}$$

where

$$\Omega_c^Z = \Omega_c(1 + \frac{Z_I}{2}), \qquad \gamma_c^Z = \gamma_c - \frac{\Omega_c Z_R}{2}. \tag{5.10}$$

Thus the effective impedance can be obtained from BTFM using the equations:

$$Z_I = \frac{2}{\Omega_c}(\Omega_c^Z - \Omega_c) \qquad Z_R = \frac{2}{\Omega_c}(\gamma_c^Z - \gamma_c), \tag{5.11}$$

or in general form

$$Z = \frac{1}{BTF_Z} - \frac{1}{BTF}. \tag{5.12}$$

The BTF without effective dipole impedance can be measured at low beam intensities. At high beam intensities the BTFM will be affected by the effective dipole impedance. Performing the BTFM with different beam intensities the effective impedance $Z_R + iZ_R$ as intensity function can be obtained. The value of Ω_c is located at the point where the BTF amplitude has maximum. The damping factor can be found from the BTF amplitude maximum A_{BTF}^{max} as

$$\gamma_c = \Omega_c/(2A_{BTF}^{max}).$$

Thus only the positions and the values of the BTF amplitude maximum in measurements with different intensities are needed in order to obtain the effective dipole impedance.

5.3 BTF of a bunch with Landau damping

In the previous section we presented a simple BTF model ignoring Landau damping. If the electron cooling is off and space charge parameter equal to zero then the expression for the BTF is written as [10]

$$BTF = \frac{\pi\omega_{s0}}{2}\int_0^{+\infty}\frac{f'(\hat{\phi})\hat{\phi}^2 d\hat{\phi}}{\omega_m - \omega_s(\hat{\phi})}. \tag{5.13}$$

The resulting BTF amplitude and BTF phase are shown in Fig. 5.3. It can be seen that the BTF amplitude and BTF phase are not symmetric as in the previous case. But in the limit of very short bunches it can be shown that Eq. (5.13) transforms to Eq. (5.6).

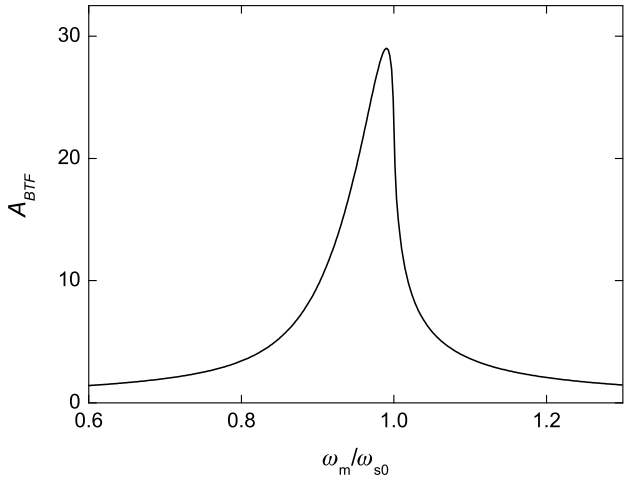

a)

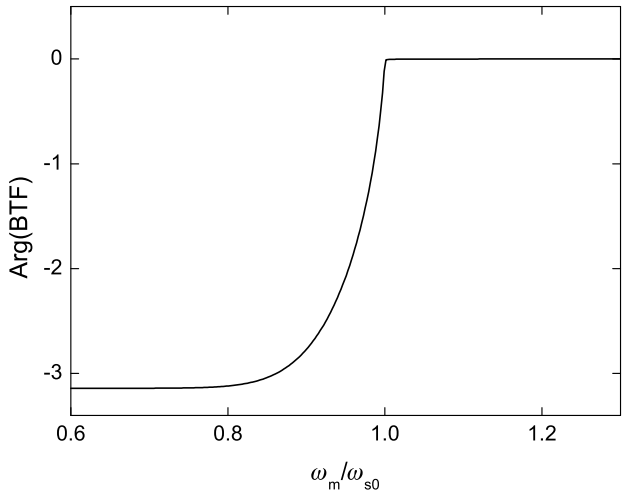

b)

Figure 5.3: BTF amplitude and BTF phase calculated from Eq. (5.13) for the bunch with a Gaussian distribution and bunch half-length 60^0.

If the space charge parameter is not zero than the BTF is obtain as (see Appendix B):

$$\frac{1}{BTF} = \frac{1}{BTF_0}\big(1 + \pi \int_0^\infty \triangle\omega_{sc}(\hat{\phi}) \frac{\psi'(\hat{\phi})^2 d\hat{\phi}}{\omega_m - \omega_s(\hat{\phi})}\big), \tag{5.14}$$

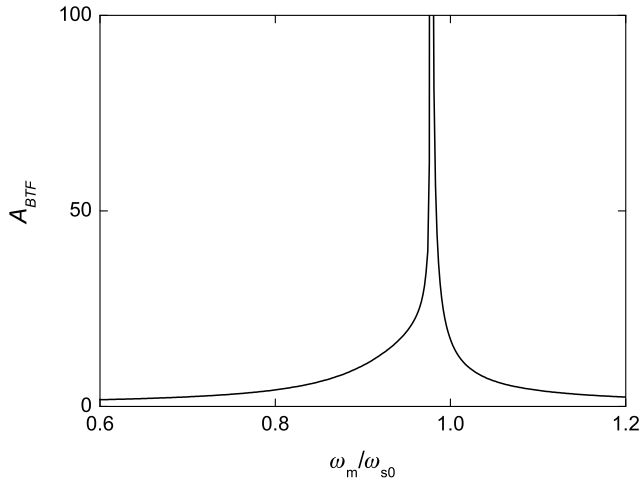

a)

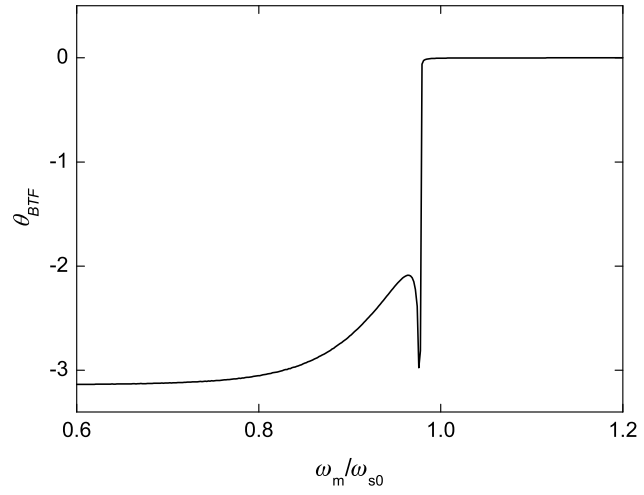

b)

Figure 5.4: BTF amplitude and BTF phase from Eq. (5.14) for the bunch with a Gaussian distribution with bunch half-length 60^0 and $\Sigma = 0.02$.

where $\triangle\omega_s(\hat{\phi})$ is synchrotron frequency shift induced by space charge from Eqs (4.12,4.13). In Fig. 5.4 it can be seen that already at very small space charge parameter the BTF curves are different from the case of BTF without space charge. Thus performing the BTFM at low intensities Σ can be obtained. Eq. (5.14) is the general expression for the bunched beam BTF with space charge. All previous cases can be extracted from this expression.

Chapter 6

BTF simulation studies

To verify the BTF models described in the previous chapter a longitudinal particle-in-cell simulation scheme [51, 52] has been developed. The scheme includes the rf fields as well as the space charge fields. In the simulation procedure the motion of all particles in bunch is taken into account. Regimes with different space charge parameters are investigated. Electron cooling and intra-beam scattering are included using Langevin forces [53]. It will be shown that when Landau damping is lost the bunch behaves as a simple oscillator with damping factor equal to the cooling rate. The BTF simulation results will be compared with the theoretical results from the previous Chapter.

6.1 The simulation scheme

PIC simulations are usually employed in studies related to plasma physics. In this method phase space is divided in small equivalent parts. Thus, the line density in a dedicated coordinate is determined by the number of particles inside the cell which corresponds to this coordinate. The simulation scheme is shown in Fig. 6.1. The simulation scheme is as follows:

- Calculation of the initial self consistent bunch distribution with space charge.
- Calculation of the space charge voltage.
- Advancing the macro-particles using the so-called "leapfrog" scheme.

The concept of macro-particles consists in reducing the number of simulated particles by increasing the charge of a simulation particle, while the total charge remains the same. The number of cells is chosen as $N_z = 256$ and the total number of macro-particles is $N_p = 10^6$. Parameters used in the code correspond to the real machine and beam parameters in the SIS-18. These parameters are: ring circumference of 216 m, harmonic number of 4, rf voltage of 10-20 kV depending on Σ, number of ions of $10^8 - 10^{10}$, typical bunch length of 60^0, type of ions U^{+73}. The beam energy is set to the SIS injection energy of 11.4 MeV/u.

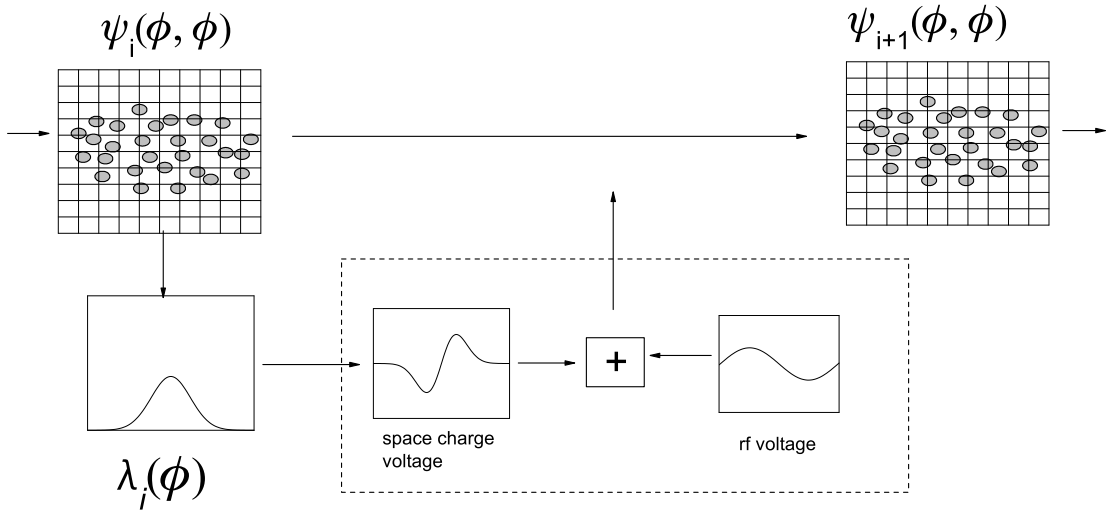

Figure 6.1: Simulation scheme.

The space charge voltage is calculated from the inverse FFT of the line density multiplied with the space charge impedance:

$$V_{sc} = Nq\beta c\frac{2\pi h}{L}FFT^{-1}\big(FFT(\lambda)\cdot iX_s\big). \tag{6.1}$$

As an option the possibility to perform rf phase modulation was added in the code. The rf voltage is written as

$$V_{rf} = V_0 \sin\big(\phi + \hat{\phi}_m PM\big), \tag{6.2}$$

where the form of phase modulation PM can be chosen from three possibilities: single frequency modulation, frequency sweep or white noise modulation. In the simulation results shown later white noise is used where

$$PM = \sum_{k=1}^{n} \sin(\omega_m^k t + \phi_k). \tag{6.3}$$

All simulation are performed with a Gaussian bunch distribution.

The particles are advanced in time using the so-called mapping equations:

$$\begin{cases} \phi_{i+1} = \phi_i + \dot{\phi}_i \triangle t \\ \\ \dot{\phi}_{i+1} = \dot{\phi}_i + \dfrac{\omega_{s0}^2}{V_0}\Big(V_{rf}(\phi_{i+1}) - V_{sc}(\phi_{i+1})\Big)\triangle t + \triangle\dot{\phi}_{i+1}^{cool} \end{cases}, \tag{6.4}$$

Number of simulated particles, N_{macro}	10^5
Number of grid points	256
Number of frequencies, n	$5 \cdot 10^5$
rf phase modulation amplitude, $\hat{\phi}_m$	0.01^0
Time step, $\triangle t$	$\frac{T_s}{100}$
Measurement time	$100 \cdot T_s$

Table 6.1: Simulation parameters.

where $\triangle\dot{\phi}_{i+1}^{cool}$ is a term which represent a simple model of electron cooling and intra-beam scattering:

$$\triangle\dot{\phi}_{i+1}^{cool} = \dot{\phi}_i \triangle t \gamma_c - \zeta\sqrt{2\gamma_c \triangle t}\dot{\phi}_{rms} \tag{6.5}$$

where ζ is random number from a Gaussian distribution. To calculate the position of the bunch center the positions of all particles in the bunch have to be summarized:

$$\bar{\phi} = \sum_{j=1}^{N_{macro}} \phi^j, \tag{6.6}$$

with N_{macro} as the number of macro-particles. The main simulation parameters are presented in Table 6.1

6.2 Comparison of simulation results with BTF models

In order to validate the numerical scheme the simulations were done for the case of the bunch without space charge. The simulations for a bunch with the half-length 60^0 was done. The simulations results are shown in Fig. 6.2. To compare these results with theory the BTF model of a bunch with Landau damping was chosen. This model is described by Eq. (5.13) presented in Chapter 5. As it can be seen from the Fig. 6.2 the simulation results agree well with the theoretical calculation.

Next simulations were done with an addition of space charge effects. The bunch half-length was chosen 60^0 as in the previous simulations. The space charge threshold parameter is obtained using Eq. (4.15). For the chosen bunch half-length 60^0 the threshold space

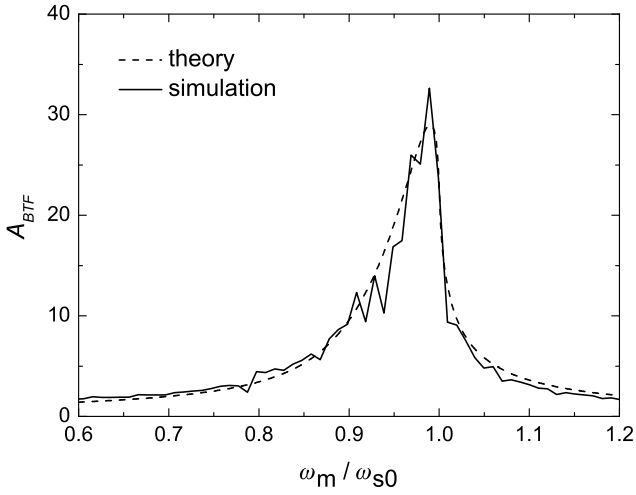

a)

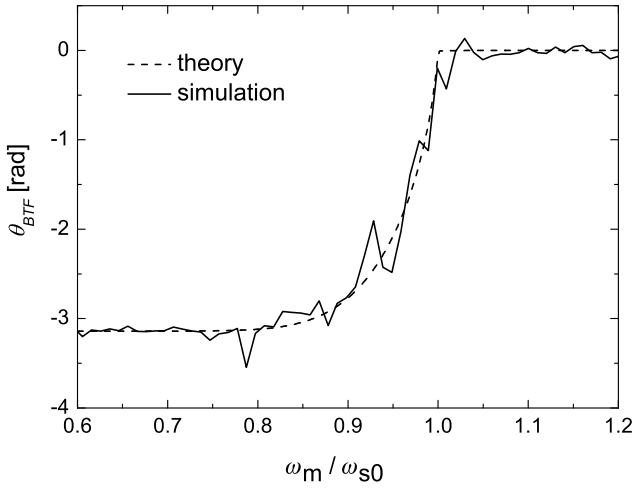

b)

Figure 6.2: Simulated BTF amplitude a) and phase b) as a function of the rf phase modulation frequency ω_m for a Gaussian bunch with $\phi_m = 60^0$ and $\Sigma = 0$. The simulation results are compared with Eq.5.14

charge parameter has a value of 0.1. Space charge parameter was chosen 0.02 that is much smaller than threshold one. In this case Landau damping is still present. The simulation results are shown in Fig. 6.3. Eq. (5.14) is chosen as theoretical BTF model in the present simulations. The simulation results with the space charge effect also give a very good

agreement with the theory.

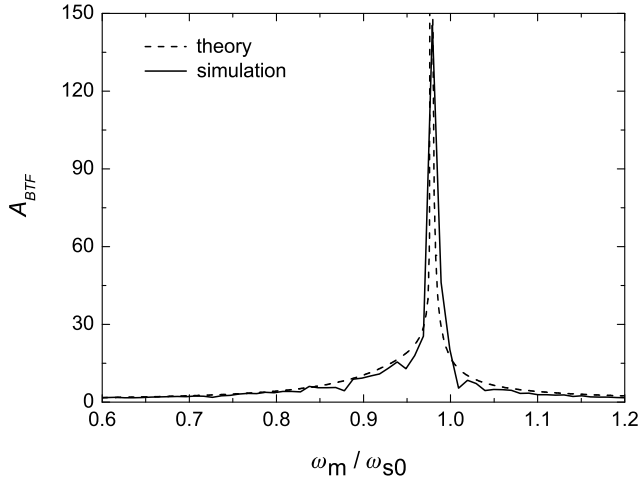

a)

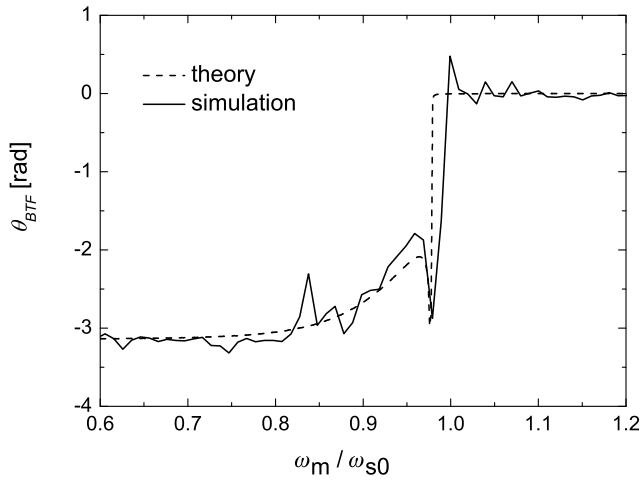

b)

Figure 6.3: Simulated BTF amplitude a) and phase b) as a function of the rf phase modulation frequency ω_m for a Gaussian bunch with $\phi_m = 60^0$ and $\Sigma = 0.02$. The simulation results are compared with Eq.5.14.

Next, we consider the electron cooled bunch. The bunch half-length was set to 60^0 and the cooling rate was set to $250s^{-1}$. The simulations were done for different values of the space charge parameter: space charge is equal zero, space charge parameter below the threshold value, space charge parameters above the threshold value. The simulation

results are presented in Fig. 6.4. The BTF model for these simulations is the model of a cold oscillator described by Eq. (5.6). The simulation results for the electron cooled bunch without space charge show that the maximum of the simulated BTF amplitude is lower than the theoretical one. This can be explained by the fact that for $\Sigma = 0$ not the only electron cooling is presented but Landau damping as well. In the simulation results for the electron cooled bunch with $\Sigma > 0$ it can be seen that as the space charge parameter exceeds the threshold one the maximum of the BTF amplitude approximates very well the theoretical value. This approves the model of a cold oscillator for the electron cooled bunches. It will be shown in the next Chapter that the model of a cold oscillator fits also

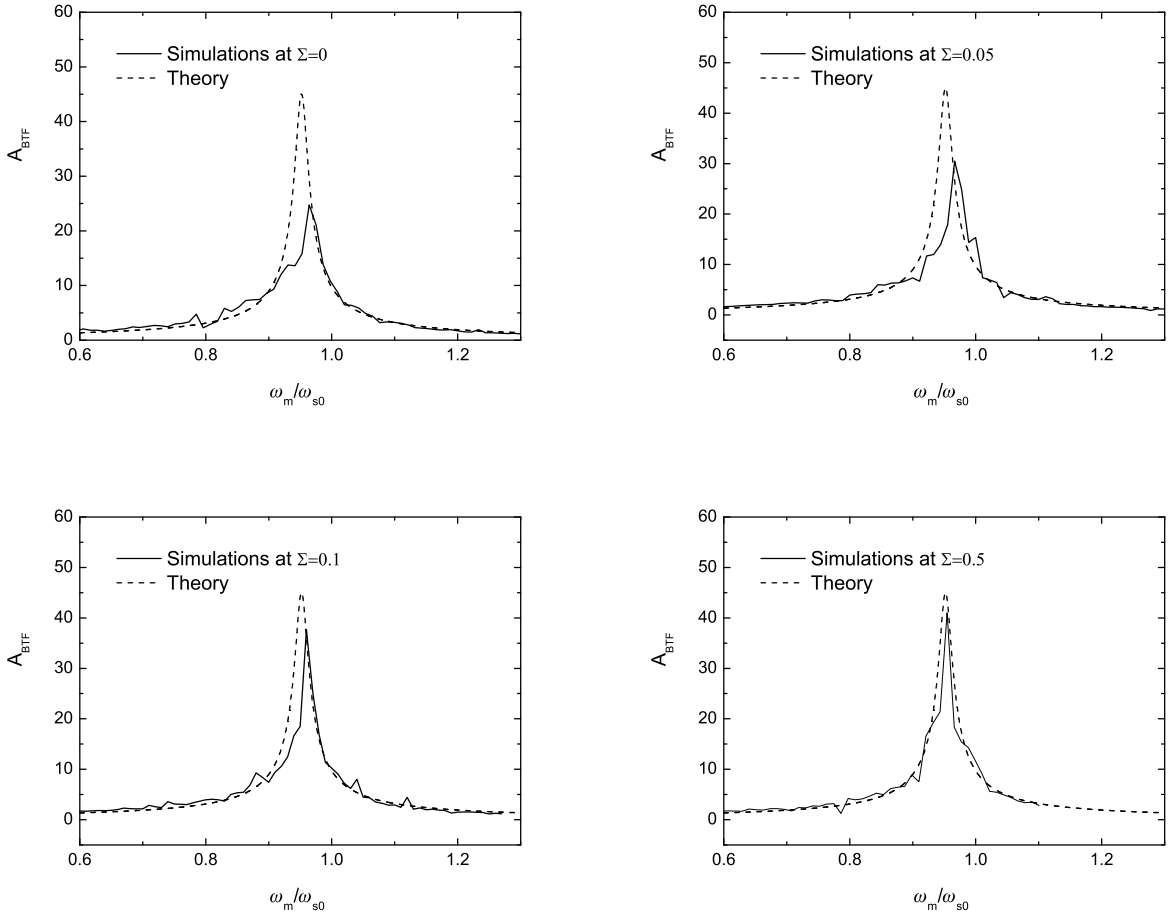

Figure 6.4: Simulated BTF amplitude as a function of the rf phase modulation frequency ω_m for a Gaussian bunch with $\phi_m = 60^0$ for different space charge parameters Σ. The simulation results are compared with the model (5.6) of a simple oscillator with damping factor which is in the present result was set to $250s^{-1}$.

to the BTFM in the SIS with electron cooled beams.

Chapter 7

Beam Transfer Function Measurements (BTFM) in the SIS

In the previous Chapter the theoretical BTF models have been checked by simulations. In this Chapter the results of the BTFM in the SIS are presented.

During the machine experiments in the SIS, it is difficult to set the required space charge parameter. Thus the BTFM were done only for two limiting cases:

- At high beam intensity and in the presence of the electron cooling. Electron cooling reduces the momentum spread in a bunch. As a result, the space charge parameter exceeds the threshold values.

- At low beam intensities and applying the rf adiabatic capture. The space charge parameter is close to zero.

Accordingly, for interpretation of the BTFM a cold oscillator model with damping factor and the BTF model of Landau damped bunch were used.

In order to work under clean conditions the excitation has been applied only during the injection plateau after the bunch was captured in the bucket and not during the capture. The rf phase modulations result from the de-tuning of the cavity. In order to measure the bunch profile the Beam Position Monitors (BPM) were used. Spectrum vector analyzer and Digital Signal Processors (DSP) system were used to obtain the longitudinal bunch offset.

7.1 rf phase modulation via cavity de-tuning

The rf phase modulation results from changing of the position of the ferrite loaded cavity resonant frequency. As it was discussed in Chapter 2 the resonant frequency depends on the bias current. The argument of rf cavity impedance at a fixed frequency depends on the bias current as well. In the Fig. 7.1 the arguments of the rf cavity impedance are shown

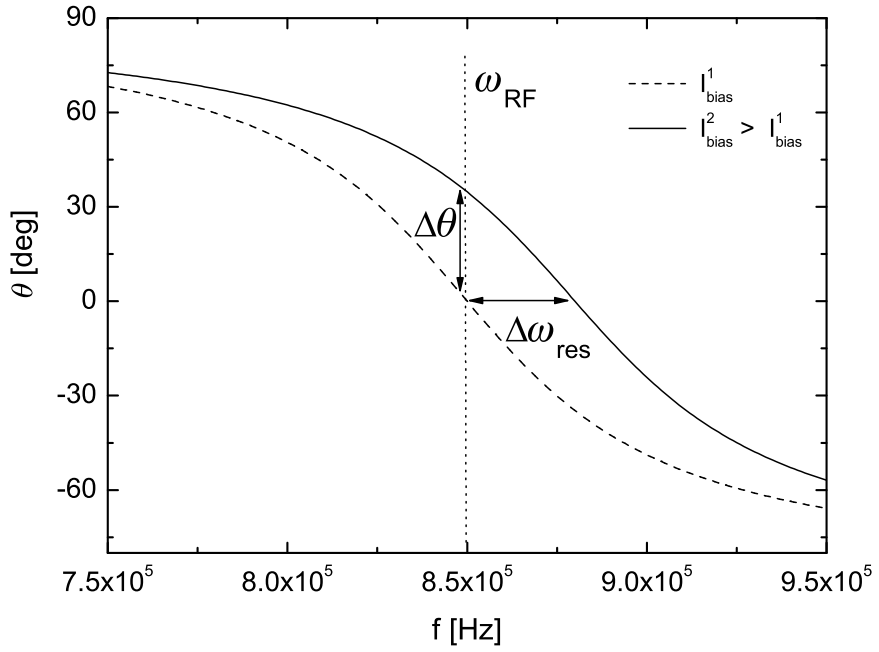

Figure 7.1: Principle of the cavity de-tuning mechanism: shift of the cavity resonant frequency induces shift of the cavity impedance phase. For small deviations the shift of impedance phase $\triangle\theta$ is directly proportional to the shift of resonant frequency $\triangle\omega_{res}$.

for two different bias currents I^1_{bias} and I^2_{bias}. The resonant frequency deviation $\triangle\omega_{res}$ and the impedance argument deviation $\triangle\theta_Z$ are defined as

$$\triangle\omega_{res} = \omega_{res}(I^2_{bias}) - \omega_{res}(I^1_{bias}), \tag{7.1}$$

$$\triangle\theta_Z = Arg(Z(I^2_{bias}, \omega_{rf})) - Arg(Z(I^1_{bias}, \omega_{rf})). \tag{7.2}$$

For a small $\triangle\omega_{res}$ the cavity impedance argument deviation $\triangle\theta_Z$ is proportional to $\triangle\omega_{res}$. As it was shown in Chapter 2, the phase of the rf signal ϕ_{mod} is equal to the $\triangle\theta$.

The schematic picture of the phase and frequency control in the SIS rf cavity is shown in Fig. 7.2. The rf signal V_a from a sweep generator goes to the the power amplifier which loads the generator current I_g to the cavity. The sweep generator also delivers the rf signal to the frequency-to-voltage converter which is used for setting the bias current I_{bias} value in order to control the resonant frequency of the cavity. For precise control the phase difference between the grid of the power amplifier V_a and the gap I_g has to be set to 180^0. The signal from the phase detector is used to correct the reference signal of the frequency-to-voltage converter. As it was discussed earlier, if the resonant frequency is shifted the rf voltage phase is shifted too. An additional voltage V_ϕ from the waveform

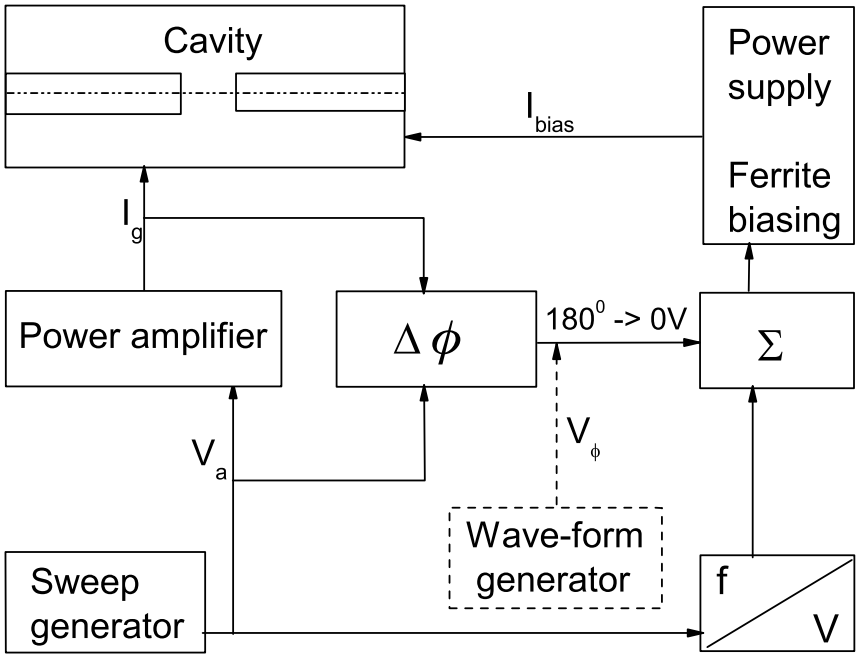

Figure 7.2: Scheme of the rf signal phase control in the SIS.

generator results in changing of the bias current and the rf phase as well. In the BTF experiments the waveform generator was used to create a harmonic signal V_ϕ for the rf phase modulation.

7.2 Longitudinal beam diagnostics in the SIS

The longitudinal bunch shape of a beam is usually determined by metallic plates. The idea is to measure on an insulated metal plate the charges induced by the electric field of the beam. The induced charges are sensed by a high impedance as a voltage on the capacity between the electrode and the surrounding vacuum chamber. The installation that consists of four plates is called a pick-up or Beam Position Monitor. In its simplest form it resembles a diagonally cut shoe-box, as it shown in Fig. 7.2. The frequency range of the SIS pick-ups is 0.2-100 MHz that allows to observe high harmonics of bunch frequency. As the beam passes by, it will induce electric charges on the metallic electrodes, more on the one which is closer, less on the other one, but their sum V_1+V_2 remaining constant, independent of the transverse beam position. The sum of the electric charges or the sum of the measured voltages from each plate depends only on the beam current. A system that consist of pick-up equipped with electronics for the measurements of the sum or difference

signal is called a Beam Position Monitors (BPM) system. The BPM sum signal can be picked up in the main control room for further analysis.

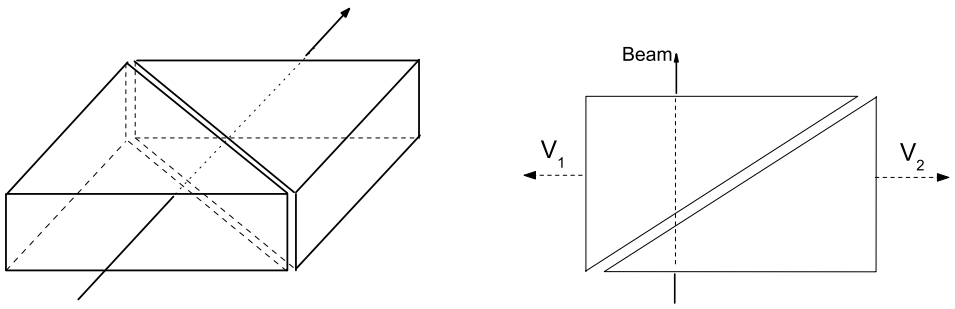

a) b)

Figure 7.3: Schematic view of pickup

The LeCroy oscilloscope of series "WaveRunner 6000A" is employed for digitizing and storing of the BPM data. It is able to record the data with a sampling rate up to 5 GHz. The recorded data can be post processed and analyzed using different software packages. Thus the bunch profiles can be fitted by different distributions and the position of the bunch center can be measured. To increase the measurement time, segmented memory can be used by the device. The LeCroy can record up to 10000 traces with individual triggering for each trace. In other words it can store 10000 bunch forms recorded at different times. This enables measurement times much longer than the synchrotron period. This method is also used to analyze the bunch behavior during the adiabatic rf capture process [54, 55] in the SIS.

Another possibility to analyze the motion in a rf bucket is via spectrum analyzer Sony Tektronix that is available in the control room. This device has the ability to measure the phase error of a harmonic signal. After narrow band filtering ($\approx$ 3 kHz bandwidth) around the rf frequency the BPM signal is compared with a reference harmonic signal of the same frequency. The disadvantage of this method is a low sampling rate. For high precision measurements a fast DSP-based phase detector should be used.

7.3 Digital signal processors system for the detection of the motion

A Digital Signal Processor (DSP) system for cavity synchronization and for beam phase control has been implemented recently at the GSI [56, 57]. The system has the ability to compare the BPM signal or the cavity gap with a reference signal and calculate the relative phase between the signals. As a result we have the excitation signal and the bunch off-set signal independently. These signals can be compared and the BTF can be obtained. A

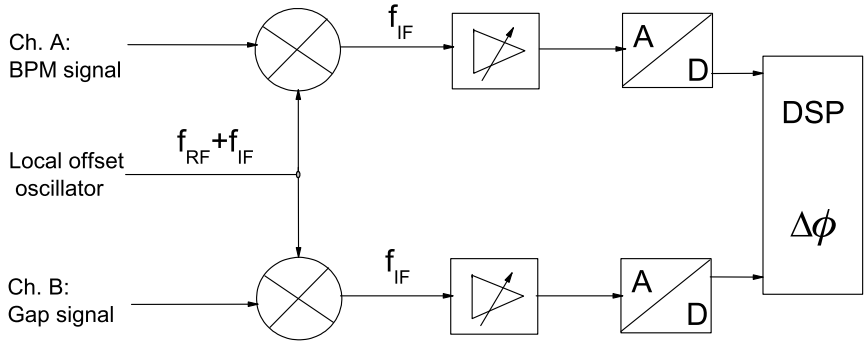

Figure 7.4: Schematic picture of the DSP based phase detection system. Non modulated rf signal is a reference signal. The BPM signal and the modulated rf signal are compared with the reference signal.

sketch of the DSP phase measurement system is shown in Fig. 7.4. The cavity gap signal or the signal from the BPM can be used as input signals. After frequency conversion of the input signals to a fixed intermediate frequency f_{IF} both signals are filtered and digitized. By choosing the intermediate frequency as high as possible the time needed to detect the phase of a signal can be minimized. Presently the intermediate frequency is equal to 21.4 MHz. A commercial filter with a bandwidth of 250 kHz is used to filter the intermediate signal. The digital signal goes to the DSP unit where the data is analyzed using a special software.

7.4 High intensity bunched beam BTFM

Using electron cooling a matched bunch with high space charge parameter is achieved. The ability of beam excitation by the de-tuning of the cavity was performed. Measured BTF amplitudes were compared with theory. The results from the measurements were analyzed by using of the BTF model for cold oscillator described in section 5.4. The effective dipole impedance was extracted. Instability thresholds in the SIS were obtained.

7.4.1 Electron cooling in the SIS

After rf capture in the SIS the bunch is not necessarily matched. Especially at high beam intensities the captured bunch still performed oscillations. Another method is to inject in standing bucket and apply electron cooling. Electron cooling system in the SIS was designed and manufactured in collaboration between GSI and BINP, Novosibirsk. The electron cooler was installed in 1998. It allows to increase the ions intensity via the beam accumulation by repeated multiturn injections. Since the typical machine cycle times are a few seconds and transverse cooling times are of the order of 100 ms the intensity gain is an order of magnitude. The maximum electron current is of 1.5 A and the electron energy is of 6.3 keV that results in effective cooling for the low energy ions at injection energy of about 11-12 MeV/u.

In the experiments with high intensity bunches, the electron cooler was used to obtain stationary bunches. It means that from one side electron cooling allows to achieve the highest intensity and from other side the electron cooling prevents persistent dipole oscillations that arises in the SIS at to high intensity [2, 3].

7.4.2 The main parameters of the experiment

The first longitudinal bunched BTFM via the rf phase modulation in the SIS were performed in December, 2005. The main goals of the performed experiment were:

- Test of the rf phase modulation.
- Measurement of the BTF amplitude as a function of the modulation frequency and the ions intensity.

In Table 7.1 the main parameters of the experiment are presented. During the experiment the multi-multiturn injection method was used. The time between two successive multiturn injections was 0.7 s that is needed to cool the ions from each injection. The longitudinal bunch profiles for different ion intensities was measured using the sum signal of one of the PU installed in the SIS. The results are shown in Fig.7.5. As the intensity increases the bunch length also grows. This can be explained by the increase of the space charge voltage which counteracts the external rf voltage. It is important to note that the areas under the measured bunch profiles are not proportional to the intensity value since the

Ion specie	Xe^{+48}
Energy	11.4 MeV/u
rf voltage amplitude	0.5 kV
Electron cooler current	0.2 A
Number of particles in one bunch	$1 \cdot 10^8 - 6 \cdot 10^8$
rf phase modulation amplitude	0.06^0

Table 7.1: The main parameters of the BTF experiment in the SIS.

amplification of the BPM signal was varied during the experiment. The bunch profiles were fitted assuming a Gaussian line density of the form:

$$\lambda(\phi) = a \cdot e^{-\frac{\phi^2}{\sigma_{rms}^2}} + b, \tag{7.3}$$

where a, b and σ_{rms} are the fits parameters of the fit. Comparisons between the experimental data and the fit data are shown in Fig.7.5. Using the rms values the space charge parameter for the rms-equivalent bunch with elliptic distribution was calculated using as well as the threshold space charge parameter for the given bunch half-length ϕ_m and intensity N. The calculated results together with the coherent frequency Ω_c and the synchrotron frequency reduced by space charge are presented in Table 7.2.

Intensity, part. per bunch	σ_{rms}, deg	ϕ_m, deg	Ω_c/ω_{s0}	Σ	Σ_{th}	$\omega_s(0)/\omega_{s0}$
$1 \cdot 10^8$	20	45	0.970	0.070	0.059	0.964
$3 \cdot 10^8$	24	55	0.956	0.117	0.091	0.946
$6 \cdot 10^8$	30	66	0.937	0.142	0.133	0.934

Table 7.2: Space charge parameters, coherent and synchrotron frequencies estimated with the Eqs. (4.10), (4.11), (4.15), (4.14) for the measured rms bunch lengthes.

It can be seen from Table 7.2 that for each intensity the space charge parameter is higher than the threshold parameter. Thus the Landau damping is lost for all intensities.

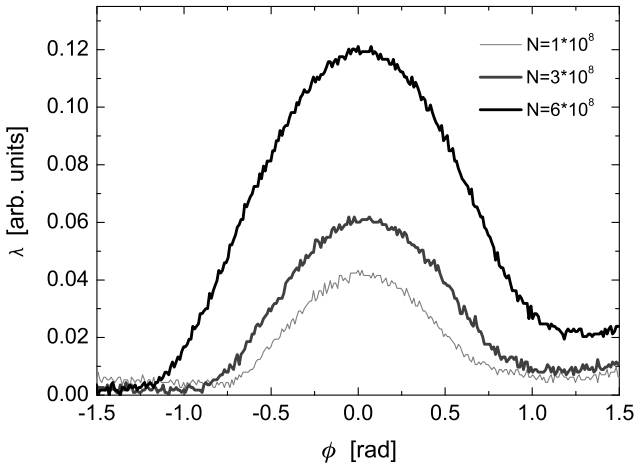

a)

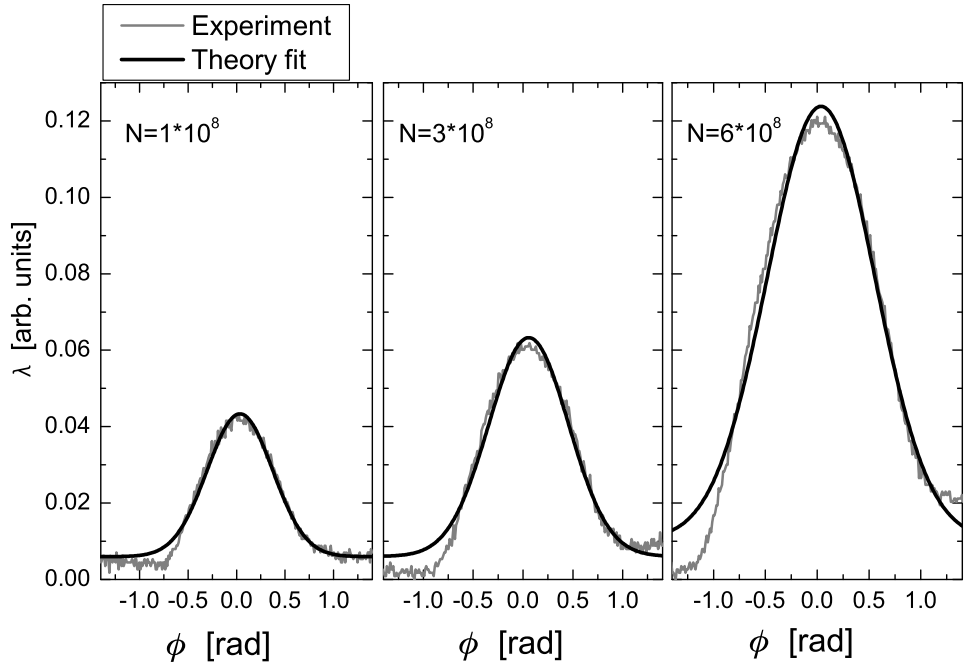

b)

Figure 7.5: Measured bunch profiles for different beam intensities a) and a Gaussian fit b).

In Fig.7.6 it is shown that for all intensities the coherent frequency Ω_c is higher than the

maximum synchrotron frequency in the bunch.

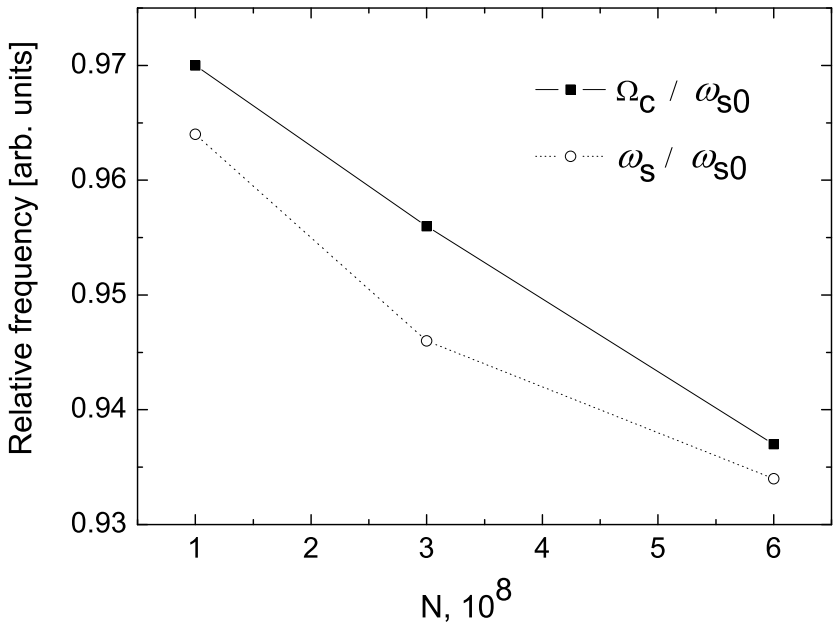

Figure 7.6: Comparison of the coherent frequency Ω_c with the maximal incoherent synchrotron frequency ω_s^0 affected by space charge.

7.4.3 BTFM scheme and results

In Fig. 7.7 the scheme of the experiment is shown. The rf voltage amplitude is set via the SIS control system. At the same time the SIS control system sends a trigger event signal in order to start the rf phase modulation and to measure the bunch oscillations. The trigger event was 1 second after the injection is completed. The modulation signal for the rf phase was provided by the arbitrary waveform function generator Agilent 33220A. The bunch oscillations were detected by the SonyTek spectrum vector analyzer using the phase error method described in section 7.2. The coherent dipole oscillations in the absence of the rf phase modulation were measured. In Figure 7.8 the data from the spectrum analyzer is shown when the rf phase modulation is off. It can be seen only a noise in the dipole motion of the bunch. The noise amplitude is less than 1^0. Following the first aim of the experiment the influence of the rf phase modulation on the bunch motion was tested with single frequency excitation. The amplitude of the output signal from the function generator was set to 5mV that corresponds to an amplitude of the rf phase modulation

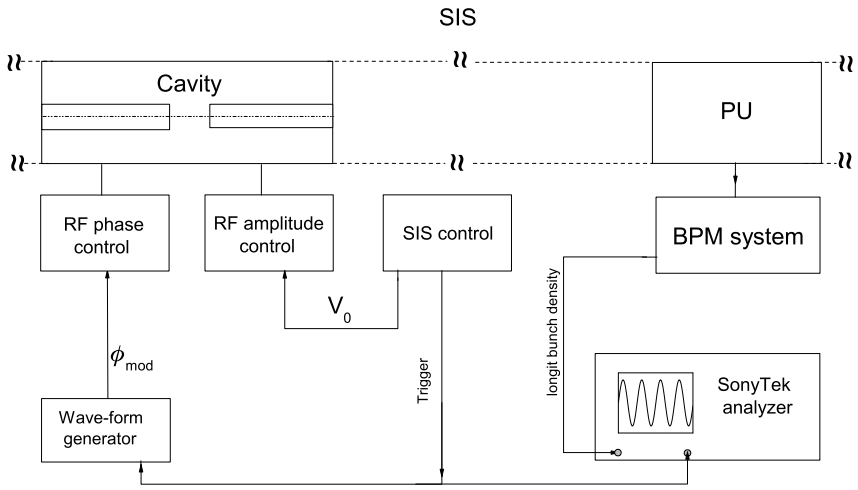

a)

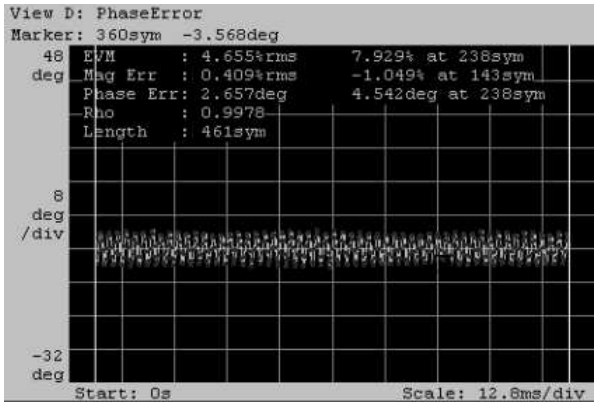

b)

Figure 7.7: Scheme of the BTF experiment in the SIS a) and SonyTek analyzer output data b) where the dipole oscillations of the bunch with the rf phase modulation on are shown. The modulation amplitude is of 0.06^0. The data were measured at the beam intensity 10^8 ions in the bunch.

equal to 0.06^0. The modulation frequency in the results shown in Fig. 7.7 was 480 kHz which is close to the estimated synchrotron frequency of 490 kHz. A clear response of the bunch to the rf phase modulation can be seen.

Changing the rf phase modulation frequency and measuring the amplitude of the bunch oscillations the frequency region around the synchrotron frequency was scanned. The frequency scan was done for three beam intensities of 10^8, $3 \cdot 10^8$ and $6 \cdot 10^8$ ions in

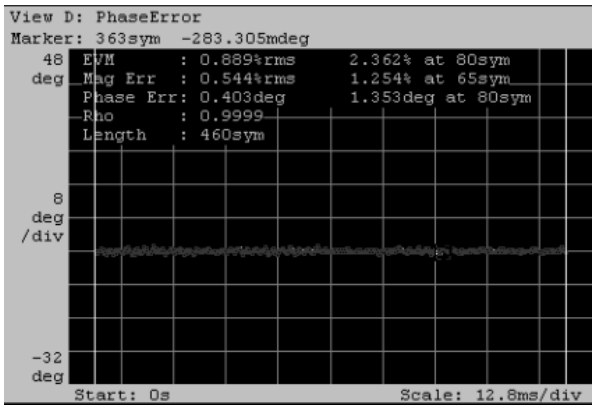

Figure 7.8: Dipole oscillations in the absence of the rf phase modulation. The amplitude of the dipole oscillations is very small.

the bunch. Dividing the measured oscillation amplitudes by the modulation the BTF amplitudes were obtained. The results are presented in Fig. 7.9. As it can be seen the

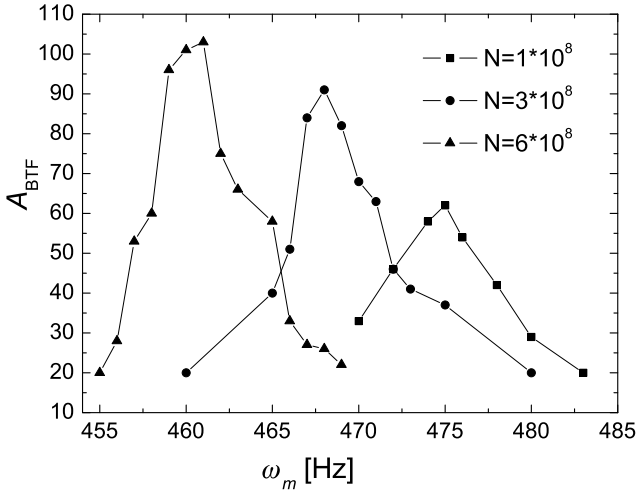

Figure 7.9: Measured BTF amplitudes from the relation $\hat{\tilde{\phi}}/\hat{\phi}_m$ for different number of particles in the bunch.

BTF amplitude as a function of frequency differs for different intensities. Firstly, the

position of the peak is shifting backwards with increasing intensity. Secondly, the peak value grows as the intensity grows. This effect will be described using the BTF model for a bunch with electron cooling and effective dipole impedance 5.9.

7.4.4 Calculation of the effective dipole impedance

The measured BTF amplitudes were fitted according to the model of a cold oscillator. The model is described by Eq.5.6. The comparison between the fit and the experimental data

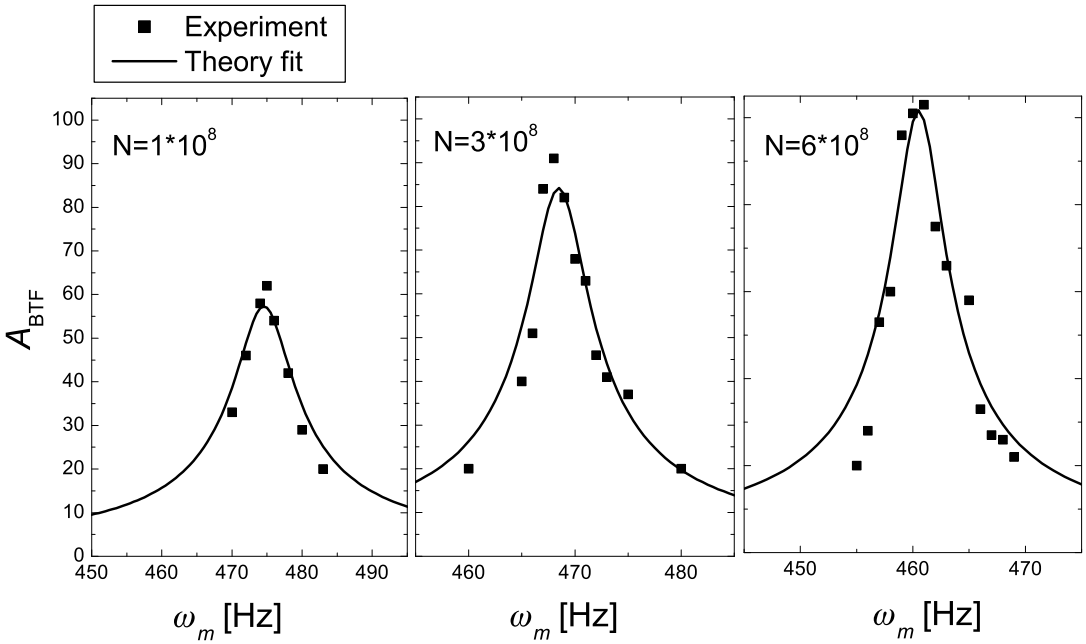

Figure 7.10: Fit of the measured BTF amplitude for different beam intensities using the model of a cold oscillator.

is shown in Fig.7.10. A good agreement between the data and the fits can be seen.

The Eqs. 5.11 for the real and imaginary parts of the effective dipole impedance can be rewritten as

$$Z_I = \frac{2}{\Omega_c}(\omega_m^{max} - \Omega_c) \qquad Z_R = \frac{2}{\Omega_c}\gamma_c - \frac{1}{A_{BTF}^{max}},$$

where ω_m^{max} and A_{BTF}^{max} are the location and the value of the measured maximum BTF amplitude. Using the Ω_c obtained for different intensities in Tab. 7.2 the imaginary part of the effective impedance as a function of intensity can be obtained. Concerning the real part the damping factor γ_c is not known. By plotting the inverted maximum BTF amplitude $\frac{1}{A_{BTF}^{max}}$ as a function of intensity and by using $Z_R = 0$ at zero intensity the

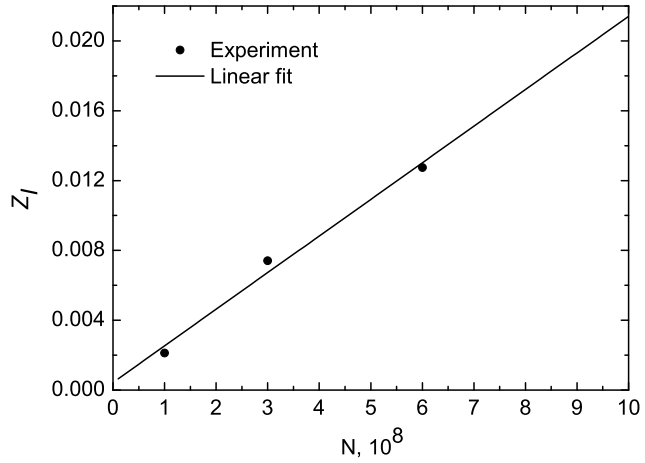

a)

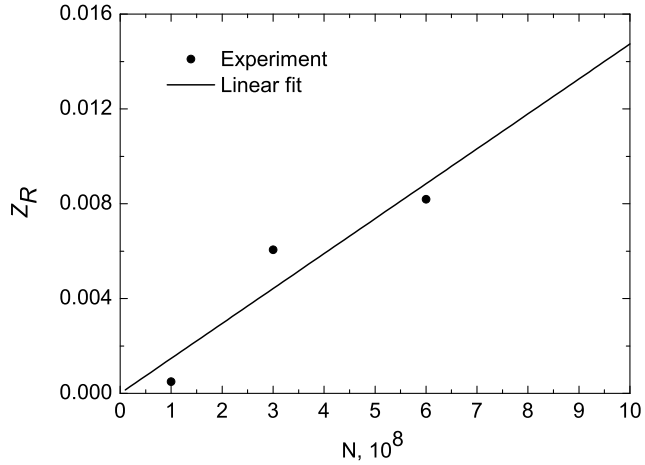

b)

Figure 7.11: Imaginary a) and real b) parts of the longitudinal effective impedance as a function of the number of particles in a bunch.

damping factor can be obtained as 27 s^{-1}. For the obtained γ_c the real part of effective impedance Z_R can be calculated for different intensities. The results are shown in Fig.7.11 together with the theoretical fit assuming a linear dependence on intensity $Z \sim N$. The final result of this experiment is the obtained effective dipole impedance fit

$$Z_{meas} = (14.7 + i20.9) \cdot 10^{-12} \cdot N. \tag{7.4}$$

7.4.5 Estimated instability thresholds and growth rates

It is important to note that the obtained values for the effective impedance are valid only for Xe-beam in the SIS. The effective dipole impedance can be presented in general form as (see Appendix A)

$$Z = \frac{Nq}{V_0} \cdot C_{\phi_m}, \tag{7.5}$$

where C_{ϕ_m} depends on the bunch distribution and on the bunch half-length ϕ_m. Comparing the Eq. (A.8) with the measured impedance the constant C_{ϕ_m} is obtained as

$$C_{\phi_m} = (14.7 + i20.9) \cdot 10^{-12} \frac{V_0^{Xe}}{q^{Xe}} = (4.6 + i6.5) \cdot 10^{10}.$$

Thus for any type of ions the effective impedance can be obtained as

$$Z = (4.6 + i6.5) \cdot 10^{10} \frac{Nq}{V_0}. \tag{7.6}$$

This formula is valid only for SIS conditions at harmonic number four and bunch half-length 60^0. Using Eq. (7.6) the effective dipole impedance for U^{+73} bunches as intensity function can be obtained. Using dispersion relation (4.21) with space charge the intensity threshold and instability growth rate for U^{+73} was calculated. In Fig. 7.12 the resulting growth rates of the instability driven by the effective dipole impedance for the U^{+73}-beam are presented. The threshold intensity equals $3.2{\cdot}10^9$ particles in the SIS. The knowledge of the growth rates values is very useful for the design of a longitudinal feedback system since it gives an approximate number for the required damping rates.

The spectra of the dipole oscillations depends on the bunch length and harmonic number. If the bunch length is known then the frequency range for potentially dangerous narrow-banded impedances can be estimated. For a bunch half-length of 60^0 that is close to the measured bunch half-lengthes the spectrum of the dipole bunch oscillations is shown in Fig. 7.13. Potentially dangerous impedances that drive dipole oscillations should be located in the frequency range where the spectrum of dipole oscillations has the highest values. For the present parameters the frequency range is ≈1.5-3.5 MHz.

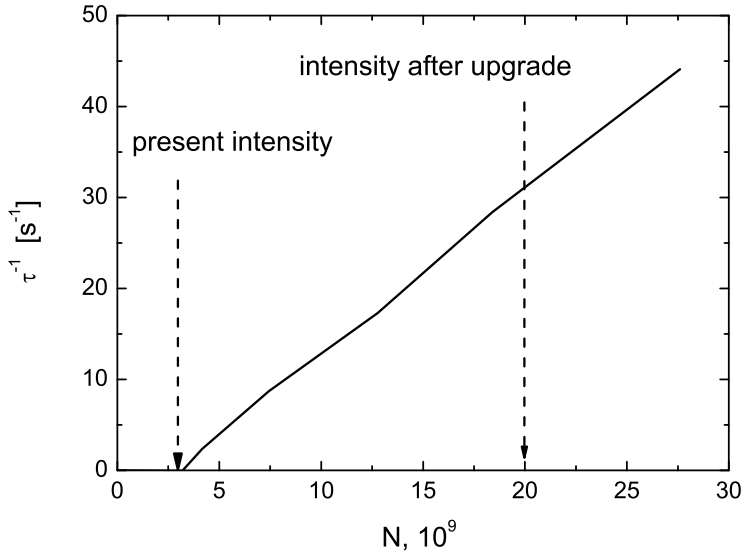

Figure 7.12: Growth rate of the instability driven by the effective dipole impedance for the U^{+73}-beam.

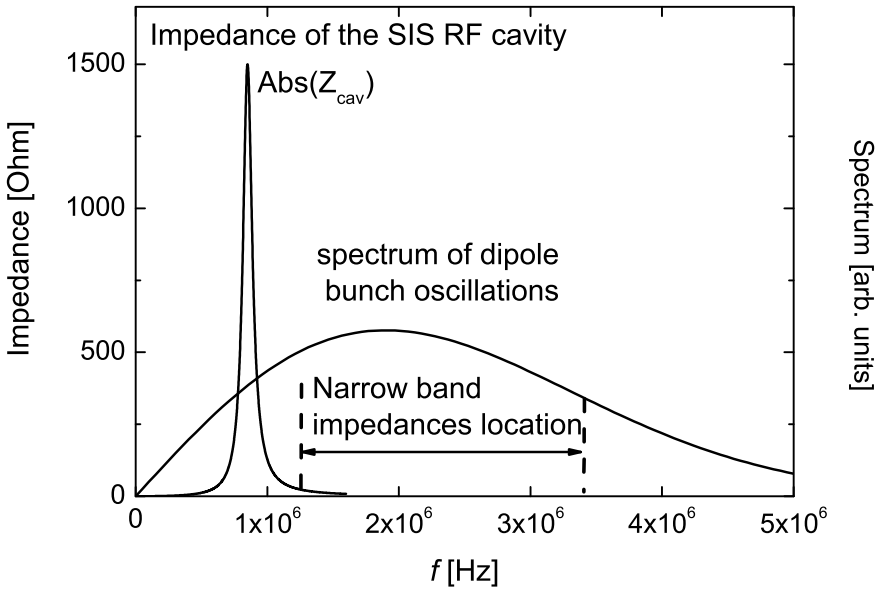

Figure 7.13: Spectrum of the bunch dipole oscillations.

7.5 BTFM with low beam intensity

In another experimental campaign with low intensity beams, where Landau damping is present, the bunches were generated by rf capture. The generation of stationary bunches is vital to the BTF method. With the existing rf ramps this is not possible in the SIS. Therefore adiabatic ramps were provided manually using the wave-form generator. The DSP system was used for the BTFM. The results are fitted by BTF model of a bunch with Landau damping. The parameters found from the fit are compared with expected results.

7.5.1 Adiabatic capture in the SIS

During adiabatic capture process the rf voltage amplitude is changed slowly in time. Thus the single particle Hamiltonian depends on time. If the amplitude ramp is slow, the Hamiltonian can be considered as quasi-static. It means that Hamiltonian parameter, such a synchrotron frequency, changes slowly so the particle orbit is characterized by the constant Hamiltonian value. The condition for adiabatic synchrotron motion is [30]

$$\alpha_{ad} = \left| \frac{1}{\omega_s^2} \frac{d\omega_s}{dt} \right| = \frac{1}{2\pi} \left| \frac{dT_s}{dt} \right| \quad << 1, \tag{7.7}$$

where α_{ad} is called the adiabaticity coefficient. An amplitude ramp is called as adiabatic if the synchrotron frequency is changed slowly enough for the distribution of particles to be at equilibrium along the whole adiabatic process.

If the adiabaticity coefficient is kept fixed and is much less than one, then the amplitude ramp is called as iso-adiabatic. The form of the iso-adiabatic ramp can be easily obtained from condition (7.7). The synchrotron period depends on the voltage as

$$T_s = 2\pi \sqrt{\frac{LRm^*}{hq}} V^{-1/2} \tag{7.8}$$

and a differential equation can be constructed as

$$\alpha_c dt = \frac{1}{2} \sqrt{\frac{LRm^*}{hq}} V^{-3/2} dV. \tag{7.9}$$

Performing integration over time period t_{ramp} the voltage is changed from V_1 to V_2 and adiabaticity coefficient is obtained as

$$\alpha_c = \sqrt{\frac{LRm^*}{hq}} \frac{1}{t_{ramp}} \left(\frac{1}{\sqrt{V_1}} - \frac{1}{\sqrt{V_2}} \right). \tag{7.10}$$

The form of the iso-adiabatic ramp can be obtained by performing the indefinite integration of Eq. (7.9):

$$\alpha_c t + C = \sqrt{\frac{LRm^*}{hq}} V^{-1/2} \tag{7.11}$$

and extracting the voltage the time dependence is obtained as

$$V(t) = \frac{1}{(\frac{t}{t_{ramp}}(\frac{1}{\sqrt{V_1}} - \frac{1}{\sqrt{V_2}}) + C)^2}, \tag{7.12}$$

where the constant C can be obtained from boundary condition $V(t_{ramp}) = V_2$. Final expression for the iso-adiabatic ramp is written as

$$V(t) = \frac{V_1}{(1 - \frac{t}{t_{ramp}}\frac{\sqrt{V_2} - \sqrt{V_1}}{\sqrt{V_2}})^2}. \tag{7.13}$$

7.5.2 The main parameters and scheme of the experiment

The second experiment with longitudinal bunched BTFM was done in March, 2007. In Table 7.3 the parameters of the performed experiment is shown. In comparison with first BTF experiment the signal detection technique as well as experimental setup has been improved. Scheme of the performed experiment is shown in Fig. 7.14. The scheme is

Ion specie	U^{+73}
Energy	11.4 MeV/u
Voltage	4-6 kV
Number of particles in one bunch	$1 \cdot 10^8$
Modulation amplitude	$2^0 - 6^0$

Table 7.3: Beam and rf parameters used in the second BTF experiment in the SIS.

similar to the scheme from the previous experiment. The feature of the new scheme is the usage of the DSP system for detection of the longitudinal bunch oscillations. Another improvement is the implementation of the "iso-adiabatic" voltage amplitude ramps. As it was mentioned already one of the important aims is the formation of stationary bunches. In order to solve this problem it was decided to provide adiabatic ramps "manually", i.e. not by using the standard ramps from the SIS control but using the so-called "self-created" adiabatic ramps. For this purpose, as well as for the phase modulation tasks, the signal generator "Agilent 3320" has been used. The feature of this generator is that it produces any form of the signal previously loaded. The "iso-adiabatic" ramp was used which is represented by the formula:

$$V(t) = \frac{4\text{kV}}{(1 - \frac{t}{100ms}\frac{\sqrt{4\text{kV}} - \sqrt{0.1kV}}{\sqrt{4\text{kV}}})^2}, \tag{7.14}$$

where the initial voltage 0.1 kV, the final voltage is 4 kV and the capturing time is 100 ms. The curve that corresponds to the given formula is shown in Fig.7.15. The results

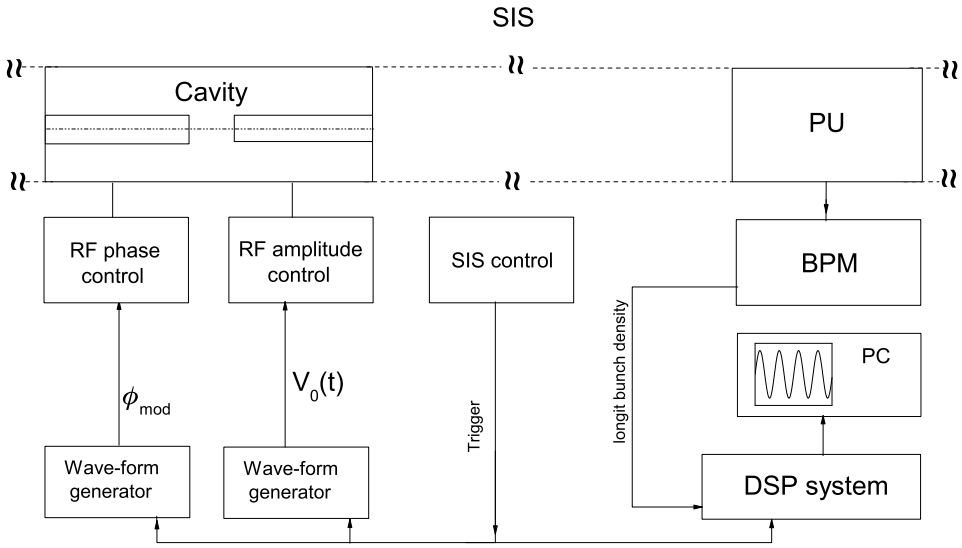

a)

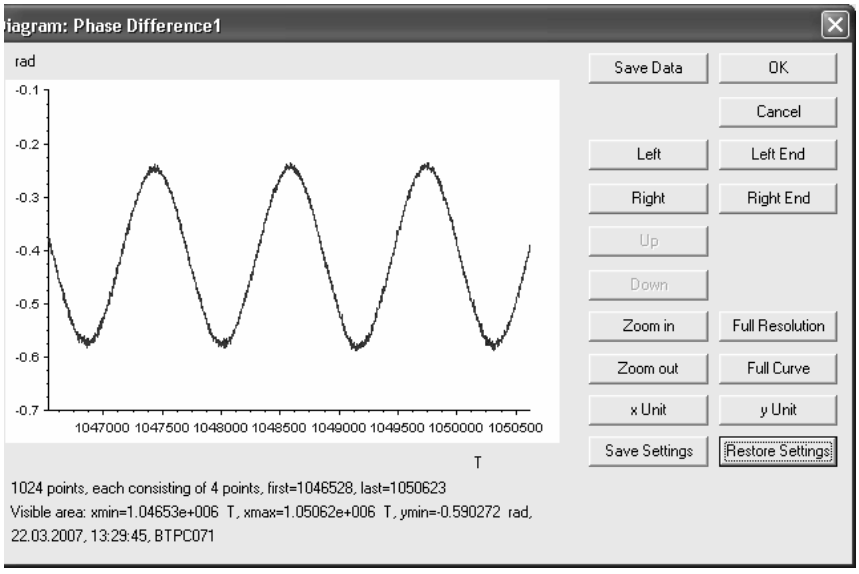

b)

Figure 7.14: Scheme of the BTF experiment a) and DSP system output data b).

from adiabatic capture process are presented in the Fig.7.16. The contour plot of the

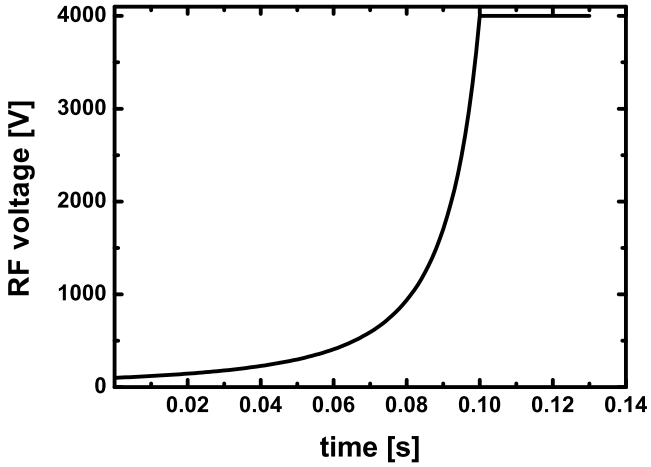

Figure 7.15: rf voltage ramp form of adiabatic capture.

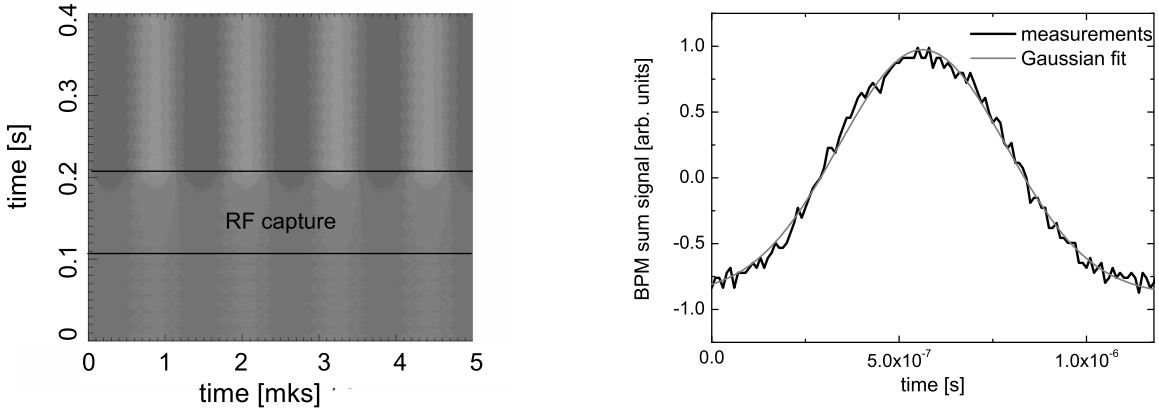

Figure 7.16: Contour plot of bunch evolution during and after the adiabatic capture (left) and bunch profile of a single bunch after adiabatic capture (right). The bunch profile (right) is fitted by a Gaussian function.

longitudinal bunch profile evolution during the adiabatic capture is shown together with the longitudinal profile which is fitted with a Gaussian function. After adiabatic ramp is finished a trigger signal goes to the waveform generator to start the phase modulation. The same trigger signal is used as a starting event for the measurements of the DSP system. In Fig. 7.17 the waterfall plots for the cases of different rf phase modulation amplitudes is

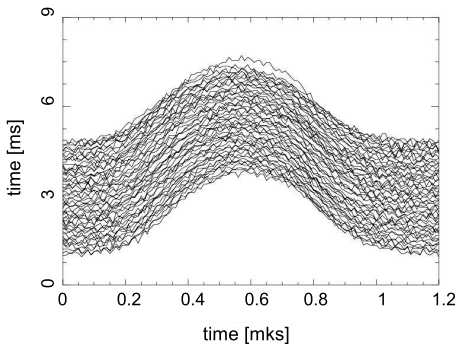

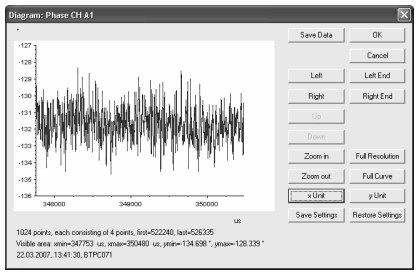

V_{mod} =0 mV

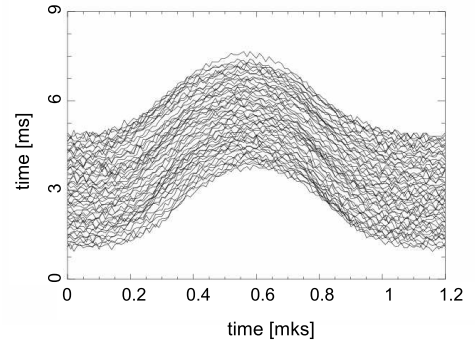

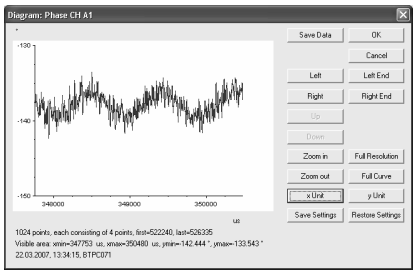

V_{mod} =50 mV

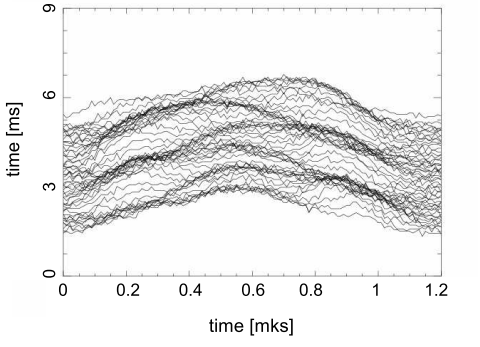

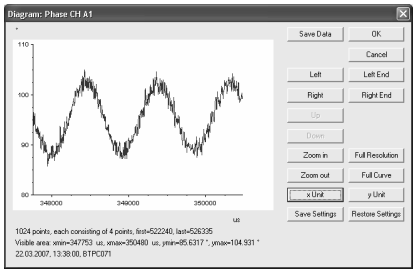

V_{mod} =500 mV

Figure 7.17: Waterfall plots of bunch evolution and the data from the DSP system during the rf phase modulation process for different modulation voltages V_{mod} from the waveform generator.

presented as well as the data about bunch phase information from the DSP system.

Type of the rf phase modulation signal has been chosen as frequency sweep. The dependence of the modulation frequency from time was described by the formula:

$$\frac{\omega_m}{2\pi} = f_m = 1000\text{Hz} + \frac{1000\text{Hz}}{1.5\text{s}}t, \tag{7.15}$$

where it can be seen that frequency region was limited by the range from 1 kHz to 2 kHz with sweeping time of 1.5 s. Synchrotron frequency estimated from the rf voltage amplitude which is 4 kV was corresponding to the value of 1223 Hz. Later it will be shown that measured synchrotron frequency was around the value of 1400 kHz. Thus the modulation frequency range covers the synchrotron frequencies range which is equal to

$$\triangle f_s = f_{s0} \cdot \frac{\phi_m^2}{16} \approx 270\text{Hz}, \tag{7.16}$$

where the bunch half-length was calculated using the rms value of 67^0 obtained from the fitted bunch profile.

7.5.3 BTFM results

The results of the measured BTF amplitudes at 4 kV rf voltage are presented in Fig.7.18. The results for two different phase modulation amplitudes are shown. The first BTF amplitude is measured with the modulation amplitude 3.2^0 and the second BTF amplitude is measured with the modulation amplitude 5.2^0. The expression for the BTF with Landau damping was used to fit the results. The parameters of the fit are the synchrotron frequency ω_{s0} and the rms momentum spread in the bunch $(\frac{\triangle p}{p})_{rms}$. A Gaussian distribution was chosen as the distribution in the BTF Eq. (5.13). The values of the parameters found by the fit are presented in Table 7.4. The small difference in the obtained rms momentum spreads occurs since the measurement for each case were done in different machine cycle and the rms value of the momentum spread varies from cycle to cycle. The rms length of the bunch line density was obtained from a Gaussian distribution. As it can be seen the values of the obtained rms bunch lengthes are not in agreement with the measured values from a Gaussian fit of the bunch profile. The possible explanation of this effect is that not all particles from the coasting beam are captured in the rf bucket. The longitudinal bunch profile measured from the BPM signal contains not only the longitudinal profile of the captured particles but also the longitudinal distribution of the particles outside the rf bucket. Thus, the particles outside the rf bucket create a background in the BPM signal that leads to a incorrect calculation of the bunch length. The main argument in the validity of the rms lengthes obtained from the BTFM was the independence of the results from the value of rf phase modulation amplitude.

The synchrotron frequency obtained from the BTFM is higher then expected. It means that the real voltage amplitude was higher than 4 kV and for obtained synchrotron frequency of 1427 Hz it has value of 5.4 kV. Additional measurements were made for the

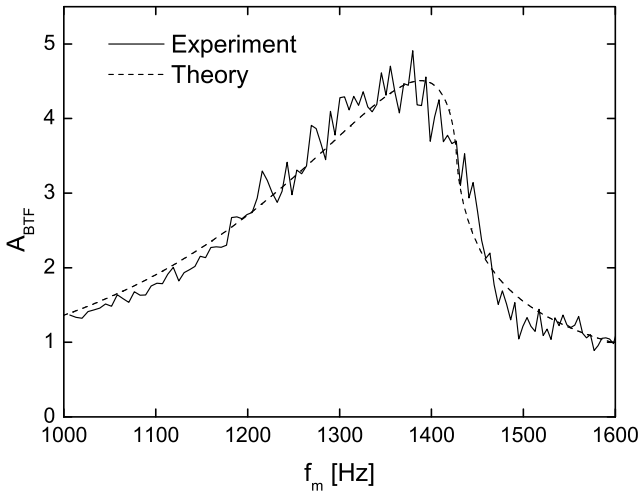

a)

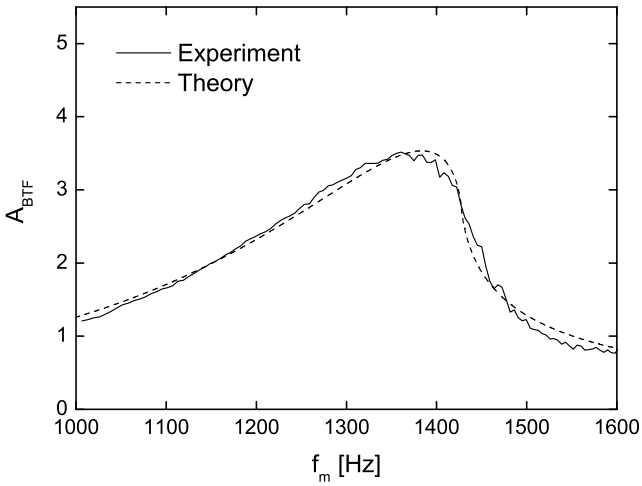

b)

Figure 7.18: BTF amplitudes measured at rf voltage 4 kV, rf phase modulation amplitude 3.2^0 a) and 5.2^0 b). The experimental data are fitted with BTF amplitudes for a bunch with Landau damping from Eq. (5.13).

rf voltage amplitude of 6 kV. The measured BTF amplitudes are presented in Fig. 7.19. The values of synchrotron frequency, rms momentum spread, rms bunch length obtained from the BTFM and rms bunch length obtained from a Gaussian fit of the bunch profile

The results expected from the BTFM			
Modulation amplitude, ^{0}	Synchrotron frequency, Hz	$(\frac{\triangle p}{p})_{rms}$	ϕ_{rms}, ^{0}
-	1223	-	67^0

The results obtained from the BTFM			
Modulation amplitude, ^{0}	Synchrotron frequency, Hz	$(\frac{\triangle p}{p})_{rms}$	ϕ_{rms}, ^{0}
3.2^0	1427	$1.2 \cdot 10^{-3}$	50^0
5.2^0	1428	$1.3 \cdot 10^{-3}$	53^0

Table 7.4: Comparison of the expected bunch parameters with the bunch parameters obtained from BTFM. The expected synchrotron frequency calculated using given rf voltage amplitude of 4 kV. The expected bunch rms length was found from a Gaussian fit of the bunch profile measured with the BPM.

are presented in Table. 7.5. In the case of rf amplitude voltage of 6 kV the synchrotron frequency obtained from the BTFM was higher then expected as well as in the previous case of 4 kV. For obtained synchrotron frequency of 1733 Hz it has value of 8.5 kV. As in the previous case the bunch rms lengthes obtained from the BTFM are different from the measured rms bunch length. Again we attribute this difference to the fact that not all particles are captured. Thus performing the BTFM with low intensity the real bunch rms lengthes can be obtained.

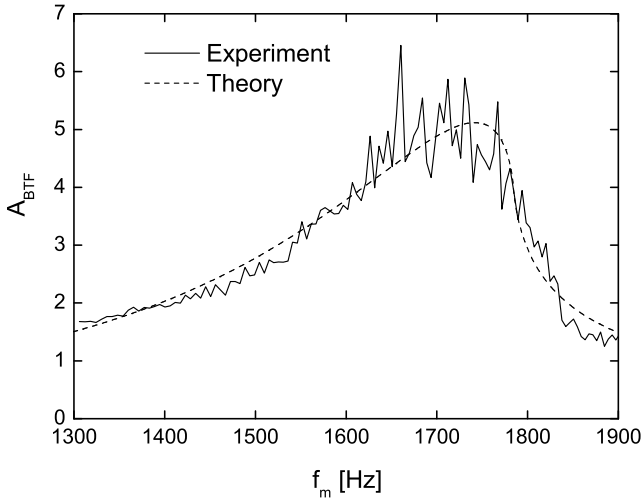

a)

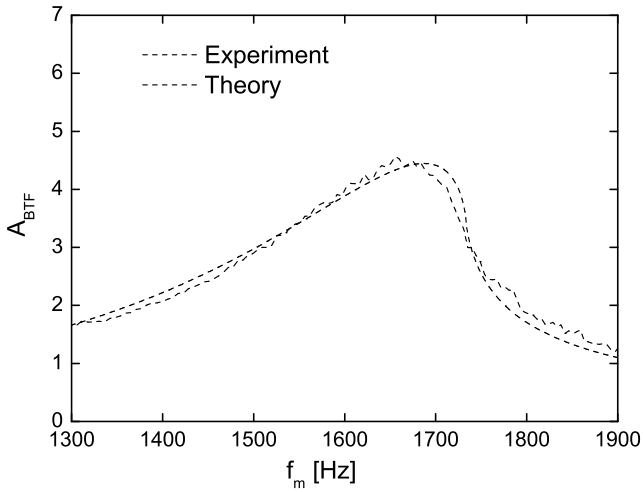

b)

Figure 7.19: BTF amplitudes measured at rf voltage 6 kV, rf phase modulation amplitude 3.2^0 a) and 5.2^0 b). The experimental data are fitted with BTF amplitudes for a bunch with Landau damping from Eq. (5.13).

The results expected from the BTFM			
Modulation amplitude, ^{0}	Synchrotron frequency, Hz	$(\frac{\triangle p}{p})_{rms}$	ϕ_{rms}, ^{0}
-	1498	-	59^0

The results obtained from the BTFM			
Modulation amplitude, ^{0}	Synchrotron frequency, Hz	$(\frac{\triangle p}{p})_{rms}$	ϕ_{rms}, ^{0}
3.2^0	1785	$1.5 \cdot 10^{-3}$	46^0
5.2^0	1733	$1.5 \cdot 10^{-3}$	49^0

Table 7.5: Comparison of the expected bunch parameters with the bunch parameters obtained from BTFM. The expected synchrotron frequency calculated using given rf voltage amplitude of 6 kV. The expected bunch rms length was found from a Gaussian fit of the bunch profile measured with BPM.

Chapter 8

Summary and outlook

In this thesis different theoretical models for the longitudinal bunched BTF have been analyzed. The work focuses on dipole oscillations in a rf bucket. One of the models is the BTF of a bunch with synchrotron frequency spread and nonlinear space charge effects. It is assumed that Landau damping is effective. The second model is the BTF of cooled beam interacting with an effective dipole impedance. According to this model, the effective dipole impedance can be obtained as the difference between inverse BTFs measured with high and low beam intensities. The cold oscillator model is applicable to the bunches cooled by electrons. Different types of RF phase modulation, such as fixed frequency, frequency sweep and noise excitation, were tested in the simulations and in the BTFM in the SIS.

In order to verify the theory numerical simulations have been performed using a simulation scheme with space charge. The simulation results were compared with the theoretical predictions. A good agreement between the simulation and theory was found. For the electron cooled bunch it was shown that for space charge parameters above a threshold the BTF can be described by a simple oscillator with damping factor. The effective dipole impedance reduces the damping factor and increases the coherent frequency. The coherent frequency and the damping factor depend linearly on the value of the effective impedance. The maximum value of the BTF amplitude depends very sensitively on the space charge parameter. This effect can be used to measure the space charge impedance or other broad band imaginary impedances in the SIS.

Two BTF experiments in the SIS are described in this thesis. During the first experiment the ability to perform the longitudinal bunched BTFM in the SIS using the existing capabilities was proved. Here the electron cooler was used to obtain reproducible conditions. The effective dipole impedance was extracted from the experimental data. Additionally, the intensity threshold for unstable dipole oscillations driven by the effective dipole impedance was estimated. In the second experiment the measurement technique was improved by installation of the DSP based phase detector. The results obtained in the experiment fit well to the BTF theory for Landau damped beams. A difference was obtain between the bunch lengthes obtained from the BTFM and the bunch lengthes measured by the BPM. The explanation is as follows: the BPM signal includes the particles which are inside and outside a RF bucket. Thus the BTFM can be used to obtain the particle

distribution inside a RF bucket and to calculate the real longitudinal rms size of a bunch. It is important to note that the measured synchrotron frequency was different from the expected one. Thus the BTFM can be used to find the effective RF voltage acting on a beam.

It was shown that the newly implemented BTFM technique is a powerful diagnostic tool which can be used during future operation of the SIS.

Appendix A

Equation for synchrotron motion with effective dipole impedance

The effective impedance is used for the determination of the coherent frequency shift for different oscillation modes m and is defined as [41, 58]

$$Z_{eff} = \frac{\sum_{p=-\infty}^{\infty} \frac{Z^{||}_{p+m\nu}}{p+m\nu}(p+m\nu)^2 I_p^2}{\sum_{p=-\infty}^{\infty}(p+m\nu)^2 I_p^2}. \tag{A.1}$$

Taking into account that $\nu << p$, Eq. (A.1) can be rewritten as

$$Z_{eff} = \frac{\sum_{p=-\infty}^{\infty} pZ^{||}_{p+m\nu} I_p^2}{\sum_{p=-\infty}^{\infty} p^2 I_p^2}.$$

Summarizing positive and negative p and taking only the dipole mode $m = 1$ we obtain:

$$\sum_{p=-\infty}^{\infty} pZ^{||}_{p+m\nu} I_p^2 = \sum_{p=-\infty}^{\infty} p(Z^{||}_p + Z^{||}_{p+\nu}) I_p^2 = \sum_{p=0}^{\infty} p(Z^{||}_p + Z^{||}_{p+\nu} - Z^{||}_{-p} - Z^{||}_{-p+\nu}) I_p^2. \tag{A.2}$$

The properties of the impedance function can be found in [59] and is written as

$$Re[Z^{||}_{-p}] = Re[Z^{||}_p] \qquad Im[Z^{||}_{-p}] = -Im[Z^{||}_p]. \tag{A.3}$$

Using these properties the real part of the effective impedance can be calculated as

$$Re[Z_{eff}] = \frac{\sum_{p=0}^{\infty} I_p^2 p(Re[Z^{||}_{p+\nu}] - Re[Z^{||}_{p-\nu}])}{\sum_{p=0}^{\infty} p^2 I_p^2}. \tag{A.4}$$

The imaginary part is obtained as

$$Im[Z_{eff}] = \frac{\sum_{p=0}^{\infty} I_p^2 p(2Im[Z_p^{||}] - Im[Z_{p+\nu}^{||}] - Im[Z_{p-\nu}^{||}])}{\sum_{p=0}^{\infty} |p^2 I_p^2|}. \tag{A.5}$$

Thus, $Z_{eff} = Re[Z_{eff}] + iIm[Z_{eff}]$ is the effective impedance for the dipole mode, or the effective dipole impedance.

Next, we will derive the force described by the effective dipole impedance. This force can be obtained from electrotechnical approach. The ion current can be decomposed as

$$I(\phi - \bar{\phi}) = \sum_{p=-\infty}^{\infty} I_p e^{ip\phi} - \frac{\hat{\bar{\phi}}}{2} \sum_{p=-\infty}^{\infty} iI_p\big((p-\nu)e^{i(p-\nu)\phi} + (p+\nu)e^{i(p+\nu)\phi}\big) =$$

$$= \sum_{p=-\infty}^{\infty} I_p e^{ip\phi} - \sum_{p=-\infty}^{\infty} iI_p e^{ip\phi}(p\bar{\phi} + i\nu\frac{\dot{\bar{\phi}}}{\Omega_c}),$$

where $\bar{\phi} = \hat{\bar{\phi}}\cos\nu\phi$ and $\dot{\bar{\phi}} = -\Omega_c\hat{\bar{\phi}}\sin\nu\phi$ is the coordinate and velocity of the bunch center with respect to the synchronous particle. The voltage induced by this current via impedance is written as

$$V(\phi) = \sum_{p=-\infty}^{\infty} Z_p^{||} I_p e^{ip\phi} - \frac{\hat{\bar{\phi}}}{2} \sum_{p=-\infty}^{\infty} iI_p\big(Z_{p-\nu}^{||}(p-\nu)e^{i(p-\nu)\phi} + Z_{p+\nu}^{||}(p+\nu)e^{i(p+\nu)\phi}\big)$$

$$= \sum_{p=-\infty}^{\infty} Z_p^{||} I_p e^{ip\phi} - \frac{1}{2} \sum_{p=-\infty}^{\infty} iI_p e^{ip\phi} p\big(\bar{\phi}(Z_{p+\nu}^{||} + Z_{p-\nu}^{||}) - \frac{i\dot{\bar{\phi}}}{\Omega_c}(Z_{p+\nu}^{||} - Z_{p-\nu}^{||})\big)$$

$$- \frac{\nu}{2} \sum_{p=-\infty}^{\infty} iI_p e^{ip\phi}\big(\bar{\phi}(Z_{p+\nu}^{||} - Z_{p-\nu}^{||}) - \frac{i\dot{\bar{\phi}}}{\Omega_c}(Z_{p+\nu}^{||} + Z_{p-\nu}^{||})\big)$$

The average voltage is determined as

$$<V>= \frac{1}{2\pi I_0}\int_{-\pi}^{\pi} I(\phi)V(\phi)d\phi.$$

Taking into account that $\nu << p$ and keeping only linear terms with respect to ϕ and $\dot{\phi}$ the average voltage is obtained as

$$<V>= \frac{1}{4\pi I_0} \sum_{p=-\infty}^{\infty} iI_p^2 p\big(\bar{\phi}(2Z_p^{||} - Z_{p+\nu}^{||} - Z_{p-\nu}^{||}) - \frac{i\dot{\bar{\phi}}}{\Omega_c}(Z_{p+\nu} - Z_{p-\nu})\big).$$

Using the properties of the impedance (A.3) and summarizing positive and negative parts the averaged voltage is simplified to

$$<V>= \frac{1}{2\pi I_0}\Bigg(\bar{\phi}\sum_{p=0}^{\infty} pI_p^2\big(Im[Z^{||}_{p+\nu}] + Im[Z^{||}_{p-\nu}] - 2Im[Z^{||}_{p}]\big) + \frac{\dot{\bar{\phi}}}{\Omega_c}\sum_{p=0}^{\infty} pI_p^2\big(Re[Z^{||}_{p+\nu}] - Re[Z^{||}_{p-\nu}]\big)\Bigg). \quad \text{(A.6)}$$

Comparing the effective voltage (A.6) with the expressions for the real (A.4) and imaginary (A.5) parts of the effective dipole impedance we obtain

$$<V>\sim -Im[Z_{eff}]\bar{\phi} + Re[Z_{eff}]\frac{\dot{\bar{\phi}}}{\Omega_c}.$$

It is more convenient to define the normalized effective dipole impedance as

$$Z = \frac{\omega_{s0}}{\Omega_c}\frac{1}{V_0 I_0} Z_{eff}\sum_{p=0}^{\infty} p^2 I_p^2. \quad \text{(A.7)}$$

Thus the effective voltage is written as

$$<V>= \frac{V_0}{\omega_{s0}}(-\Omega_c Z_I\bar{\phi} + Z_R\dot{\bar{\phi}}).$$

With normalized effective dipole impedance the longitudinal equation of motion can be presented in a simple way:

$$\ddot{\bar{\phi}} + \omega_{s0}^2\sin\phi = -\omega_{s0}\Omega_c Z_I\bar{\phi} + \omega_{s0}Z_R\dot{\bar{\phi}},$$

where $Z = Z_R + iZ_I$. In this thesis we will use the term "effective dipole impedance" instead of "normalized effective dipole impedance"

It is important to note that the effective dipole impedance (A.7) can be re-written in a simple form

$$Z = \frac{Nq}{V_0}\cdot C_{\phi_m}, \quad \text{(A.8)}$$

where C_{ϕ_m} contains only the bunch distribution and ring parameters.

Appendix B

Longitudinal bunched BTF with space charge

The stationary bunch is characterized by the particle distribution $\psi(\phi, \dot{\phi})$ or $\psi(\hat{\phi})$ in phase space, where $\hat{\phi}$ is the amplitude of particle oscillation. To describe the evolution of distribution the Vlasov equation is involved. The Vlasov equation is written as

$$\frac{\partial \psi}{\partial t} + \dot{\phi}\frac{\partial \psi}{\partial \phi} + \ddot{\phi}\frac{\partial \psi}{\partial \dot{\phi}} = 0.$$

Under the influence of rf phase modulation the time dependent part is taken into account in the distribution:

$$\psi(\hat{\phi}, \theta, t) = \psi_0(\hat{\phi}) + \psi_1(\hat{\phi}, \theta)e^{i\Omega t},$$

where Ω is the frequency of rotation of the perturbed part in phase space. Assuming that the perturbed part ψ_1 is small in comparison with the stationary part ψ_0 the Vlasov equation can be linearized with respect to ψ_1 and is written as

$$i\Omega\psi_1 e^{i\Omega t} - \omega_s \frac{\partial \psi_1}{\partial \theta}e^{i\Omega t} + \frac{F}{\omega_{s_0}} sin\theta \frac{d\psi_0}{dr} = 0, \tag{B.1}$$

where F is determined by the right side of the longitudinal equation of motion:

$$\ddot{\phi} + \omega_{s0}^2 \sin\phi + \omega_{s0}^2 F_{sc}(\phi) = \omega_{s0}^2 \hat{\phi}_m e^{i\omega_m t} + \omega_{s0}^2 F'_{sc}(\phi)\bar{\phi}, \tag{B.2}$$

where $F_{sc}(\phi) = V_{sc}(\phi)/V_0$ depends on space charge voltage and $\bar{\phi} = \hat{\bar{\phi}}e^{i\Omega t}$ is the coordinate of the bunch center. Perturbed part of the distribution can be written as

$$\psi_1(\hat{\phi}, \theta) = \psi_1(\hat{\phi}) \cdot e^{i\theta}. \tag{B.3}$$

Using F from Eq. (B.2) and ψ_1 from Eq. (B.4) the linearized Vlasov equation (B.1) can be written:

$$(\omega_m - \omega_s)\psi_1(\hat{\phi})e^{i\theta} = \frac{\sin\theta}{\omega_{s_0}} \cdot \psi'_0(\hat{\phi})\big(\omega_{s0}^2\hat{\phi}_m + F'_{sc}(\hat{\phi}, \theta)\big), \tag{B.4}$$

where the equivalence of the coherent frequency Ω to the modulation frequency ω_m is assumed. Integrating (B.4) over θ we obtain

$$\psi_1(\hat{\phi}) = \omega_{s0}\hat{\phi}_m\pi\frac{\psi_0'(\hat{\phi})}{\omega_m - \omega_s} + \omega_{s0}\pi f(\hat{\phi})\frac{\psi_0'(\hat{\phi})}{\omega_m - \omega_s},$$

where the function $f(\hat{\phi})$ will be obtained later. Position of the bunch center is defined as an average over the distribution

$$\bar{\phi} = \int_0^\infty \int_0^{2\pi} \hat{\phi} cos(\theta)\psi(\hat{\phi}, \theta, t)\hat{\phi}d\hat{\phi}\frac{d\theta}{2\pi}.$$

This results in equation of bunch center motion

$$\bar{\phi} = \omega_{s0}\frac{\pi}{2}\Big(\hat{\phi}_m\int_0^\infty \frac{\psi_0'(\hat{\phi})\hat{\phi}^2 d\hat{\phi}}{\omega_m - \omega_s(\hat{\phi})} + \int_0^\infty f(\hat{\phi})\frac{\psi_0'(\hat{\phi})\hat{\phi}^2 d\hat{\phi}}{\omega_m - \omega_s(\hat{\phi})}\Big)e^{i\omega_m t},$$

where $\omega_s(\hat{\phi})$ is the synchrotron frequency

$$\omega_s(\hat{\phi}) = \omega_{s_0} - \omega_{s_0}\cdot\frac{\hat{\phi}^2}{16} + \triangle\omega_{sc}(\hat{\phi})$$

The first term in the equation of bunch center motion is due to external modulation and the second term is due to space charge. Without external modulation $\hat{\phi}_m = 0$ and with distribution function consisting of one particle the equation of bunch center motion should represent the equation of single particle motion in nonlinear external field with coherent frequency $\Omega = \omega_{s_0}(1 - \frac{\hat{\phi}^2}{16})$. It does not include the space charge shift because space charge does not affect the coherent frequency. Making substitution $\omega_m = \Omega$ it can be obtained:

$$\hat{\bar{\phi}} = \omega_{s0}\frac{\pi}{2}\int_0^\infty f(r)\frac{\psi_0'(\hat{\phi})\hat{\phi}^2 d\hat{\phi}}{\triangle\omega_{sc}(\hat{\phi})} \tag{B.5}$$

Assuming $f(\hat{\phi}) = C\triangle\omega_{sc}(\hat{\phi})$ and canceling $\triangle\omega_{sc}(\hat{\phi})$ the integral (B.5) can be calculated by parts. Using $\int \psi_0(\hat{\phi})2\pi\hat{\phi}d\hat{\phi} = 1$ it can be obtained:

$$\hat{\bar{\phi}} = -\frac{-C\omega_{s0}}{2}, \qquad C = -\frac{2\hat{\bar{\phi}}}{\omega_{s0}}.$$

The expression for the bunch center will looks like

$$\bar{\phi} = \Big(\frac{\omega_{s_0}\hat{\phi}_m\pi}{2}\int_0^\infty \frac{\psi_0'(\hat{\phi})\hat{\phi}^2 d\hat{\phi}}{\Omega - \omega_s(\hat{\phi})} - \hat{\bar{\phi}}\pi\int_0^\infty \triangle\omega_{sc}(\hat{\phi})\frac{\psi_0'(\hat{\phi})\hat{\phi}^2 d\hat{\phi}}{\Omega - \omega_s(\hat{\phi})}\Big)e^{i\Omega t}.$$

Extracting the amplitude of the bunch center motion $\hat{\bar{\phi}}$ and dividing by the modulation amplitude $\hat{\phi}_m$ the expression for the BTF can be obtained:

$$BTF = \frac{\frac{\omega_{s_0}\pi}{2}\int_0^\infty \frac{\psi_0'(\hat{\phi})\hat{\phi}^2 d\hat{\phi}}{\omega_m - \omega_s(\hat{\phi})}}{1 + \pi\int_0^\infty \triangle\omega_{sc}(\hat{\phi})\frac{\psi_0'(\hat{\phi})\hat{\phi}^2 d\hat{\phi}}{\omega_m - \omega_s(\hat{\phi})}}.$$

In the case of $\Sigma = 0$ BTF is obtain as

$$BTF = \frac{\omega_{s_0}\pi}{2}\int_0^\infty \frac{\psi_0'(\hat{\phi})\hat{\phi}^2 d\hat{\phi}}{\omega_m - \omega_s(\hat{\phi})}. \tag{B.6}$$

Thus the BTF with $\Sigma \neq 0$ can be simplified to

$$\frac{1}{BTF} = \frac{1}{BTF_0}\big(1 + \pi\int_0^\infty \triangle\omega_{sc}(\hat{\phi})\frac{\psi'(\hat{\phi})^2 d\hat{\phi}}{\omega_m - \omega_s(\hat{\phi})}\big). \tag{B.7}$$

Bibliography

[1] http://www.gsi.de/.

[2] Y. Liu. *Theory, measurements and simulation of longitudinal stability of bunched beams at the heavy ion synchrotron SIS*. Dissertation, Institue of modern physics in Lanzhou, 2003.

[3] O. Boine-Frankenheim, I. Hofmann, Y. Liu, and G. Rumolo. 2003.

[4] O. Boine-Frankenheim. *"Collective effects" activities at GSI and TUD as part of the EU-design study "DIRACsecondary beams"*. www-linux.gsi.de/ boine/CARE/Day2/Boine1.ppt.

[5] H. G. Hereward. Landau damping. (89-05):255–263, 1985.

[6] F. Pedersen and F. Sacherer. Theory and performance of the longitudinal active damping system for the cern ps booster. *IEEE Trans. Nucl. Sci.*, 24:1396–1398, 1977.

[7] J. M. Byrd. Longitudinal Beam Response Measurements at CESR. Prepared for IEEE 1991 Particle Accelerator Conference (APS Beam Physics), San Francisco, California, 6-9 May 1991.

[8] E. N. Shaposhnikova. Bunched beam transfer matrices in single and double rf systems. CERN-SL-94-19-RF.

[9] E. Shaposhnikova, T. Bohl, and T. Linnecar. Beam transfer functions and beam stabilisation in a double rf system. CERN-AB-2005-026.

[10] J. Byrd. Longitudinal beam transfer function diagnostics in the als. Prepared for 17th IEEE Particle Accelerator Conference (PAC 97): Accelerator Science, Technology and Applications, Vancouver, British Columbia, Canada, 12-16 May 1997.

[11] J. M. Byrd. Longitudinal beam response measurements at cesr. Prepared for IEEE 1991 Particle Accelerator Conference (APS Beam Physics), San Francisco, California, 6-9 May 1991.

[12] M. G. Minty and F. Zimmermann. Longitudinal beam-transfer-function measurements at the slc damping rings. Talk given at 17th IEEE Particle Accelerator Conference (PAC 97), Vancouver, Canada, 12-16 May 1997.

[13] M. Ellison. Driven response of the synchrotron motion of a beam. *Phys. Rev.*, E70, 1993.

[14] M. Ellison and H.-J. Shih. Theorethical study of longitudinal beam splitting and related phenomena. *Phys. Rev.*, E49, 1994.

[15] H. Huang et al. Experimental determination of the hamiltonian for synchrotron motion with rf phase modulation. *Phys. Rev.*, E48:4678–4688, 1993.

[16] M. Syphers. Experimental study of synchro-betatron coupling induced by dipole modulation. *Phys. Rev. Lett.*, 71, 1993.

[17] D. Li et al. Experimental measurement of resonance islands induced by the rf voltage modulation. *Phys. Rev.*, E48:1638–1641, 1993.

[18] J. M. Byrd et al. Nonlinear longitudinal dynamics studies at the als. Contributed to IEEE Particle Accelerator Conference (PAC 99), New York, 29 Mar - 2 Apr 1999.

[19] N. P. Abreu, R. H. A. Farias, and P. F. Tavares. Longitudinal dynamics with rf phase modulation in the lnls electron storage ring. *Phys. Rev. ST Accel. Beams*, 9:1433, 2006.

[20] U. Schaaf. *Schottky-Diagnose und BTF-Messungen an Gekuhlten Strahlen im Schwerionen-Speicherring ESR.* Dissertation, Frankfurt University, 1991.

[21] I. Hofmann, K. Beckert, S. Cocher, and U. Schaaf. Diagnostics and instability studies of cooled ion beams. Given at EPAC90: 2nd European Particle Accelerator Conference, Nice, France, 12-16 Jun 1990.

[22] I. Hoffmann. Beam dynamics of cooled heavy ion beams. 1991.

[23] U. Schaaf et al. Impedances and instability studies at the esr. Darmstadt GSI - Prepr. GSI 92-25-F (92/04,rec.Apr.) 3 p.

[24] G. Kalisch, K. Beckert, B. Franzke, I. Hofmann, and U. Schaaf. Longitudinal space charge effects in cooled bunched beams. Darmstadt GSI - Prepr. GSI 92-25-G (92/04,rec.Apr.) 3 p.

[25] http://www.gsi.de/library/gsi-report-2006-1.

[26] FAIR baseline technical report, GSI, September 2006.

[27] P. Huelsmann and W. Vinzenz. GSI-Acc-Note-2004-11-001(2004).

[28] G. Dome. Theory of rf acceleration. IN *OXFORD 1985, PROCEEDINGS, ADVANCED ACCELERATOR PHYSICS, VOL. 1*, 110-158.

[29] W. Pirkl. Longitudinal beam dynamics. Prepared for CERN Accelerator School: Course on Advanced Accelerator Physics (CAS), Rhodes, Greece, 20 Sep - 1 Oct 1993.

[30] S.Y. Lee. *Accelerator Physics*. World Scientific Publishing Co. Pte. Ltd., second edition, 2004.

[31] P. Huelsmann, O. Boine-Frankenheim, H. Klingbeil, and G. Schreiber. GSI-Acc-Note-2004-08-001(2004).

[32] J. Le Duff. Longitudinal beam dynamics in circular accelerators. In *Gif-sur-yvette 1984, Proceedings, General Accelerator Physics, Vol. 1*, 125-143.

[33] L. D. Landau and E. M. Lifshitz. *Course of theoretical physics. VOL. 1: MECHANICS*. Pergamon Press, third edition, 1976.

[34] A. Piwinski. Intrabeam scattering. In *Noordwijkerhout 1991, Proceedings, Advanced accelerator physics* 226-242. (see HIGH ENERGY PHYSICS INDEX 30 (1992) No. 9905).

[35] M. Reiser. Theory and design of charged particle beams. New York, USA: Wiley (1994) 607 p.

[36] A. Hofmann and F. Pedersen. Bunches with local elliptic energy distribution. *IEEE Trans. Nucl. Sci.*, 26:3526, 1979.

[37] I.N. Bronstein, K.A. Semendyayev, K. Musiol, and H. Mühlig. *Handbook of mathematics*. Springer, fourth edition, 2004.

[38] O. Boine-Frankenheim and T. Shukla. Space charge effects in bunches for different rf wave forms. *Phys. Rev. ST Accel. Beams*, 8:034201, 2005.

[39] F. J. Sacherer. Bunch lengthening and microwave instability. *IEEE Trans. Nucl. Sci.*, 24:1393–1395, 1977.

[40] A. Sessler and V. Vaccaro. Longitudinal instabilities of azimuthally uniform beams in circular vacuum chambers with walls of arbitrary electrical properties. CERN-67-02.

[41] A. Chao. Physics of collective beam instabilities in high energy accelerators. SSC-N-802.

[42] S. Nagaitsev. *Space charge dominated beams in the IUCF cooler*. Dissertation, Indiana University, 1995.

[43] O. Boine-Frankenheim and O. Chorniy. Stability of coherent synchrotron oscillations with space charge. *Phys. Rev. ST Accel. Beams*, 10:104202, 2007.

[44] H. G. Hereward. The elementary theory of landau damping. CERN-65-20.

[45] K. Y. Ng. Decoherence and landau damping. FERMILAB-FN-0763-AD.

[46] K. Y. Ng. Comments on landau damping due to synchrotron frequency spread. FERMILAB-FN-0762-AD.

[47] D. Mohl. On landau damping of dipole modes by nonlinear space charge and octupoles. *Part. Accel.*, 50:177–187, 1995.

[48] G. I. Budker. An effective method of damping particle oscillation in proton and antiproton rings. *Sov. J. Atom. Energy.*

[49] G. I. Budker et al. Experimental studies of electron cooling. *Part. Accel.*, 7:197–211, 1976.

[50] G. Budker, G. Dimov, and V. Dudnikov. (VIII-6-1), 1966.

[51] C. K. Birdsall and A. B. Langdon. *Plasma Physics via Computer Simulation.* IOP Publishing, 1991.

[52] R. W. Hockney and J. W. Eastwood. *Computer Simulation using Particles.* IOP Publishing, 1994.

[53] H. Risken. *The Fokker-Plank Equation.* Springer, 1984.

[54] H. Damerau, M. Kirk, and Y. Liu. Maschinenexperimente zum longitadinalen strahlverhalten waerend des hoch frequenzeinfangs. 2002.

[55] O. Chorniy, H. Damerau, G. Schreiber, and B. Zipfel. Machine development experiments on cavity synchronization in the sis12/18. 2005.

[56] H. Klingbeil. Digitale kavitaetensynchronisation. 2004.

[57] H. Klingbeil. A fast dsp-based phase detector for closed loop rf control in synchrotrons. pages 1209–1213, 2005.

[58] B. Zotter. Potential well bunch lengthening. CERN SPS/81-14.

[59] A. Hofmann. Beam instabilities. Prepared for CERN Accelerator School and PSI: Course on Synchrotron Radiation and Free Electron Lasers, Brunnen, Switzerland, 2-9 Jul 2003.

Acknowledgements

Here I want to thank all who help me during this work.

First of all I am would like to thank Prof.Dr.-Ing. Thomas Weiland for his support and useful comments concerning this work.

Special thanks go to Prof. Dr. Oliver Boine-Frankenheim who guided me in the ocean of beam dynamics and collective effects and help a lot in the questions concerning the numerical simulations.

I am thankful to Prof. Dr. Ingo Hoffmann for organizing very informative and interesting division meetings. I would like to thank to all people from Accelerator Theory division at GSI: Dr. Giuliano Franchetti, Priv.Doz. Dr. Rainer Hasse, Dr. Vladimir Kornilov, Dr. Edil Mustafin, Dr. Stefan Sorge, Dr. Andrey Plotnikov, Tripti Mohite, Angelina Parfenova for creating a nice atmosphere in the division.

I would like to thank Dr. Heiko Damerau for his sincere interest in my work and for the help in performance the first bunched BTF measurements in the SIS that was the first significant experiment in my life.

Thanks to Bernhard Zipfel, Hans-Gunter Koenig, Harald Klingbeil and others people from the rf group at GSI for useful discussions and help in organizing the experiments.

I would like to thank also Dr. Oleksiy Dolinskiy for organizing a very nice evening discussions on accelerator physic topics. This discussions would be not so useful without my colleagues: Vitaliy Gostishchev, Oleksiy Gorda, Sergiy Litvinov.

I am thankful to my colleagues Sergiy Trotsenko, Olga Lepyoshkina, Irina Poltoratska and Yuliya Plotroratska who make me more optimistic than I am.

Finally, I want to thank especially my wife Irina Chorna for taking care about our family during this work.

Curriculum vitae

Name:	Oleksandr Chorniy
Born on:	26 October 1980 in Smolino, Ukraine

Education

1987-1998	Energodar Secondary School No.3, Zaporizka Region, Ukraine
1998-2004	Student of V.N. Karazin Kharkiv National University, Ukraine Department of Physics and Technology. Specialization in Nuclear Physics
2002	Bachelor thesis "Data acquisition system for registration of pulses from neutron generator", V.N. Karazin Kharkiv National University, Ukraine
2003	2nd German-Ukrainian Nuclear and Accelerator Physics Summer School, Darmstadt
2004	Master thesis "The equivalent dose rate of a spent fuel assembly from the nuclear reactor VVER-1000" V.N. Karazin Kharkiv National University, Ukraine

Professional experience

since 2005	Work at FAIR Accelerator Theory Division, Gesellschaft fur Schwerionenforschung (GSI)